UC Santa Cruz
UC Santa Cruz Electronic Theses and Dissertations

Title

Paleoceanography of the Pacific: studies of high latitude Pleistocene climate and low latitude sea surface temperatures since the late Miocene

Permalink

https://escholarship.org/uc/item/5nx2w7ww

Author

Drake, Michelle

Publication Date

2021

Copyright Information

Peer reviewed|Thesis/dissertation

UNIVERSITY OF CALIFORNIA
SANTA CRUZ

**PALEOCEANOGRAPHY OF THE PACIFIC: STUDIES OF HIGH
LATITUDE PLEISTOCENE CLIMATE AND LOW LATITUDE SEA
SURFACE TEMPERATURES SINCE THE LATE MIOCENE**

A dissertation submitted in partial satisfaction
of the requirements for the degree of

DOCTOR OF PHILOSOPHY

in

OCEAN SCIENCES

by

Michelle K. Drake

June 2021

The Dissertation of Michelle K. Drake is
approved:

_____
Professor Ana Christina Ravelo, chair

_____
Professor James Zachos

_____
Professor at San Jose State University,
Moss Landing Marine Laboratories
Ivano Aiello

_____
Quentin Williams
Interim Vice Provost and Dean of Graduate Studies

Table of Contents

List of Figures and Tables

Abstract
Paleoceanography of the Pacific: studies of high latitude Pleistocene climate and low latitude sea surface temperatures since the late Miocene
By Michelle K. Drake

This dissertation investigates the climate system response during periods of relative warmth over the last 10 million years (Myr) at different temporal scales: thousand-year (i.e., orbital) timescales during the warmer glacial cycles of the early Pleistocene and million-year timescales during the warm mean-state of the late Miocene. The relatively warmer and less intense glacial cycles of the early Pleistocene are an ideal period to investigate what drives high latitude climate during the ice ages, which remains not entirely understood. The warm mean-state of the late Miocene is a period not currently well characterized especially in the western equatorial Pacific (WEP) therefore, we investigate how WEP climate responds as the mean-state shifts from the warm late Miocene into the Pleistocene ice ages. This dissertation is presented in three parts.

Chapter 2 provides an efficient method to characterize changes in high-resolution multi-sensor track data (i.e., Gamma Ray Attenuation (GRA) bulk density) as a function of sediment composition and/or grain size. This sedimentological study focuses on the diatom-rich sediments of the high latitude Bering Sea. An interpretation of the GRA bulk density data is developed based on laser particle size and smear slide analysis. Results show that down-core variability in GRA reflects changes in the sediment packing due to changings in diatom valve abundance and fragmentation.

The method presented in Chapter 2 is adapted and applied in Chapter 3, which studies the cyclicity of the Bering Sea cryosphere to test theories of what causes ice ages. We focus on the warmer early Pleistocene glacial cycles because they are shorter (40 thousand years (kyr)), less intense, and are thought to be a more straightforward response to insolation forcing than the most recent ice ages. To measure local high latitude ice variability Chapter 3 presents an orbitally resolved Ice Rafted Debris (IRD) flux record that is interpreted with help from the sedimentological method of Chapter 2, modified to interpret Natural Gamma Radiation (NGR) instead of GRA. Results suggest the record dominantly represents transport of IRD by sea ice. While spectral analysis reveals there are no 40 kyr cycles, there is significant sub-orbital variability in the record, which suggests the Bering Sea cryosphere is sensitive to local seasonal forcing.

Chapters 4 evaluates the long-term (~10 Myr) evolution of sea surface temperatures (SST) in the WEP warm pool since the late Miocene. There is little data from the WEP warm pool, but over this ~10 Myr period many other regions show a long-term cooling trend. We also assess whether the tropical Pacific El Padre mean-state, characteristic of the early Pliocene, is present in the late Miocene. The SST record presented in Chapters 4 use the Mg/Ca paleothermometer by measuring trace metal ratios of planktic foraminifer *Trilobatus trilobus*. Results show there is long-term stability in the SSTs of the WEP warm pool, and the El Padre mean-state is present during the late Miocene.

Overall, this dissertation broadly investigates the climate system response during past periods of relative warmth. Chapters 2 and 3 focus on the high-latitude Bering Sea at orbital timescales and show that Bering Sea cryosphere is sensitive to local seasonal forcing during the early Pleistocene. Chapter 4 focuses on the low-latitude WEP over million-year timescales and finds long-term stability in the WEP warm pool SSTs since the late Miocene. Synthesized, this work finds strong regional responses, since the 40 kyr cycles were not found in Chapter 3, and the long-term cooling trend was not found in Chapter 4.

Dedication

In Loving Memory of my mother

Dr. Diane Reiko Murakami

Acknowledgements

I first want to thank my PhD advisor and mentor Christina Ravelo for pushing me to think deeper and harder than I thought I could and for her patience while helping me improve my writing skills. She supported my dream to sail on the D/V JOIDES Resolution even though it extended my time as her advisee. Most of all her support through the years when my mom was dying were crucial to my completion of this dissertation.

I would also like to sincerely thank my committee members Ivano Aiello and James Zachos for their mentorship and thoughtful feedback.

I have appreciated the support from all the UCSC Ocean Sciences faculty and staff, particularly Phoebe Lam who was on my qualifying exam committee as well as Matt McCarthy and Chris Edwards who tested me during my departmental exam. A special thank you to Rondi Robison for logistical and generous emotional support throughout the years.

I am very grateful to Dyke Andreasen and Colin Carney of the UCSC Stable Isotope Laboratory as well as Rob Franks and Bryan Dreyer of the Marine Analytical Lab for patiently teaching me about our instrumentation. A special thank you to Colin Carney for going out of his way to help me complete my data collection after I moved back to the Bay Area to take care of my mother.

My lab-mates past and present have helped me learn complex lab techniques, paleoceanographic concepts, and have been a constant source of encouragement. A special thank you to Sarah White, Wilson Sauthoff, Heather Ford, and Karla

Knudson. I also received help from many undergraduates including Dan Mendoza, Isabella De La Rosa, Carman Ma, Linda Pineda, and Tori Andrade, and others. I would never been able to process so many samples without their help. Thank you to my Ocean Sciences cohort and my officemates from the fifth-floor penthouse (EMS C580) and the few of us that were exiled to Thimann Labs, which I lovingly refer to as the Ocean Sciences "villas".

Finally, I would like to thank my family and friends for their unconditional support especially my husband, Roger Chu.

Chapter 1: Introduction

The overall aim of this dissertation is to investigate how the climate system responds to different forcings (i.e., internal versus external, local versus global) during intervals of relative warmth over the last ~10 million years (Myr). Since the climate system has both fast and slow responses, this dissertation studies past periods of relative warmth at two different temporal scales: thousand-year (i.e., orbital) timescales during the warmer glacial cycles of the early Pleistocene and million-year timescales during the warm mean-state of the late Miocene. The projects referenced in this dissertation focus on what drives high latitude climate in the Bering Sea during the shorter and less intense glacial cycles of the early Pleistocene (Chapters 2 and 3) and on the long-term evolution of sea surface temperatures (SST) in the western equatorial Pacific (WEP) since the warmer mean-state of the late Miocene (Chapter 4).

Chapters 2 and 3 are fundamentally sedimentological studies of Bering Sea sediment. Chapter 2 provides an efficient method to characterize changes in high-resolution multi-sensor track data (i.e., Gamma Ray Attenuation (GRA) bulk density) as a function of sediment composition and/or grain size. This sedimentological study focuses on the diatom-rich sediments of the high latitude Bering Sea. An interpretation of the GRA bulk density data is developed based on laser particle size and smear slide analysis. Results show that down-core variability in GRA reflects changes in the sediment packing due to changings in diatom valve abundance and

fragmentation. The sedimentological method presented in Chapter 2 is modified to interpret Natural Gamma Radiation (NGR) instead of GRA in Chapter 3.

Chapter 3 set out to test theories for the early Pleistocene glacial cycles (e.g., Huybers, 2006; Raymo et al., 2006). What drives high latitude climate variability and more specifically the cause of ice ages are long-standing questions in paleoceanography that are not fully understood. We focus on the early Pleistocene because relative to the late Pleistocene ice ages, the shorter (40 thousand years (kyr)) and less intense glacial cycles (Lisiecki & Raymo, 2005) of the early Pleistocene (Herbert et al. 2010; Snyder et al., 2016; Sosdian & Rosenthal, 2009) are thought to be a more straightforward response to orbitally induced changes in incoming solar radiation. Therefore, the early Pleistocene is considered an excellent period to test astronomical theories for the ice ages (Raymo & Huybers, 2008).

Ambiguity around what drives variability in the high latitude cryosphere comes from a lack of high latitude proxy records that are sensitive to changes in local ice (Raymo & Huybers, 2008). Therefore, Chapter 3 presents an orbitally resolved record of Bering Sea Ice Rafted Debris (IRD) flux to assess the cyclicity of Bering Sea cryosphere. The presence of IRD in high latitude deep-sea sediment it is one of the most direct pieces of evidence for the occurrence of ice. Chapter 3 uses the method presented in Chapter 2 to understand if the IRD flux record represents sea ice or iceberg rafted debris. Rather than interpreting variations in GRA, the method was modified in Chapter 3 to interpret the NGR record as a proxy for clay mineral abundance, leading to the interpretation that the IRD was primarily transported by sea

ice. Finally, the cyclicity of the IRD flux record was assessed through spectral analysis. The record of IRD flux has significant variability at precession (1/23 cycles/kyr) and half-precession (1/12-10 cycles/kyr) frequencies that suggests the Bering Sea cryosphere responds to local seasonal forcing during the early Pleistocene.

Zooming out from orbital scale variability, Chapter 4 investigates the long-term trends in SST from the Western Equatorial Pacific (WEP) warm pool since the late Miocene. The late Miocene is a period of global warmth and a more equitable SST distribution that is followed by a period of long-term cooling into the Pleistocene Ice Ages (Herbert et al., 2016; Steinthorsdottir et al., 2020). There is a large discrepancy between late Miocene paleo-proxy data and paleoclimate model simulations, with models generally underestimating high latitude SSTs and overestimating tropical SSTs such as in the WEP warm pool (e.g., Burls et al., 2021). Therefore, it is critical to create good SST records from the WEP warm pool during the late Miocene because there is currently a dearth of data and it is a region where there is a significant model-data discrepancy (Burls et al., 2021; Herbert et al., 2016).

Chapter 4 further examines if the El Padre mean-state conditions are present during the late Miocene. El Padre is a well-documented tropical Pacific mean-state during the early Pliocene (Ford et al., 2015) characterized by a reduced zonal SST gradient (e.g., Wara et al., 2005), a deeper and/ or warmer thermocline (Ford et al., 2015), and far-field changes in precipitation (e.g., Goldner et al., 2011; Molnar & Cane, 2002). To investigate the evolution of SST in WEP warm pool from the warm mean-state of the late Miocene to the present, a long-term record of SST was

generated using the Mg/Ca paleothermometer. The results of Chapter 4 indicate there is long-term stability in SST of the WEP warm pool and our findings also suggest the early Pliocene El Padre conditions are present during the late Miocene.

This dissertation is presented in three chapters. Chapters 2 and 3 present sedimentological analyses of Bering Sea sediments, and Chapter 3 also assess the cyclicity of the cryosphere during the early Pleistocene glacial cycles. Chapter 4 investigates the evolution of SST in the WEP warm pool from the warm mean-state of the late Miocene to modern climate conditions. The chapters are written as independent manuscripts for submission to peer-reviewed journals. Overall, this dissertation broadly contributes to our understanding of how the climate system responds during periods of relative warmth, both at orbital timescales during the less intense glacial cycles of the early Pleistocene and at million-year timescales during the warmer mean state of the late Miocene and early Pliocene. Synthesized, this work finds strong regional responses, since the 40 kyr cycles were not found in Chapter 3, and a long-term cooling trend was not found in Chapter 4.

References:

Burls, N. J., Bradshaw, C. D., De Boer, A. M., Herold, N., Huber, M., Pound, M., … Zhang, Z. (2021). Simulating Miocene Warmth: Insights From an Opportunistic Multi-Model Ensemble (MioMIP1). *Paleoceanography and Paleoclimatology*, *36*(5). https://doi.org/10.1029/2020pa004054

Ford, H. L., Ravelo, A. C., Dekens, P. S., Lariviere, J. P., & Wara, M. W. (2015). The evolution of the equatorial thermocline and the early Pliocene El Padre mean state. *Geophysical Research Letters*, *42*(12), 4878–4887. https://doi.org/10.1002/2015GL064215

Goldner, A., Huber, M., Diffenbaugh, N., & Caballero, R. (2011). Implications of the permanent El Niño teleconnection "blueprint" for past global and North American hydroclimatology. *Climate of the Past*, *7*(3), 723–743. https://doi.org/10.5194/cp-7-723-2011

Herbert, T. D., Lawrence, K. T., Tzanova, A., Peterson, L. C., Caballero-Gill, R., & Kelly, C. S. (2016). Late Miocene global cooling and the rise of modern ecosystems. *Nature Geoscience*, *9*(11), 843–847. https://doi.org/10.1038/ngeo2813

Herbert, T. D., Peterson, L. C., Lawrence, K. T., & Liu, Z. (2010). Tropical ocean temperatures over the past 3.5 million years. *Science*, *328*(5985), 1530–1534. https://doi.org/10.1126/science.1185435

Huybers, P. (2006). Early Pleistocene glacial cycles and the integrated summer insolation forcing. *Science*, *313*(5786), 508–511. https://doi.org/10.1126/science.1125249

Lisiecki, L. E., & Raymo, M. E. (2005). A Pliocene-Pleistocene stack of 57 globally distributed benthic 18O records. *Paleoceanography*, *20*(1), 1–17. https://doi.org/10.1029/2004PA001071

Molnar, P., & Cane, M. (2002). El Niño's tropical climate and teleconnections as a blueprint for pre-Ice Age climates. *Paleoceanography*, *17*(2), 1021-undefined. https://doi.org/10.1029/2001PA000663

Raymo, M. E., & Huybers, P. (2008). Unlocking the mysteries of the ice ages. *Nature*, *451*, 284–285. https://doi.org/10.1038/nature06589

Raymo, M. E., Lisiecki, L. E., & Nisancioglu, K. H. (2006). Plio-Pleistocene ice volume, Antarctic climate, and the global delta18O record. *Science*, *313*(5786), 492–495. https://doi.org/10.1126/science.1123296

Snyder, C. W. (2016). Evolution of global temperature over the past two million years. *Nature*, *538*(7624), 226–228. https://doi.org/10.1038/nature19798

Sosdian, S., & Rosenthal, Y. (2009). Deep-Sea Temperature and Ice Volume Changes Across the Pliocene-Pleistocene Climate Transitions. *Science*, *325*, 306–311. https://doi.org/10.1126/science.1169938

Steinthorsdottir, M., Coxall, H. K., de Boer, A. M., Huber, M., Barbolini, N., Bradshaw, C. D., … Strömberg, C. A. E. (2020). The Miocene: the Future of the Past. *Paleoceanography and Paleoclimatology*. https://doi.org/10.1029/2020pa004037

Wara, M. W., Ravelo, A. C., & Delaney, M. L. (2005). Permanent El Niño-like Conditions during the Pliocene Warm Period. *Science*, *309*(5735), 758–761. https://doi.org/10.1126/science.1112596

Chapter 2: Gamma-ray attenuation bulk density as an indicator of diatom valve abundance and fragmentation in Pleistocene biosiliceous sediments of the Bering Sea

Michelle K. Drake[1*], Ivano W. Aiello[2*], and Ana Christina Ravelo[1]

[1] *Ocean Sciences Department, University of California, 1156 High Street, Santa Cruz, California, 95064, USA*

[2] *Moss Landing Marine Laboratories, Moss Landing, California 95039, USA*
email: mkdrake@ucsc.edu; iaiello@mlml.calstate.edu

Abstract

Multi-sensor track measurements are a non-destructive method to produce continuously measured high-resolution physical property datasets that are a great asset to a wide range of research including geotechnical studies and paleoceanography. Interpretation of these physical property data can be challenging because they are typically influenced by multiple variables. This paper specifically focuses on the interpretation of gamma-ray attenuation (GRA) data (a proxy for sediment bulk density) in biosiliceous sediments. The Bering Sea is a basin dominated by biosiliceous sediment and the late Pleistocene to present core record of Sites U1340 and U1339 drilled during IODP Expedition 323 has subtle meter-scale changes in the concentration of fine-grained siliciclastic sediment that produce lithologic alternations between diatom ooze and diatom mud. We produce a detailed sedimentologic dataset that combines smear slide petrography, scanning electron microscopy, and grain size analysis for both Sites U1340 and U1339 and correlate to shipboard GRA bulk density measurements. Results show that bulk density is inversely correlated with diatom abundance and positively correlated with the

fragmentation of diatom valves. This study argues that diatom abundance and fragmentation influence sediment packing and drive downcore variability in GRA bulk density. Therefore, denser diatom mud is a result of tightly packed highly fragmented diatom valves that alternate with diatom ooze, a less dense sediment dominated by whole and less fragmented diatom valves. We suggest GRA data can be used as a proxy for diatom abundance and an indicator of diatom fragmentation. We include a discussion of how these results may impact the interpretation of ancient bedded siliceous rocks.

Introduction

Biosiliceous oozes are sedimentary deposits with a dominant biogenic component derived from the accumulation of plankton tests (mainly diatoms and radiolarians) made of amorphous silica (opal-A). The accumulation of biosiliceous sediments is limited because seawater is undersaturated with respect to silica. In the modern ocean biogenic silica accumulates on the seafloor beneath regions with well-mixed surface waters, high nutrient availability, and high export production (Abrantes et al., 2016; Calvert, 1966; Lisitsyn et al., 1967; Romero et al., 2001; Romero and Hebbeln, 2003). Multiple factors other than export production affect the preservation of biosiliceous oozes such as zooplankton grazing, water depth, and bioturbation of the seafloor (Ragueneau et al., 2000). In paleoceanographic reconstructions, the presence of biosiliceous sediments is often interpreted as an indication of upwelling-driven productivity (Abrantes & Moita, 1999; Calvert, 1983; Schuette & Schrader,

1981;). Changes in biosilica are commonly measured as the concentration of opal-A through alkaline leaching (e.g., Mortlock & Froelich, 1989), which is destructive and time consuming. Expanding our understanding of how multi-sensor track (MST) physical property data relate to biosiliceous lithologies will improve our ability to use these quickly measured non-destructive datasets for paleoceanographic studies, geotechnical studies (e.g., interpretation of lithologic units in synthetic seismic studies), or modeling diagenetic processes. This paper specifically focuses on how to interpret gamma-ray attenuation (GRA) MST measurements collected from biosiliceous sediments.

Generally, downcore variability in physical properties is correlated with changes in sediment lithology, but a more nuanced understanding of how these measurements relate to sediment properties is necessary. Accurate interpretation of physical properties data is of great interest because physical property measurements can be produced continuously at high-resolution (centimeter scale) through non-destructive core scanning processes (Rothwell & Rack, 2006). Interpretation of physical properties can be challenging because they are influenced by multiple variables. Early studies of this show wet-bulk density of unconsolidated sediments measured by GRA is influenced by the volume of water-saturated pores, grain density, and porosity (Boyce, 1976; Hamilton, 1971). Bulk density and porosity are linearly and inversely correlated (Hamilton, 1974). They are influenced by mean grain size, sorting, mineralogy (i.e., density) and sediment micro-fabric (i.e., sediment packing) (Hamilton, 1974; Hamilton & Bachman, 1982).

Our understanding of how to interpret sediment bulk density largely comes from studies in carbonate-rich and terrigenous sediments. In carbonate-rich sediments it is well established that variations in sediment bulk density reflect a shift in lithology, with alternations between high density calcareous oozes and lower density lithologies rich in either clay minerals or biosiliceous microfossils (Herbert & Mayer, 1991; Nobes et al., 1991; Wilkens & Handyside, 1985). Study of North Pacific Site 882 showed low-density sediments correlate with biogenic opal and high-density sediment reflect terrigenous sediments (Kotilainen & Shackleton, 1995). The change in bulk density can be driven by a change in the relative abundance of particles with different grain densities and or a change in sediment packing (Hamilton,1974; Wilkens & Handyside, 1985). Site specific studies of alternating calcareous-biosiliceous oozes suggest both the difference in grain density between opal-A (2.00-2.30 g/cm^3) and calcium carbonate (2.65 g/cm^3) as well as the more open sediment framework produced by the shape of siliceous microfossils contribute to the lower density of biosiliceous sediments relative to nannofossil-rich calcareous ooze sediments (Nobes et al., 1991; Rack & Palmer-Julson, 1992; Wilkens & Handyside, 1985). A multi-regional study of carbonate-rich sediments suggest that the variation in bulk density is driven by a difference in sediment packing between the carbonate-rich lithology and the non-carbonate lithology, more than the change in the grain densities of sediment components (Herbert & Mayer, 1991). This paper will investigate how GRA bulk density data specifically relates to biosiliceous sediments.

10

To our knowledge, there has not been a rigorous interpretation of bulk density in a sedimentary basin dominated by biosiliceous sediments.

The Bering Sea is an ideal location for this study because it has been dominated by sedimentation of mainly biosiliceous (diatom) sediments over the last five million years (Takahashi et al., 2000, 2002, 2011). Subtle lithologic variability has been observed in the sediments collected during IODP Expedition 323 (Exp 323) in the Bering Sea, where the biosiliceous sediment (diatom ooze) alternates at sub-meter- to meter-scale with diatom mud, a lithology where diatoms are mixed with siliciclastic sediment (Takahashi et al., 2011; Aiello & Ravelo, 2012). Gamma-ray attenuation bulk density was measured on Exp 323 cores and rhythmic down-core variability was observed (Takahashi et al., 2011).

In a basin dominated by biosiliceous sediments changes in GRA are driven by changes in the sediment composition that drive changes in grain density or by changes in sediment packing? Is this relationship consistent throughout the Bering Sea basin? To investigate these questions, we characterize the composition of the sediment through smear slide and scanning electron microscope (SEM) analysis and measure grain size statistics through laser particle size analysis. Analyses on samples from Site U1340 Bowers Ridge and Site U1339 on the Umnak Plateau. The relationship between sediment properties and shipboard GRA bulk density measurements are analyzed with regression analysis.

Results from this study show that at both sites variability in sediment bulk density change as a result of diatom valve abundance and fragmentation, which we

11

suggest influence sediment packing. Therefore, we propose denser diatom mud is a result of tightly packed highly fragmented diatom valves that alternate with diatom ooze, a less dense sediment dominated by whole and less fragmented diatom valves. We suggest GRA data can be used as a proxy for diatom abundance and an indicator of diatom fragmentation. We discuss the implications of these findings for silica diagenesis models and the interpretation of ancient bedded siliceous rocks such as those found in the Monterey Group.

Methods

Site locations and age control

Expedition 323 to the Bering Sea offers an opportunity to examine how sediment properties change in contrasting depositional environments within a basin dominated by biosiliceous sediment. This study focuses on Site U1339 on the Umnak Plateau and Site U1340 on Bowers Ridge. Site U1339 represents deposition in an ocean margin-like setting, proximal to the modern sea ice edge and the broad continental shelf, which is a major source of terrigenous sediment. The average sedimentation rate at Site U1339 is ~24 cm/1000 yr (Cook et al., 2016). Site U1340 represents deposition in an open ocean-like setting with a sedimentation rate of ~30 cm/1000 yr (Schlung et al., 2013; Figure 1).
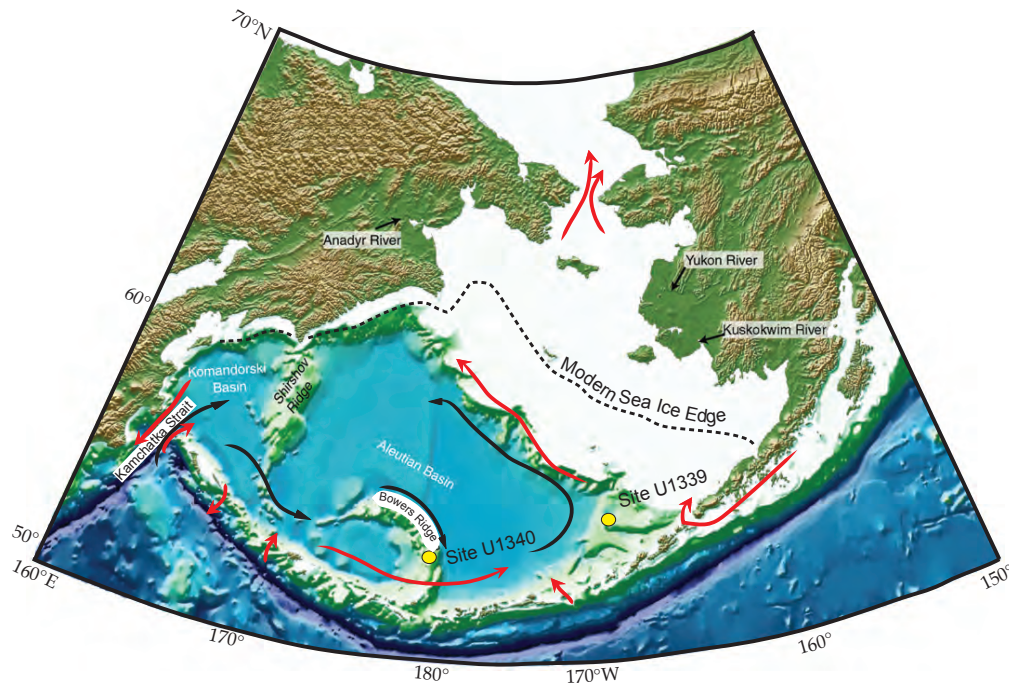
Figure 1

Figure 1. Bathymetric map of Bering Sea and regional physiography. Site U1339 on Umnak Plateau (54.47N, 169.97W; water depth, 1866m), is within the Bering Slope current and proximal to the modern sea-ice limit (dashed line, Fetterer et al., 2016). Site U1340 on the eastern slope of Bowers Ridge (53.4N, 179.52W; water depth, 1294m), is directly influenced by the eastward flowing Aleutian North Slope Current. Simplified surface currents (red arrows) and sub-surface water-circulation (black arrows). Map modified from Takahashi et al. (2011).

In this study we investigate late Pleistocene to Holocene samples of the last ~700,000 years (n=214). The sedimentologic dataset is interpreted within the chronostratigraphic framework produced during Exp 323 and further refined by post-cruise stable isotope studies (Schlung et al., 2013; Cook et al., 2016). The age model for Site U1339 is based on the oxygen isotope stratigraphy of Cook et al. (2016). The age model for Site U1340 is improved by ^{14}C dating and oxygen isotope stratigraphy of Schlung et al. (2013). The sediment bulk density record at each site reflects

13

different scales of climate variability: orbital scales at Site U1339 (Cook et al., 2016) and sub-orbital scales at Site U1340 (Schlung et al., 2013). Therefore, sampling resolution for the upper ~100 ka varies between the two sites to capture this variability. Site U1340 was sampled at ~0.5 kyr resolution, while Site U1339 was sampled at ~2 kyr resolution. lower portion of each record was sampled at ~45 kyr sample resolution, which represent 682-100 ka at Site U1339 and 824-279 ka at Site U1340.

Smear slide analysis

Smear slide petrography was used to determine the relative abundance of each constituent of the sediment. The ODP and IODP shipboard scientists commonly use this visual method for core descriptions, as it offers a relatively rapid way to identify the components in marine sediments and estimate their relative abundances (e.g. Marsaglia et al., 2015, 2013; Rothwell, 1989).

A method was developed to improve the statistical confidence and reproducibility of smear slide estimates using a subset of sediment samples from Sites U1339 and U1340 (Drake et al., 2014). Smear slide counts (i.e., determining the percent cover of each sedimentary component within a single field of view) were performed with a petrographic microscope at 400x magnification. The location of each field of view was selected through a systematically randomized process, where the slide cover was divided into a six-box grid and a random number generator was used to determine within which grid box the field of view would be located. A

particular field of view was excluded when sediments were covering less than 10% or greater than 30% of the total visible area. This ensured that a representative portion of the sample was analyzed and that the field of view was not too crowded thus obstructing identification. The percent cover of each particle type was counted with reference to a standardized visual estimation chart (e.g., Rothwell, 1989). The initial estimate of total percent cover should be used as a reference point to assess the final sum of all individual components estimated, these two estimates of total percent cover should be within five percent. The final calculation of relative percent abundance for each particle type is the average of three fields of view counted on one smear slide. Data are reported as a relative percent abundance of each sedimentary component.

A qualitative assessment of centric diatom valve fragmentation was incorporated into the counting procedure. The procedure was adapted from the conventional approach used by marine micropaleontologists (e.g., Johnson, 1976). When assessing the relative percent abundance of centric diatoms, the observer first estimates the percent cover of total centric diatoms, followed by an estimate of the percent cover of only whole centric diatom valves. A whole centric diatom was defined as a valve with ≥80% of the valve face intact. The definition of a 'whole' centric diatom is adapted from the micropaleontology assemblage count procedure, where >50% of centric diatom species must be present to be counted (Schrader & Gersonde, 1976). A larger percentage is used as the cut off for the definition of 'whole' because other procedures such as the identification of diatom valve

microstructures wasn't compatible with smear slide analysis. The percent cover of whole centric diatoms is normalized to the percent cover of total centric diatoms and reflects the level of fragmentation in the sample.

Clay minerals were visually identified based on reference images from Marsaglia et al. (2013). The percent volume of clay-sized particles was also measured for each sample in this study (discussed in following section). The relative percent cover of fine-grained siliciclastic material was based on the abundance of non-biogenic material visible in cross-polarized light. Individual mineral types were not systematically identified or counted, but most abundant minerals were generally quartz and feldspar. This operational definition likely led to the underestimate of weakly pleochroic minerals (i.e., biotite) but they are not thought to be a major percentage of the fine-grained siliciclastic material.

Particle sizes

Smear slide analyses are paired with particle size analysis measured by a laser diffraction particle size analyzer (LPS) for each sample in this study (Table 1). Grain size distributions of pelagic and hemipelagic sediments have been used as tools to interpret changes in composition (e.g. Aiello & Ravelo, 2012) and physical properties (e.g. Warner & Domack, 2002). This study used a Beckman Coulter LS 13 320 equipped with an aqueous module. The instrument generates particle size distributions between 0.04 and 2000 μm (using geometric statistics). The proprietary software uses a spherical approximation to quantify the grain size, which can

16

overestimate the size of platy particles (Beckman Coulter Inc., 2003). Flocculation of small platy particles can also bias grain size statistics by underestimating the smaller end of the particle size spectrum, defined as less than 4 μm in this study. To test this possible source of bias randomly chosen samples (n=35) were analyzed with two treatments: (1) untreated bulk sediment and (2) bulk sediment with sodium-hexametaphosphate, a disaggregating solution. No treatment effect was found using a Wilcoxon signed-rank test (α=0.01; Z= -0.82, p=0.935), suggesting that flocculation is not significantly biasing the LPS analyses. Mean grain size (μg) and the percent volume of clay-sized particles are used in correlation analysis and data provided in Supplemental Information (Table S1, Table S2). Note that the percent volume of clay-size particles is an operational definition based on size (particles <4 μm) distinct from the previously described measure of clay minerals by smear slide petrography.

Table 1

	Site U1340	Site U1339
Major sedimentary components		
Total Diatom (Pennate + Centric)	51.64 ± 1.29	46.19 ± 1.48
Pennate Diatoms	12.95 ± 0.52	9.55 ± 0.63
Centric Diatoms	38.68 ± 1.02	36.69 ± 1.14
Whole Centric*	14.02 ± 1.21	13.77 ± 1.35
Clay Minerals	17.52 ± 0.72	21.79 ± 0.84
Fine-grained Siliciclastic	14.93 ± 0.60	15.97 ± 0.68
Minor sedimentary components		
Volcanic Material	6.52 ± 0.48	11.79 ± 1.00
Opaque Material	4.79 ± 0.24	3.55 ± 0.31
Trace sedimentary components		
Sponge Spicules	0.69 ± 0.09	0.07 ± 0.03
Radiolarian	0.05 ± 0.02	0.00 ± 0.00
Silicoflagellates	0.29 ± 0.08	0.08 ± 0.06
Foraminifera	1.17 ± 0.20	0.01 ± 0.01
Coccolithophores	2.13 ± 0.26	0.27 ± 0.17
Particle size statistics		
Standard deviation	3.66	4.20
Mean grain size (µm)	19.17 ± 0.81	12.18 ± 0.56
Clay	15.88 ± 0.74	24.30 ± 0.97
Silt	67.66 ± 0.58	63.02 ± 0.62
Sand- very fine	12.45 ± 0.72	7.77 ± 0.44
Sand- fine	3.89 ± 0.47	4.97 ± 0.60
Sand- medium	0.10 ± 0.03	0.04 ± 0.01

*"Whole centric" diatoms is normalized to the abundance of centric diatoms

Table 1. Average relative abundance of sedimentary components identified by smear slide petrography, Site U1340 (n=138) and U1339 (n=76). Particle size statistics quantified by laser particle size analysis, data reported as average value and standard error. Clay, silt, and sand-size fractions follow the Wentworth scale and represent the percent volume of a sample.

Results

Overall, the comparisons between smear slide, LPS analysis and shipboard bulk density show the dependence between sediment composition, grain size, and sediment bulk density at both sites. The first section reports the sedimentological analysis of the upper ~200m meters of Sites U1340 and U1339. The second section is a comparison of these data to shipboard GRA bulk density data. Statistical analyses include the results of Pearson correlations (r), simple linear regressions (adjusted R^2),

and t-tests (t) between the variables measured (all values are p>0.001 unless otherwise noted).

Sediment composition and texture

Smear slide analysis identified three main sediment constituents as well as secondary and trace constituents. Diatoms (pennate and centric) are the most common sedimentary component, and in all analyzed samples diatom abundance is greater than 20% (Figure 2a). The other two major components are clay minerals and fine-grained siliciclastic particles of mainly silt size. Volcanic ash and opaque minerals are secondary components, on average accounting for less than ~13% of the sediment. Silicoflagellates, radiolarians, foraminifera, sponge spicules, and coccolithophores were identified and counted in trace amounts (relative abundance less than 5%) at both sites (Table 1, Supplemental Information Table S1, Table S2).
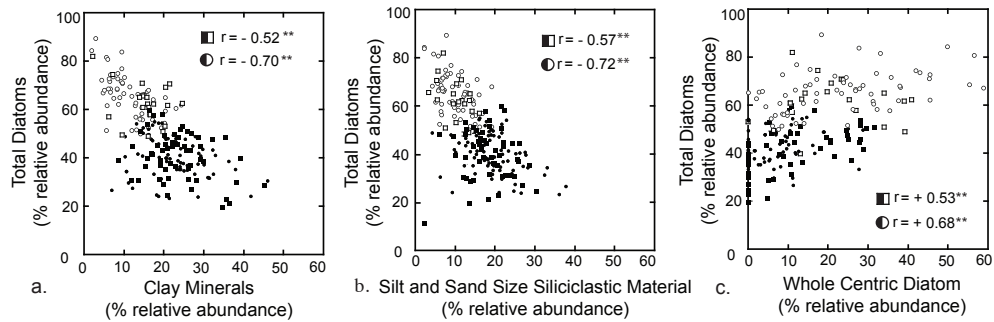
Figure 2. Bivariate graphs of sediment composition. The relative percent abundance of total diatoms (both centric and pennate) correlated to relative percent abundance of clay minerals (A), fine-grained siliciclastic sediments (B), and whole centric diatoms (C). Site U1340 (n=138) represented by circles (●,○) and U1339 (n=76) represented by squares (■,□). Open symbols indicate diatom ooze and closed symbols indicate diatom mud. Correlation coefficient (r) reported for Pearson correlation analyses. Double asterisk (**) indicates p-value <0.001.

Correlation trends between the three main sediment components are consistent between sites (Figure 2). The most significant correlations are the inverse relationships between the relative abundance of diatoms with both clay minerals (U1339 r=-0.52; U1340 r=-0.70) and fine-grained siliciclastic particles (U1339 r=-0.57; U1340 r=-0.72; Figure 2a, 2b). Clay mineral abundance and the silt- to sand-sized siliciclastic abundance are weakly correlated with each other at Site U1340 (r=+0.25, p<0.05) and are not correlated at Site U1339 (r=0.05, p>0.05). There is a significant positive correlation between the abundance of whole centric diatom valves and the total abundance of diatoms (both centric and pennate) at both sites (U1339 r=+0.53; U1340 r=+0.68; Figure 2c).

Sediment composition and grain size data indicate that sites U1340 and U1339 broadly have the same lithologies, but there are a few very subtle differences

20

(Table 1). The average diatom content is greater at Site U1340, whereas Site U1339

has a higher clay mineral content, percent abundance of volcanogenic particles, and

percent volume of clay-size particles (Table 1). The mean grain size of Site U1340 is

significantly larger than Site U1339 (t = 5.9; Table 1). The differences between sites

can be summarized as sediments at U1340 are more abundant in diatoms with larger

mean grain size and sediments at U1339 are more abundant in clay minerals and clay-

sized particles with smaller mean grain size.

Ultimately the lithology of sediment from both sites range from diatom ooze

to diatom mud (Figure 3). These lithologies were previously defined in Aiello &

Ravelo (2012). Diatom ooze is a biosilica-rich lithology primarily composed of

generally well-preserved valves of centric and pennate diatoms (> ~50%) as well as

clay minerals (< ~20%), fine siliciclastics (< ~10%), and minor (< 10%) amounts of

other biogenic components, including nannofossils and foraminifers (Aiello &

Ravelo, 2012). The diatom mud lithology is classified with an intermediate

composition between diatom ooze and pelagic mud. Pelagic mud is primarily

composed of clay minerals (> ~30%) as well as biogenic material (< ~20%) and fine-

grained siliciclastic and/or volcanic material (< ~10%) (Aiello & Ravelo, 2012).

Samples in this study were classified as diatom ooze if the relative ratio of diatom

valves to terrigenous material was greater than or equal to the minimum proportion

(50%/30%) outlined by Aiello & Ravelo (2012; Figure 2, Figure 3, Figure 4, Figure

9). No sample in this study has less than 20% biogenic material, which is the

threshold for the pelagic mud lithology and therefore samples with a ratio less than

50% diatom valve to 30% terrigenous material were classified as diatom mud (Aiello

& Ravelo, 2012; Figure 2, Figure 3, Figure 4, Figure 9).
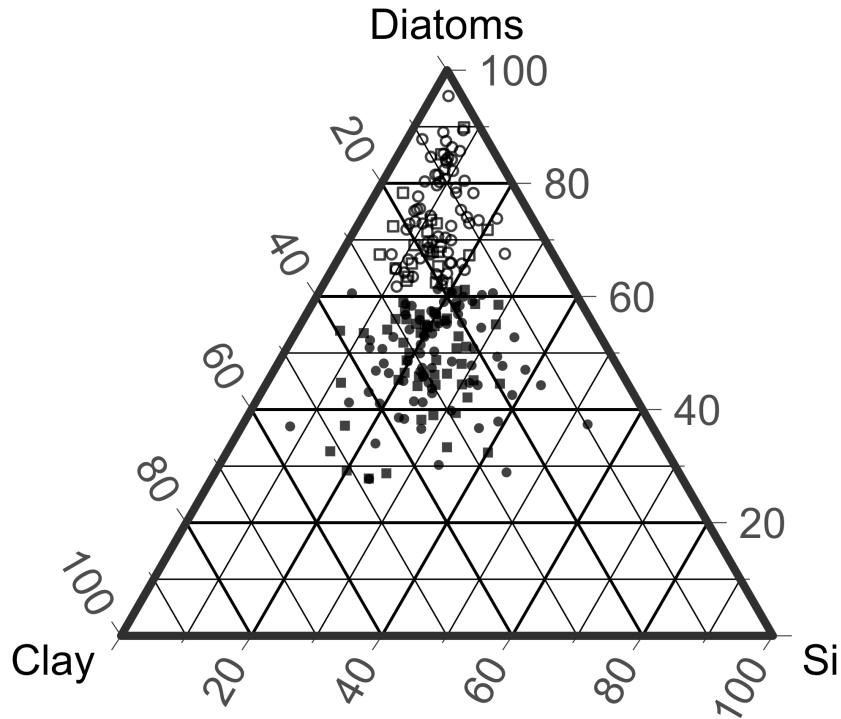
Figure 3. Ternary diagram of the three major sedimentary components. Diatoms =
relative percent abundance of centric and pennate diatom valves, Clay = relative
percent abundance of clay minerals, and Si = relative percent abundance of fine-
grained siliciclastic sediments. Site U1340 (n=138) represented by circles (●,○) and
U1339 (n=76) represented by squares (■,□). Open symbols indicate diatom ooze
lithology and closed symbols indicate diatom mud lithology.

A qualitative comparison of samples classified as diatom ooze and diatom

mud shows clear differences in the grain size-frequency distribution. The grain size-

frequency distributions of diatom ooze from both sites have a well-defined modal

peak in the coarse-silt to very fine sand size-range (mainly diatom valves; Figure 4a,

4b). Whereas, diatom mud grain size-frequency distributions are platykurtic, with

greater than about one-third of the percent size volume occurring in the clay to very

fine silt range (composed of clay minerals and broken up diatoms) and several other

peaks in the silt range (composed of fine siliciclastics and whole diatoms; Figure 4c,

4d). In summary, diatom ooze at both sites are characterized by a higher abundance of

whole centric diatoms (Figure 2c) and a lower percent volume of clay-sized particles

(Figure 4) compared to diatom mud.
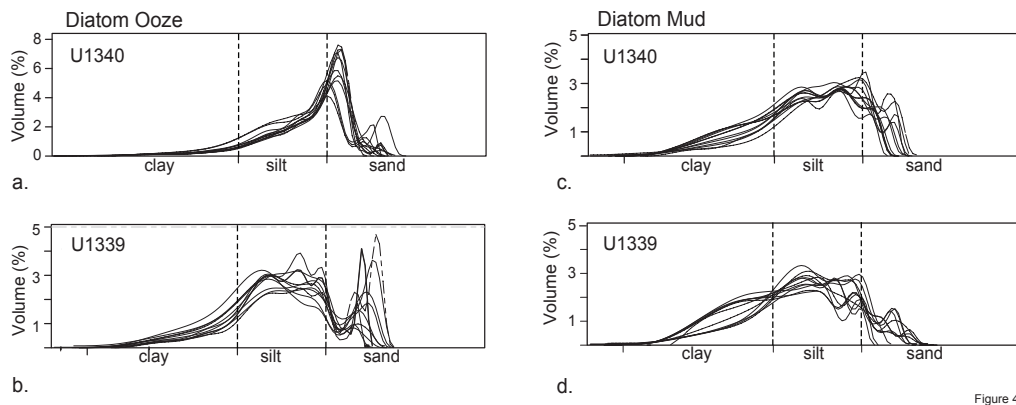
Figure 4. Grain size-frequency distributions of diatom ooze and diatom mud
lithologies. Lithology defined by the ratio of diatom valves to siliciclastic particles,
diatom ooze > (50% diatom / 20% clay + 10% fine-grained siliciclastic sediments) >
diatom mud. U1340 diatom ooze, n=13 (A). Site U1339 diatom ooze, n =9 (B).
U1340 diatom mud n=11 (C). Site U1339 diatom mud n=9 (D). Log scale in micro-
meters (μm).

Relationships between sediment composition, grain size, and bulk density

Grain size increases with increasing abundance of diatoms and these two

variables are most strongly correlated to bulk density. There is a significant positive

correlation between mean grain size and the abundance of diatoms (U1339 r=+0.65;

U1340 r=+0.60; Figure 5a). There is a corresponding negative correlation between

the percent volume of clay-size particles and diatom abundance (U1339 r=-0.64;

U1340 r=-0.67; Figure 5b). Mean grain size has a significant inverse correlation to sediment bulk density at both sites (U1339 R^2=-0.51; U1340 R^2=-0.37; Figure 6d). Lower bulk density values correspond to higher diatom content and larger mean grain sizes at both sites (Figure 6a, 6d). Higher bulk density values correspond to lower diatom content, smaller mean grain size, and an increased volume of clay-sized particles (Figure 6a, 6d. 6e).
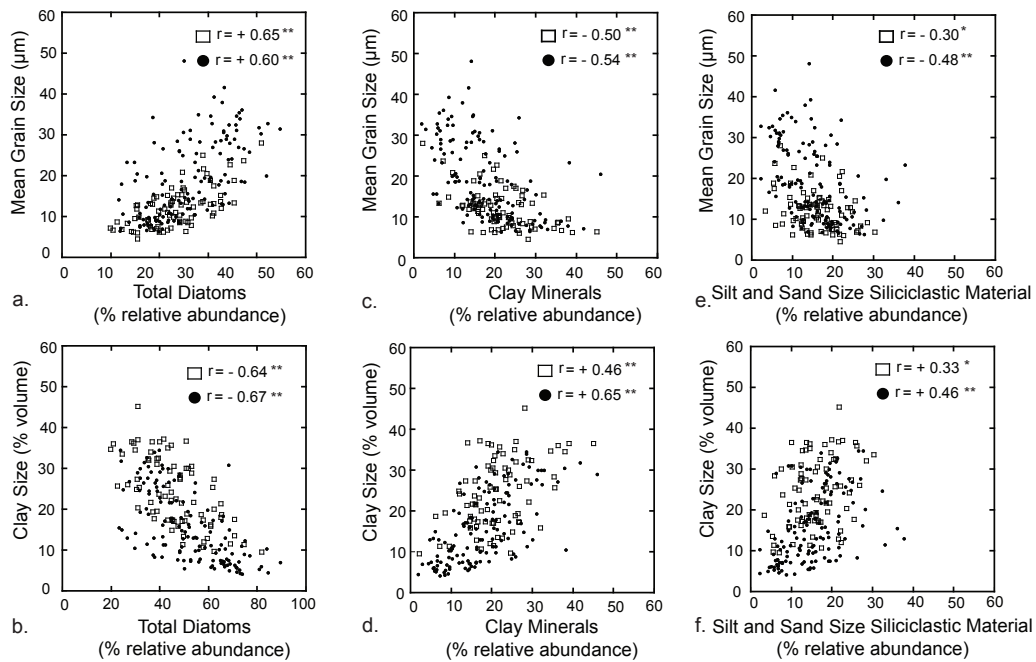
figure 5

Figure 5. Bivariate graphs of grain size parameters correlated to sedimentary components. Mean grain size (μm) (A, C, E) and % volume of clay-sized (<4 μm) material (B, D, F) in relation to the relative abundance of total diatom, clay minerals, and fine siliciclastic respectively. Site U1340 (n=138) represented by a closed circle (●) and U1339 (n=76) represented by an open square (□). Correlation coefficient (r) reported for Pearson correlation analyses. A single asterisk (*) indicates p-value ≤0.05 and double asterisk (**) indicates p-value <0.001.

24

Sediment bulk density has a stronger correlation to the volume of clay-sized particles than the abundance of clay minerals. Bulk density has a significant positive relationship with the percent volume of clay-size particles at both sites (U1339 $R^2=+0.40$; U1340 $R^2=+0.32$; Figure 6e). However, the correlation with clay minerals is weak at Site U1340 ($R^2=+0.11$, $p<0.05$) and the two parameters are not correlated at Site U1339 ($R^2=+0.05$, $p>0.05$; Figure 6b). A change in sediment bulk density is not strongly dependent on the abundance of clay mineral.

The correlation between the abundance of fine siliciclastics and bulk density is different between the two sites. But at both sites the abundance of fine siliciclastics is negatively correlated to mean grain size (U1339 $r=-0.30$, $p<0.05$; U1340 $r=-0.48$; Figure 5e) and positively correlated to the percent volume of clay-sized particles (U1339 $r=+0.33$, $p<0.05$; U1340 $r=+0.46$; Figure 5f). At Site U1340 there is a significant positive correlation between bulk density and the abundance of fine siliciclastics ($R^2=+0.41$) while the two parameters are not significantly correlated in samples from Site U1339 ($R^2=0.05$, $p>0.05$; Figure 6c).
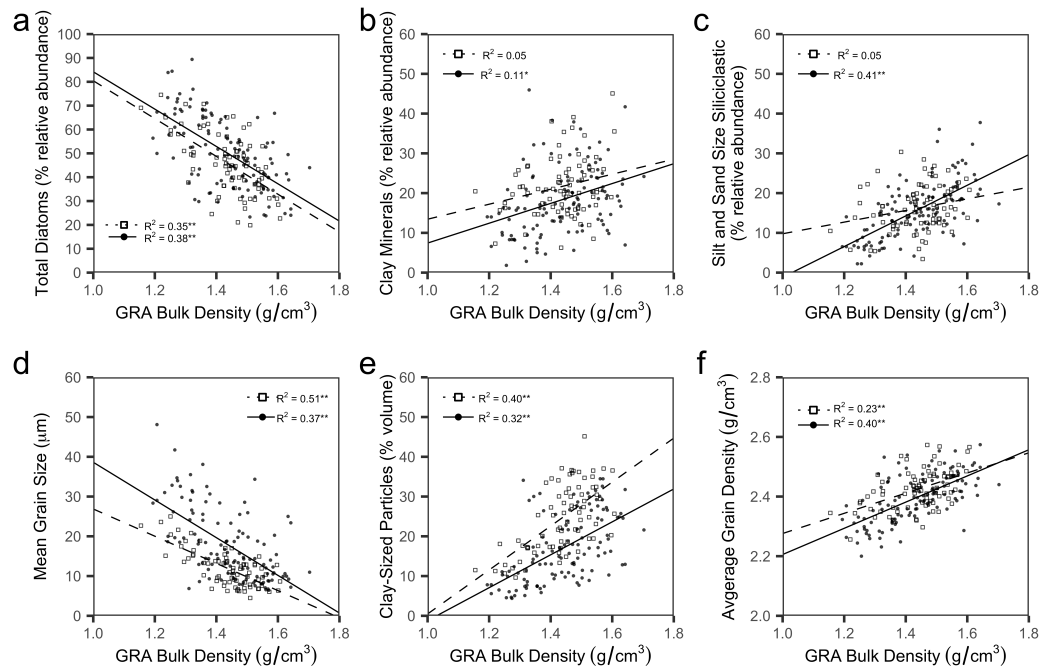
Figure 6. Linear regressions of sediment bulk density with major sedimentary components. (A, B, C), grain size parameters (D, E), and an estimate of average grain density (F). Sediment bulk density is measured as gamma-ray attenuation (GRA) bulk density (g/cm^3). Site U1340 (n=122) represented by a closed circle (●) and solid line. Site U1339 (n=74) represented by an open square (□) and dashed line. Coefficient of determination (R^2) reported for simple linear regression. A single asterisk (*) indicates p-value ≤0.05 and double asterisk (**) indicates p-value <0.001.

Discussion

Bulk density changes due to sediment packing

The correlation analysis demonstrates a predictable relationship between sediment composition, grain size, and bulk density for diatom ooze and diatom mud lithologies that is consistent at both sites (Figure 2, Figure 5, Figure 6). Grain size parameters (mean size and the percent volume of clay-sized particles) and sediment bulk density are primarily driven by changes in the abundance and fragmentation of

26

diatom valves (Figure 5a, 5b; Figure 6) and the influence of other sediment

components (e.g., clay minerals and fine siliciclastics) is only secondary. The finding

that diatom abundance is the primary controlling factor of mean grain size has been

previously reported at various sites on Bowers Ridge and the Bering slope including

U1340 and U1339 (Aiello & Ravelo, 2012). This study confirms that result and

demonstrates that diatom abundance and grain size parameters strongly influence

sediment bulk density (Figure 6a, 6d). Generally, intervals dominated by diatom ooze

coincide with lower bulk densities while diatom mud is correlated to higher bulk

densities (Figure 7). We propose that variability in GRA bulk density is driven by a

difference in sediment packing between the diatom ooze and diatom mud lithologies.
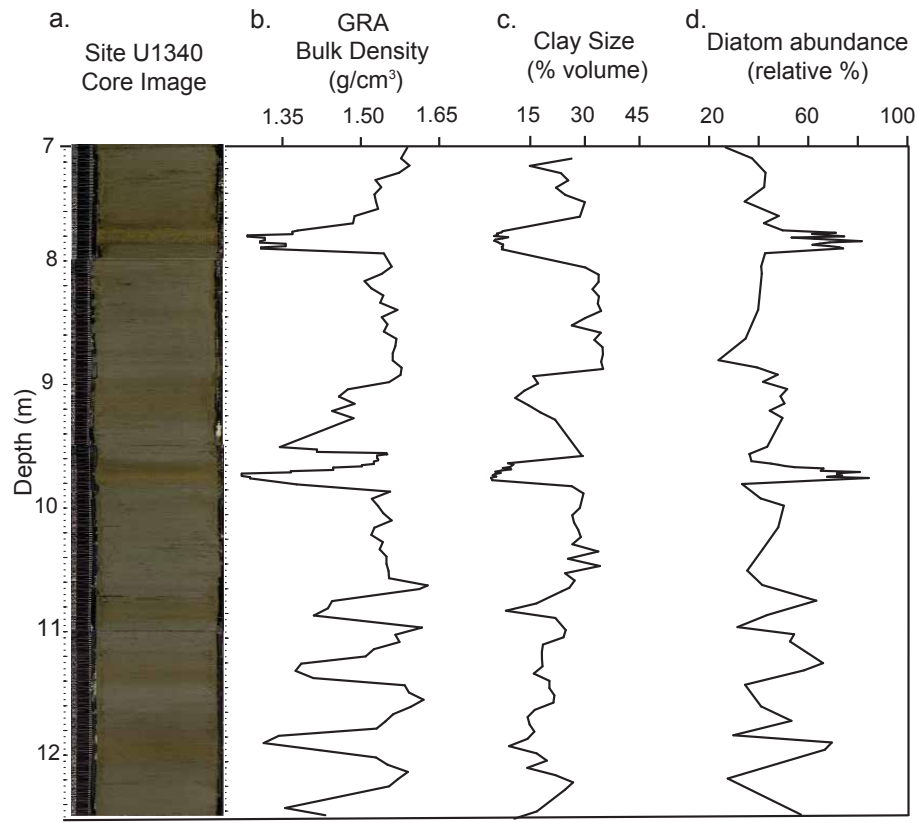
Figure 7. Core U1340A_2H bedding and associated variations in sediment parameters. Site U1340A core images from 7-12.5 m (A), shipboard GRA bulk density (g/cm³) (B), clay-sized particles (% volume) (C), and relative percent abundance of diatoms (D).

Sediment bulk density reflects the lithology of sediments and is controlled by changes in the average grain density and or the porosity of the sediment (Hamilton, 1971, 1976). A change in bulk density can reflect a change in the relative abundance of particles with different grain densities. Alternatively, a change in bulk density can reflect a change in porosity, which is a result of the interrelationship between grain size, grain shape, and grain sorting that ultimately influence sediment packing. To investigate which variable is driving the change in bulk density we estimate the

28

average grain density for each sample. This estimate is calculated using the measured

relative percent abundance of diatoms, clay minerals, and fine-grained siliciclastic

material and an assumed constant average grain density for opal (2.18 ± 0.18 g/cm^3),

clay minerals (2.75 ± 0.25 g/cm^3), and quartz (2.68 ± 0.03 g/cm^3) (Breitzke, 2006). The

estimated average grain density does have a significant relationship to GRA bulk

density (U1339 $R^2= 0.23$; U1340 $R^2=0.40$), but the strength of this relationship may

be influenced by the data used to calculate this estimate (Figure 6f). Discrete

shipboard measurements of grain density and sediment bulk density show a weaker

correlation (U1339 $R^2= 0.12$; U1340 $R^2=0.28$), these samples are taken from the same

depth range as the samples in this study (Figure 8a). A much stronger correlation is

found between discrete shipboard measurements of bulk density and porosity ($R^2 =$

0.74; Figure 8b). This suggests that changes in grain density are not the primary

driver of variability in bulk density.
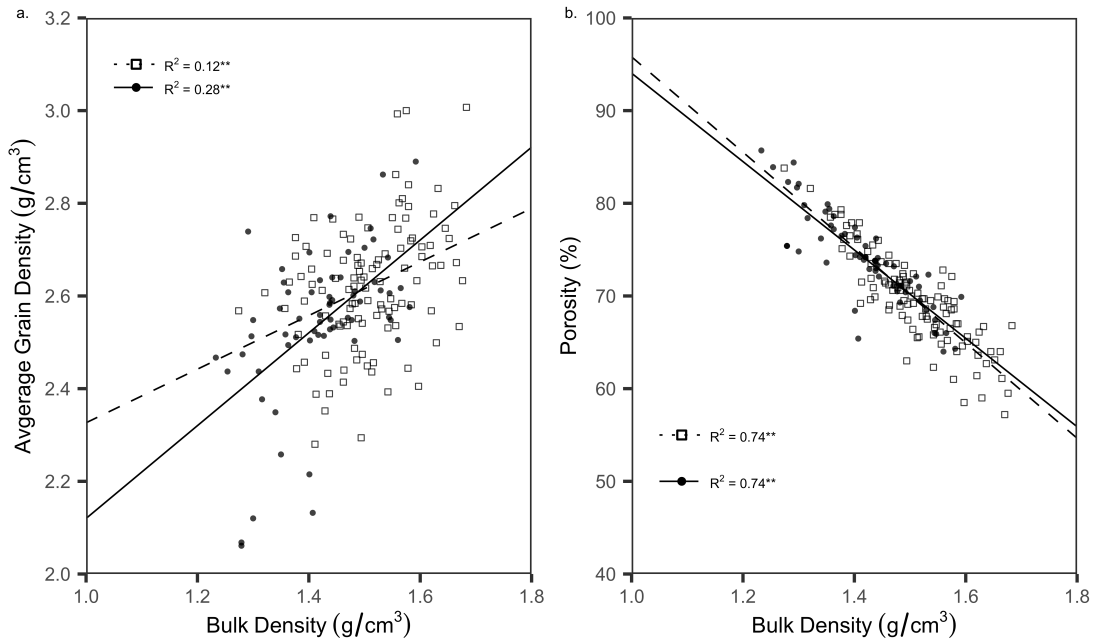
Figure 8. Linear regression of Exp 323 shipboard discrete measurements of bulk density, grain density, and porosity. Site U1340A (0-214m, n=64) represented by a closed circle (●) and solid line. Site U1339B (0-193m, n=109) represented by an open square (□) and dashed line. Coefficient of determination (R^2) reported for simple linear regression. Double asterisk (**) indicates p-value <0.001.

Furthermore, we find that the change in bulk density is not strongly dependent on clay mineral abundance (Figure 6b). In this study there are two measures of clay, one defined by size (particles < 4 μm) and another visually identified by smear slide analysis (relative percent abundance of clay minerals). Two measures of the same variable should result in near one-to-one agreement but there is a weaker than expected positive correlation between clay minerals and the percent volume of clay-sized particles (U1339 r=+0.46; U1340 r=+0.65; Figure 5d). Furthermore, we find a strong correlation between percent volume of clay-sized particles and bulk density (Figure 6e), but there is a weak or no correlation between bulk density and clay

30

minerals (Figure 6b). High-magnification SEM imaging reveals the clay-size fraction

includes clay-sized fragments of diatoms (Figure 9e, 9f). This indicates diatom

fragmentation influences bulk density more than the abundance of clay minerals.
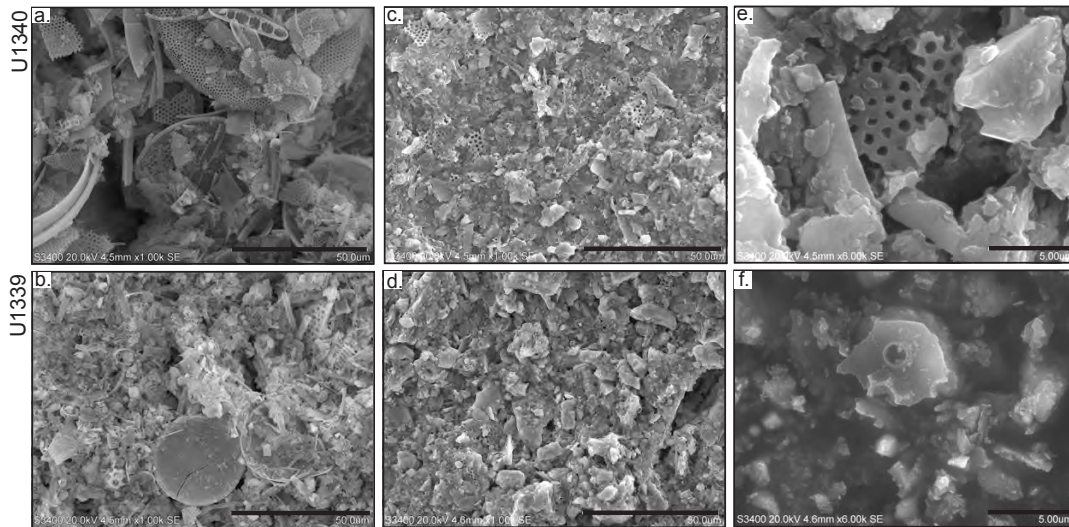
Figure 9. Scanning electron micrographs of diatom ooze (A, B) and diatom mud
(C, D, E, F). Diatom ooze image at x1000 magnification, U1340A_1H_1_146cm (A)
and U1339_1H_1_10cm (B). Diatom mud image at x1000 magnification,
U1340A_2H_5_52cm (C) and U1339A_2H_2_XRD (D). Diatom mud samples
highlighting clay-sized diatom valve fragment at x6000 magnification,
U1339A_2H_2_XRD (E) and U1340A_2H_5_52cm (F).

We suggest that the abundance and fragmentation of diatom valves alter

sediment packing, which ultimately drives variability in sediment bulk density.

Samples with high diatom abundance have less diatom fragmentation (Figure 2c,

Figure 5b) and larger mean grain size (Figure 5a). Therefore, we propose low density

diatom ooze is loosely packed fine sand-size whole centric diatoms and silt size

diatom fragments with fewer clay-size biosilica particles filling interparticle voids

(Figure 4a, 4b; Figure 9a, 9b). Conversely, we propose higher bulk density diatom

31

mud is more tightly packed with micron-scale fragments of biosilica filling the intraparticle pore space and interparticle void space between very fine sand- and silt-size valve fragments (Figure 4c, 4d; Figure 9c, 9d). These observed differences in the abundance and fragmentation between diatom ooze and diatom mud lithologies suggest that differences in sediment packing drive bulk density variability. Sediment packing is also a factor in explaining bulk density correlating to organic carbon content in the California Borderlands where organic carbon adhered to clay minerals and clay minerals kept the sediment framework open reducing sediment density (Janik et al., 2004).

The interpretation that the abundance and fragmentation of diatom valves can significantly influence physical properties is similar to observations of biosiliceous sediment intervals from the Southern Ocean, which found valve orientation as well as the type of siliceous microfossil dramatically changed the micro-fabric of sediment (Rack & Palmer-Julson, 1992). Herbert and Mayer (1991) found the variability in bulk density is driven by a difference in the sediment packing between dramatically different carbonate-rich versus non-carbonate rich (biosiliceous ooze or pelagic clay) lithologies. While our study shows large variations in sediment packing between lithologies with very subtle differences, where the degree of diatom fragmentation changes sediment packing and therefore bulk density. The change in bulk density within sediments of similar minerology has been observed in pelagic clays where loosely packed sediment result from the accumulation of platy clay particles in a

random orientation and densely packed sediment occur when aggregates of clay minerals stack in a more uniform manner (Bennet et al., 1989).

Our interpretation of GRA as an indicator of diatom abundance and fragmentation within Bering Sea sediments should be applicable to other regions. But it is likely limited to areas with a two-component system of terrigenous and biosiliceous sediment. Furthermore, sedimentation driven by surface productivity is likely an important qualification when considering where this interpretation can be applied. The recent review of diatom-rich sediments of the North Pacific Ocean (Koizumi & Yamamoto, 2018) provide insight into where these findings may be applied, such as the Sea of Japan, Northeast Japan, North Pacific Detroit Seamounts, and the California Margin. Although sites along the California Margin include sediments rich in calcareous microfossils and previous studies suggest that the GRA signal would be highly sensitive to this (Herbert & Mayer, 1991). The very low preservation of carbonate in Bering Sea sediments meant this study was unable to assess how calcareous microfossils may influence GRA as an indicator of diatom abundance and fragmentation.

Implications for the interpretation of ancient bedded siliceous rocks

Understanding the sedimentary properties of modern unconsolidated biosiliceous sediments may be useful to those studying the formation of diagenetically related bedded siliceous rock units (e.g., Monterey Group, Franciscan Complex- Marine Headlands Terrane, Western Tethys Radiolarites etc.). There are

multiple, and sometimes contrasting, hypotheses on the origin of bedding in siliceous rocks. Bedding has been interpreted to reflect primary depositional cycles of terrigenous versus biogenic sediment flux (Hiro et al., 1993; Iijima & Utada, 1983), or the cyclic changes in surface productivity and biosilica export (Behl & Smith, 1992; Garrison & Fischer, 1969; Heath & Moberly, 1971; Pisciotto & Garrison, 1981). Other authors have interpreted bedding as the result of pure diagenetic segregation of homogeneous sediments (Murray et al., 1992), or as the result of a combination of depositional and diagenetic processes (Tada, 1991).

Biosiliceous sediments of the Bering Sea are fundamentally homogeneous when compared to the striking lithologic changes that produce bedding in rock outcrops of units like the Monterey with bedding of porcellanite and organic shale (e.g., Isaac et al., 1983; Pisciotto & Garrison, 1981) or the Jurassic radiolarites with bedded chert and claystone (e.g., Hiro et al., 1993). The statistical relationships between composition, grain size and bulk density that define the very subtle meter-scale alternations in the biosiliceous sediment of the Bering Sea may offer clues as to what might affect silica phase reactions during diagenesis and the formation of bedded siliceous rocks. Silica phase change involves a two-step process of complete dissolution and re-precipitation from opal-A to diagenetic opal-CT (interlayered cristobalite and tridymite) and from opal-CT to quartz (Hesse & Schacht, 2011). These transformations are controlled by temperature, burial depth, sediment composition, and physical properties such as porosity and permeability (Behl, 1999; Kastner and Gieske, 1983). As shown in classic studies on the Monterey Formation of

California, silica phase transitions are not abrupt but can occur across broad transition zones of interbedded lithologies containing different silica phases (Isaacs, 1982). The occurrence of different silica phases within the same stratigraphic intervals has been explained by other mineralogic phases mixed with biosilica affecting the paragenetic sequence (Kastner et al., 1977).

If biosiliceous sediments with the same characteristics as the ones observed at Sites U1339 and U1340 were to experience diagenesis we hypothesize precipitation of opal-CT would occur earlier in diatom ooze. Diatom mud has a greater abundance of clay minerals (Figure 3) that limit the opal-A to opal-CT transition (Kastner et al., 1977). Furthermore, diatom mud has a larger component of fragmented diatoms (Figure 2c, Figure 4, Figure 9), these fine silt- and clay-size biosilica particles have higher specific surface areas compared to whole diatom valves and would enhance opal-A dissolution. Diatom ooze layers with higher biogenic silica and lower clay mineral may dissolve opal-A and precipitate opal-CT first. This mechanism describes what Tada (1991) defined as a 'silica pump' initiated by the differential onset of silica diagenesis (opal-A to opal-CT phase change) between adjacent sediment layers that have subtle compositional and textural differences. Once the silica pump turns on and silica concentration gradients develop in pore waters, a positive feedback is created. Opal-CT precipitation increase in the silica-rich layers (diatom ooze) due to silica moving from solution into mineral form, while the interbedded clay-rich layers (diatom mud) become progressively depleted of opal-A. Clay-rich layers (diatom mud) would undergo compaction due to the loss of siliceous microfossils. If this

mechanism were applied to the Bering Sea biosiliceous sediments, diagenesis would produce bedded siliceous rocks where originally small changes in the composition and texture of alternating sediment intervals would be enhanced. Interestingly even though the two Bering Sea sites represent contrasting environments and record different scales of climate variability, we speculate diagenesis could produce similar bedded sequences. If true, siliceous rocks with similar sedimentologic characteristics and bedding styles can form from biosiliceous deposits that have accumulated in different environments and where primary lithologic variability represents very different scales of climate variability. Further analysis of the bedding structures as well as application of a diagenetic model to Sites U1339 and U1340 would be necessary to evaluate this speculation. The Bering Sea has not been classically considered a modern depositional analogue to the Monterey formation (Donegan & Schrader, 1981; Soutar et al., 1981), but this work suggests the sedimentological characteristics of the Bering Sea sediment may provide insight into the deposition and diagenesis of the siliceous facies found in the Monterey Group.

Conclusions

Detailed sedimentological analysis of core sediments from the upper ~200 m of Sites U1339 and U1340 are used to interpret the sedimentological significance of shipboard GRA bulk density measurements. Downcore variability in bulk density is a

result of variable diatom abundance and degree of diatom valve fragmentation. We show bulk density significantly correlates with changes in diatom abundance, mean grain size, and percent volume of clay-size particles (Figure 6a, 6d, 6e, Figure 7). We show that the clay-size fraction includes micron-size fragments of biosilica (Figure 9e, 9f) and suggest that lithologies with higher diatom valve fragmentation results in a more tightly packed sediment and higher bulk density (Figure 9c, 9d). These relationships caution the interpretation of a physical property such as bulk density solely as a proxy for composition especially in sediments that have a significant biosiliceous component. Ultimately, we suggest GRA bulk density can be used as a proxy for diatom abundance and fragmentation. To interpret the reason behind the change in abundance and fragmentation of diatom valves is outside the scope of this study because production and accumulation of biogenic opal is influenced by many factors (Ragueneau et al., 2000) as is diatom fragmentation (Scherer et al., 2004). Further work to combine micropaleontology data with this dataset could result in an interpretation of GRA data that has stronger ecological significance.

We speculate that the subtle lithologic variability observed in the sediments of the Bering Sea may provide insight into what characteristics in the precursor sediments of ancient siliceous rock formations could control the formation of bedding during diagenesis. In a biosiliceous sediment with the same characteristics as Sites U1339 and U1340, subtle differences in composition and grain size between diatom ooze and diatom mud could influence the kinetics of silica-phase transformations during diagenesis. The differential onset of diagenesis initiates a 'silica pump' (Tada,

1991) and would result in higher silica concentrations and earlier opal-CT precipitation in the diatom oozes, while the interbedded diatom muds would become progressively depleted in biosilica. We speculate that if this diagenetic mechanism was applied to the Bering Sea sediments it could produce similar bedded rocks since lithologic variability is very similar in the two sites. Further modeling of this silica diagenesis mechanism would be necessary to verify this speculation.

References

Abrantes, F., Cermeno, P., Lopes, C., Romero, O., Matos, L., Van Iperen, J., … Magalhães, V. (2016). Diatoms Si uptake capacity drives carbon export in coastal upwelling systems. *Biogeosciences*, *13*(14), 4099–4109. https://doi.org/10.5194/bg-13-4099-2016

Abrantes, F., & Moita, M. T. (1999). Water column and recent sediment data on diatoms and coccolithophorids, off Portugal, confirm sediment record of upwelling events. *Oceanologica Acta*, *22*(3), 319–336. https://doi.org/10.1016/S0399-1784(99)80055-3

Aiello, I. W., & Christina Ravelo, A. (2012). Evolution of marine sedimentation in the bering sea since the pliocene. *Geosphere*, *8*(6), 1231–1253. https://doi.org/10.1130/GES00710.1

Beckman Coulter, I. (2003). LS 13 320 particle size analyzer manual. Miami, Florida. Retrieved from https://www.beckmancoulter.com/wsrportal/techdocs?docname=B05577AB.pdf

Behl, R J, & Smith, B. M. (1992). Silicification of deep-sea sediments and the oxygen isotope composition of diagentic rocks from the western Pacific, Pigafetta and East Mariana Basins, Leg 129. In R. L. Larson & Y. Lancelot (Eds.), *Proc. ODP, Sci. Results, 129* (pp. 81–117). College Station, TX: Ocean Drilling Program. https://doi.org/10.2973/odp.proc.sr.129.112.1992

Behl, Richard J. (1999). Since Bramlette (1946): The Miocene Monterey Formation of California revisited. *Geological Society of America Special Papers*, *338*(1946), 301–313. https://doi.org/10.1130/0-8137-2338-8.301

Bennett, R. H., Fischer, K. M., Lavoie, D. L., Bryant, W. R., & Rezak, R. (1989). Porometry and fabric of marine clay and carbonate sediments: determination of permeability. *Marine Geology*, *89*, 127–152. https://doi.org/10.1016/0025-3227(89)90030-3

Boyce, R. E. (1976). Definitions and laboratory techniques of compressional sound velocity parameters and wet-water content, wet-bulk density, and porosity parameters by gravimetric and gamma ray attenuation techniques. In S. O. Schlanger, E. D. Jackson, & E. Al. (Eds.), *Initial Report Deep Sea Drilling Project, Volume 33* (pp. 931–958). Washington: U.S. Government Printing Office. https://doi.org/10.1017/CBO9781107415324.004

Breitzke, M. (2006). Physical Properties of Marine Sediments. In H. D. Schulz & M. Zabel (Eds.), *Marine Geochemistry* (pp. 27–71). Berlin, Heidelberg: Springer. https://doi.org/10.1007/3-540-32144-6_2

Calvert, S. E. (1966). Origin of Diatom-Rich, Varved Sediments from the Gulf of California. *Journal of Geology*, *74*(5), 546–565. https://doi.org/www.jstor.org/stable/30059298

Calvert, S. E. (1983). Sedimentary Geochemistry of Silicon. In S. R. Aston (Ed.), *Silicon*

Geochemistry and Biogeochemistry (pp. 143–186). London: Academic Press Inc.

Cook, M. S., Ravelo, A. C., Mix, A., Nesbitt, I. M., & Miller, N. V. (2016). Tracing subarctic Pacific water masses with benthic foraminiferal stable isotopes during the LGM and late Pleistocene. *Deep Sea Research Part II: Topical Studies in Oceanography*, *126*, 84–95. https://doi.org/10.1016/j.dsr2.2016.02.006

Donegan, D., & Schrader, H. (1981). Modern Analogues of the Miocene Diatomaceous Monterey Shale of California: Evidence from Sedimentologic and Micropaleontologic Study. In R. E. Garrison & R. G. Douglas (Eds.), *The Monterey Formation and Related Siliceous Rocks of California: Soiety of Economic Paleontologists and Mineralogists* (pp. 149–157). Pacific Section SEPM.

Drake, M. K., Aiello, I. W., & Ravelo, A. C. (2014). New Method for the Quantitative Analysis of Smear Slides in Pelagic and Hemi-Pelagic Sediments of the Bering Sea. *Fall Meeting, AGU*, *December 1*.

Fetterer, F., Knowles, K., Meier, W., Savoie, M., & Windnagel, A. K. (2016). *Sea Ice Index, Version 2 [Monthly Sea Ice Extent]*. Boulder, Colorado USA. https://doi.org/http://dx.doi.org/10.7265/N5736NV7

Garrison, R. E., & Fischer, A. G. (1969). Deep Water Limestones and Radiolarites of the Alpine Jurassic. In G. M. Friedman (Ed.), *Depositional Enviornments in Carbonate Rocks* (pp. 20–56). https://doi.org/10.2110/pec.69.03.0020

Hamilton, E. L. (1971). Elastic properties of marine sediments. *Journal Geophysical Research*, *76*(2), 579–604. https://doi.org/10.1029/JB076i002p00579

Hamilton, E. L. (1974). Prediction of deep-sea sediment properties: state-of-the-art. In A. L. Inderbitzen (Ed.), *Deep-Sea Sediments* (Vol. 2). New York: Springer, Boston, MA. https://doi.org/10.1007/978-1-4684-2754-7_1

Hamilton, E. L. (1976). Variations of density and porosity with depth in deep-sea sediments. *Journal of Sedimentary Petrology*, *46*(2), 280–300. https://doi.org/10.1306/212F6F3C-2B24-11D7-8648000102C1865D

Hamilton, E. L., & Bachman, R. (1982). Sound velocity and related properties of marine sediments. *The Journal of the Acoustical Society of America*, *72*(6), 1891. https://doi.org/10.1121/1.388539

Heath, G. R., & Moberly, R. (1971). Cherts from the Western Pacific, Leg 7, Deep Sea Drilling Project. In E. L. Winterer & et al. (Eds.), *Initial Reports of the Deep Sea Drilling Program, Volume 7* (pp. 991–1007). Washington (U.S. Government Printing Office). https://doi.org/10.2973/dsdp.proc.7.119.1971

Herbert, T. D., & Mayer, L. A. (1991). Long climate time series from sediment physical property measurements. *Journal of Sedimentary Petrology*, *61*(7), 1089–1108.

https://doi.org/10.1306/D4267843-2B26-11D7-8648000102C1865D

Hesse, R., & Schacht, U. (2011). Early diagenesis of deep-sea sediments. In H. Huneke & T. Mulder (Eds.), *Developments in Sedimentology* (Vol. 63, pp. 557–713). Amsterdam: Elsevier. https://doi.org/10.1016/B978-0-444-53000-4.00009-3

Hori, R., Cho, C.-F., & Umeda, H. (1993). Origin of cyclicity in Triassic-Jurassic radiolarian bedded cherts of the Mino accretionary complex from Japan. *The Island Arc*, *3*, 170–180. https://doi.org/10.1111/j.1440-1738.1993.tb00084.x

Iijima, A., & Utada, M. (1983). Recent developments in the sedimentology of siliceous deposits in Japan. *Developments in Sedimentology*, *36*, 45–64. https://doi.org/10.1016/S0070-4571(08)70083-9

Isaacs, C. M., Pisciotto, K. A., & Garrison, R. E. (1983). Facies and Diagenesis of the Miocene Monterey Formation, California: A Summary. *Developments in Sedimentology*, *36*, 247–282. https://doi.org/10.1016/S0070-4571(08)70094-3

Janik, A., Lyle, M. W., & Liberty, L. M. (2004). Seismic expression of Pleistocene paleoceanographic changes in the California Borderland from digitally acquired 3.5 kHz subbottom profiles and Ocean Drilling Program Leg 167 drilling. *Journal of Geophysical Research*, *109*, B07101. https://doi.org/10.1029/2003JB002439

Johnson, T. C. (1976). Controls on the Preservation of Biogenic Opal in Sediments of the Eastern Tropical Pacific. *Science*, *192*(4242), 887–890.

Kastner, M., & Gieske, J. M. (1983). Opal-A to opal-CT transformations: A kinetic study. *Siliceous Deposits in the Pacific Region*, 211–226. https://doi.org/10.1017/CBO9781107415324.004

Kastner, M., Keene, J. B., & Gieske, J. M. (1977). Diagenesis of siliceous oozes-Chemical controls on the rate of opal-A to opal-CT transformation- an experimental study. *Geochimica et Cosmochimica Acta*, *41*(8), 1041–1059. https://doi.org/10.1016/0016-7037(77)90099-0

Koizumi, I., & Yamamoto, H. (2018). Diatom ooze and diatomite–diatomaceous sediments in and around the North Pacific Ocean. *JAMSTEC Report of Research and Development*, *27*(0), 26–46. https://doi.org/10.5918/jamstecr.27.26

Kotilainen, A. T., & Shackleton, N. J. (1995). Rapid climate variability in the North Pacific Ocean during the past 95,000 years. *Nature*, *377*(6547), 323–326. https://doi.org/10.1038/377323a0

Lisitsyn, A. ., Belyayev, Y., Bogdanov, Y., & Bogoyavlenskiy, A. (1967). Distribution relationships and forms of silicon suspended in the waters of the World Ocean. *International Geology Review*, *9*(4), 604–623. https://doi.org/10.1080/00206816709474491

Marsaglia, K., Milliken, K., & Doran, L. (2013). *IODP Digital Reference for Smear Slides Analysis of Marine Mud. Part 1 : Methodology and Atlas of Siliciclastic and Volcanogenic Components*. IODP Technical Note 1. https://doi.org/10.2204/iodp.tn.1.2013

Marsaglia, K., Milliken, K., Leckie, R. M., Tentori, D., & Doran, L. (2015). *IODP Smear Slide Digital Reference for Sediment Analysis of Marine Mud. Part 2: Methodology and Atlas of Biogenic Components*. IODP Technical Note 2. https://doi.org/10.2204/iodp.tn.2.2015

Matsumoto, R., & Iijima, A. (1983). Chemical and sedimentology of some Permo-jurassic and tertiary bedded cherts in central Honshu, Japan. In *Siliceous Deposits in the Pacific Region* (Vol. Chapter 11, pp. 175–191). https://doi.org/10.1017/CBO9781107415324.004

Mortlock, R., & Froelich, P. (1989). A simple method of the rapid determination of biogenic opal in pelagic marine sediments. *Deep Sea Research Part I: Oceanographic Research Papers*, *36*(9), 1415–1426.

Murray, R. W., Jones, D. L., & Buchholtz ten Brink, M. R. (1992). Diagenetic formation of bedded chert: Evidence from chemistry of the chert-shale couplet. *Geology*, *20*(3), 271–274. https://doi.org/10.1130/0091-7613(1992)020<0271:DFOBCE>2.3.CO;2

Nobes, D. C., Mienert, J., & Dirksen, G. J. (1991). Lithologic control of physical-property interrelationships. In P. Ciesielski & Y. Kristoffersen (Eds.), *Proc. ODP, Sci. Results, 114* (pp. 657–669). College Station, TX: Ocean Drilling Program. https://doi.org/10.2973/odp.proc.sr.114.162.1991

Pisciotto, K. A., & Garrison, R. E. (1981). Lithofacies and Depositional environments of the Monterey Formation, California. In R. E. Garrison & R. G. Douglas (Eds.), *The Monterey Formation and Related Siliceous Rocks of California, special publicatoin of the Pacific Section Soiety of Economic Paleontologists and Mineralogists* (pp. 97–112). Pacific Section SEPM.

Rack, F. R., & Palmer-Julson, A. (1992). Sediment microfabric and physical properties record of late Neogene Polar Front migration, Site 751. In S. W. Wise, R. Schlich, & et al. (Eds.), *Proc. ODP, Sci. Results, 120* (pp. 179–205). College Station, TX: Ocean Drilling Program. https://doi.org/10.2973/odp.proc.sr.120.145.1992

Ragueneau, O., Treguer, P., Leynaert, A., Anderson, R. F., Brzezinski, M. A., DeMaster, D. J., … Queguiner, B. (2000). A review of the Si cycle in the modern ocean : recent progress and missing gaps in the application of biogenic opal as a paleoproductivity proxy. *Global and Planetary Change*, *26*, 317–365. https://doi.org/10.1016/S0921-8181(00)00052-7

Romero, O. E., & Hebbeln, D. (2003). Biogenic silica and diatom thanatocoenosis in surface

sediments below the Peru–Chile Current: controlling mechanisms and relationship with productivity of surface waters. *Marine Micropaleontology*, *48*(1–2), 71–90. https://doi.org/10.1016/S0377-8398(02)00161-5

Romero, O. E., Hebbeln, D., & Wefer, G. (2001). Temporal and spatial variability in export production in the SE Pacific Ocean: evidence from siliceous plankton fluxes and surface sediment assemblages. *Deep Sea Research Part I: Oceanographic Research Papers*, *48*(12), 2673–2697. https://doi.org/10.1016/S0967-0637(01)00037-1

Rothwell, R. (1989). *Minerals & Mineraloids in Marine Sediments*. (R. G. Rothwell, Ed.) (1st ed.). Crown House, England: Springer Netherlands. https://doi.org/10.1007/978-94-009-1133-8

Rothwell, R. G., & Rack, F. R. (2006). New techniques in sediment core analysis: an introduction. *Geological Society, London, Special Publications*, *267*(1), 1–29. https://doi.org/10.1144/GSL.SP.2006.267.01.01

Scherer, R. P., Sjunneskog, C. M., Iverson, N. R., & Hooyer, T. S. (2004). Assessing subglacial processes from diatom fragmentation patterns. *Geology*, *32*(7), 557–560. https://doi.org/10.1130/G20423.1

Schlung, S. A., Christina Ravelo, A., Aiello, I. W., Andreasen, D. H., Cook, M. S., Drake, M. K., … Takahashi, K. (2013). Millennial-scale climate change and intermediate water circulation in the Bering Sea from 90 ka: A high-resolution record from IODP Site U1340. *Paleoceanography*, *28*(1), 54–67. https://doi.org/10.1029/2012PA002365

Schrader, H. J., & Gersonde, R. (1976). Diatoms and Silicoflagellates. In W. J. Zachariasse, Riedel. W.R. A, R. R. Schmidt, A. Sanfilippo, M. J. Brolsma, H. J. Schrader, … J. A. Broekman (Eds.), *Micropaleontological Counting Methods and Techniques an Exercise on an Eight Metres Section of the Lower Pliocene of Capo Rosello, Sicily* (pp. 129–176). Utrecht: Utrecht Micropaleontology.

Schuette, G., & Schrader, H. (1981). Diatoms in surface sediments: A reflection of coastal upwelling. In F. A. Richards (Ed.), *Coastal and Esuarine Sciences* (Vol. 1, pp. 372–380). https://doi.org/10.1029/CO001p0372

Soutar, A., Johnson, S. R., & Baumgartner, T. R. (1981). In Search of Modern Depositional Analogs to the Monterey Formation. In R. E. Garrison & R. G. Douglas (Eds.), *The Monterey Formation and Related Siliceous Rocks of California, special publicatoin of the Pacific Section Soiety of Economic Paleontologists and mineralogists* (pp. 123–147). Pacific Section SEPM.

Tada, R. (1991). Compaction and cementation in siliceous rocks and their possible effect on bedding enhancement. In G. Einsele, W. Ricken, & A. Seilacher (Eds.), *Cycles and Events in Stratigraphy* (pp. 480–491). Springer-Verlag.

Takahashi, K., Fujitani, N., & Yanada, M. (2002). Long term monitoring of particle fluxes in

the Bering Sea and the central subarctic Pacific Ocean, 1990-2000. *Progress in Oceanography*, *55*(1–2), 95–112. https://doi.org/10.1016/S0079-6611(02)00072-1

Takahashi, K., Ravelo, A. C., Alvarez Zarikian, C., & Expedition 323 Scientists. (2011). *Proc. IODP, 323*. Tokyo. https://doi.org/10.2204/ iodp.proc.323.2011

Takahashi, Kozo, Fujitani, N., Yanada, M., & Maita, Y. (2000). Long-term biogenic particle fluxes in the Bering Sea and the central subarctic Pacific Ocean, 1990-1995. *Deep Sea Research Part I: Oceanographic Research Papers*, *47*, 1723–1759. https://doi.org/10.1016/S0967-0637(00)00002-9

Warner, N. R., & Domack, E. (2002). Millennial- to decadal-scale paleoenvironmental change during the Holocene in the Palmer Deep, Antarctica, as recorded by particle size analysis. *Paleoceanography*, *17*(3). https://doi.org/10.1029/2000PA000602

Wilkens, R. H., & Handyside, T. (1985). Physical properties of equatorial Pacific sediments. In L. Mayer, F. Theyer, & et al. (Eds.), *Initial Reports Deep Sea Drilling Project, Volume 85* (pp. 839–847). Washington: U.S. Govt. Printing Office. https://doi.org/10.2973/dsdp.proc.85.128.1985

Chapter 3: Precession and sub-orbital cyclicity of ice rafted debris in the Bering Sea (IODP Site U1341) during the early Pleistocene

Michelle K. Drake[1*], Ana Christina Ravelo[1], and Ivano W. Aiello[2]

[1] Ocean Sciences Department, University of California, 1156 High Street, Santa Cruz, California, 95064, USA

[2] Moss Landing Marine Laboratories, Moss Landing, California 95039, USA

Abstract

The growth and contraction of the cryosphere is well documented in paleo-proxy records throughout the Pleistocene 2.58-0.012 Ma. The pace of the cryosphere fluctuations is associated with the fundamental frequencies of the orbital parameters, as well as higher sub-orbital frequencies (i.e., 1/12-1/10 cycles/kyr). Although the pace of the fluctuations is clear in the paleo-archives, the ultimate cause of glacial cycles or higher-frequency sub-orbital variability is not entirely understood. The classic astronomical theory of the ice ages theorizes that glacial cycles are a direct response to insolation received during the northern hemisphere high latitude summer, but the theory is not entirely supported by the proxy data. To study the relationship between the cryosphere and insolation we focus on the shorter 40 kyr glacial cycles of the early Pleistocene, because unlike the more recent ~100 kyr ice ages, they are thought to be a more straight-forward response to orbitally induced changes in insolation. To measure the cyclicity of the cryosphere we generate a record of ice rated debris (IRD) flux and carry out advance spectral analysis. In this study we present an orbitally resolved record of IRD flux from the Bering Sea (IODP Site

U1341) between 1.87-1.61 Ma. From our results we interpret the IRD flux record primarily represents sea ice variability. Spectral analysis the record has significant power at precession band and half-precession frequencies (1/12-1/10 cycles/kyr). The presence of precession band frequencies suggests the cryosphere is sensitive to the high-latitude seasonal insolation cycle and the sub-orbital frequencies suggest a non-linear response of the system. We present scenarios with possible forcings that could explain the variability in the IRD flux record.

Introduction

Paleoclimate records of the cryosphere (i.e., glaciers and sea ice) reveal fluctuations at orbital timescales during the Pleistocene ice ages (Jansen et al., 2000; Lisiecki & Raymo, 2005). It is accepted that the frequencies in benthic foraminifer oxygen isotope ($\delta^{18}O$) records, a proxy of global ice volume, match the fundamental frequencies of the orbital parameters eccentricity (1/100 cycles/kyr), obliquity (1/40 cycles/kyr), and precession (1/23 cycles/kyr) (e.g., Hays et al., 1976; Imbrie et al., 1993). This finding supports the idea that orbitally induced changed in insolation 'pace' the glacial cycles, but the definitive cause of the ice ages is still not entirely understood. The conventional astronomical theory of the ice ages posits the growth and decay of ice sheets is regulated by the intensity of insolation received during high latitude northern hemisphere summer because the extent of ablation ultimately controls ice growth (Milankovitch, 1941). The intensity of insolation received during high latitude northern hemisphere summer is influenced by both the obliquity and

precession parameters (Berger & Loutre, 1991; Laskar et al., 2004). Therefore, if the astronomical theory of ice ages is correct, we would expect $\delta^{18}O$ records to have 40 thousand years (kyr) and 23 kyr cycles to match the obliquity and precession cycles. But when analyzed the $\delta^{18}O$ records reveal that the late Pleistocene ice ages occur every 100 kyr (on average) and have spectral power at frequencies associated with all three orbital parameters and the early Pleistocene ice ages occur every 40 kyr and have spectral power associated with only obliquity, therefore the geologic record does not categorically corroborate Milankovitch's theory (Huybers, 2006; Lisiecki & Raymo, 2005; Raymo & Huybers, 2008). Theories to explain the 100 kyr cycle of the late Pleistocene ice ages initially suggested they were a non-linear amplification of eccentricity related changes in insolation (Ghil et al., 1994); but more recent theories propose they are not associated with eccentricity, rather the timing of late Pleistocene glacial terminations occur at multiples of either precession cycles (Ridgewell et al., 1999), obliquity cycles (Huybers & Wunsch, 2005), or a combination of the two cycles (Huybers et al., 2011). A completely alternative theory for the ice ages does not require external insolation forcing, instead the theory posits glacial cycles are a non-linear self-sustaining oscillation intrinsic to the climate system that terminate through a 'sea-ice switch' mechanism and can phase lock to orbital frequencies (Ashkenazy & Tziperman, 2004; Gildor & Tziperman, 2000). The longer and more intense late Pleistocene glacial cycles are more complex than the relatively straightforward 40 kyr glacial cycles of the early Pleistocene and therefore many

researchers focus on the early Pleistocene to test astronomical theories for the ice ages (Raymo & Huybers, 2008).

Numerous theories have been proposed to explain the early Pleistocene glacial cycles (Huybers, 2006; Lee & Poulsen, 2009; Raymo et al., 2006; Raymo & Nisancioglu, 2003; Tabor et al., 2015). Raymo et al. (2006) suggests Milankovitch's (1941) original theory is correct and proposes that the precession signal is absent from the $\delta^{18}O$ data because the proxy represents a global average and thus the precession signal is 'cancelled out' because it has an anti-symmetric effect between hemispheres. An alternative theory proposes the summer energy metric (Figure 1i) would be a more accurate measure of how insolation controls ice sheet growth because it captures both the intensity of summer insolation and the duration of the summer season (Huybers, 2006). The summer energy metric varies at a frequency of 1/40 (cycles/kyr), which matches the frequency of the obliquity parameter (Figure 1) and is therefore consistent with the $\delta^{18}O$ records (Huybers, 2006). These competing theories can be tested by determining if the precession frequency (1/23 cycles/kyr) is present in a proxy record that is sensitive to the signal of local continental ice variability (Raymo & Huybers, 2008).

Figure 1. (a) Global benthic foraminifer oxygen isotope stack (Lisiecki & Raymo, 2004). (b) Obliquity parameter (red; Laskar et al., 2004) and summer energy 65°N with threshold of 250 W/m^2 (black; Huybers, 2006). (c) Daily insolation June 21 at 65°N (Laskar et al., 2004). (d) Site U1341 Natural Gamma Radiation (Takahashi et al., 2011). (e) Natural log of Site U1341 IRD flux. (f) Occurrence of authigenic glauconite (green circles) and detrital plant matter (orange squares) in the coarse fraction (>250μm) of Site U1341. Black markers indicate absence, open markers indicate rare occurrence (1-5 grains), and colored markers indicate presence (>5 grains). (g) Site U1341 IRD flux (IRD grains/cm^2/kyr). (h, i, j) Spectral estimates using the Blackman-Tukey method during the interval 2.0-1.4 Ma for records: (h) global benthic oxygen isotope stack, (i) summer energy, and (j) daily insolation June 21 at 65°N. Black circles on d, e, g correspond to the sub-samples used for the coarse fraction composition analysis reported in Figure 5. Absolute age of data in a, b, c is found on the upper x-axis in black. Relative age model of Site U1341 data in d, e, f, g is found on lower x-axis in blue.
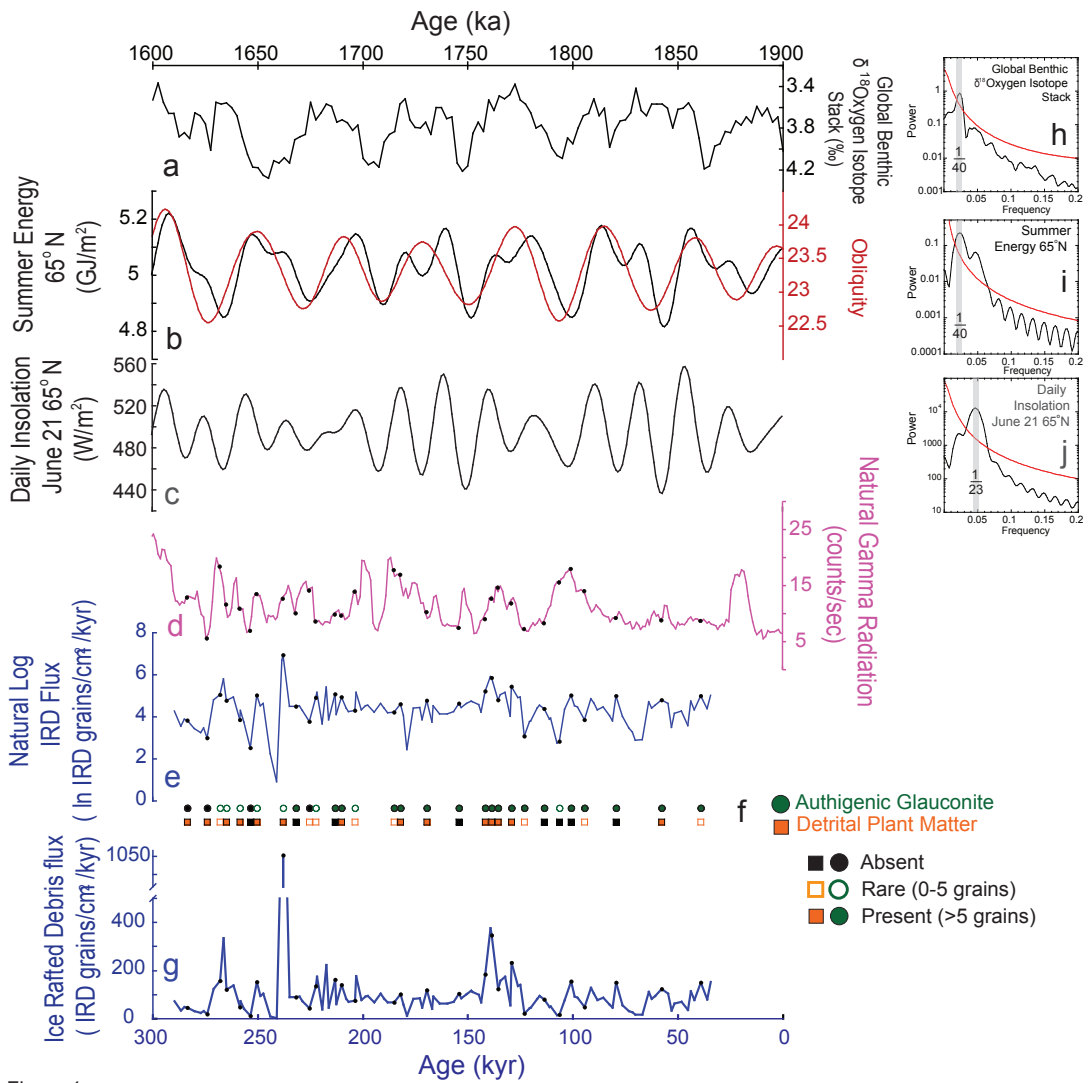
Figure 1

Paleoclimate records of the Pleistocene cryosphere also have sub-orbital variability, primarily documented in the records from the North Atlantic (e.g., Billups & Scheinwald, 2014; Ferretti et al., 2015; Hagelberg et al., 1994; McIntyre et al., 2001; McIntyre & Molfino, 1996; Wara et al., 2000; Yiou et al., 1994). The underlying forces driving these sub-orbital fluctuations (e.g., half precession) is not fully understood. The origin of half precession frequencies (1/12-1/10 cycles/kyr) in paleo-records has been attributed to multiple sources. These frequencies are observed in equatorial insolation because there is a double maximum that occurs at both the spring and fall equinoxes (Berger et al., 2006, 1991). In addition, climate models predict a half precession signal arises from the non-linear response of temperatures to equatorial insolation (e.g., Short et al., 1991). Furthermore, bi-spectral analysis has established some high latitude sub-orbital variability can originate from low latitudes and the signal is transmitted through a dynamical link between the low and high latitude climate systems (Hagelberg et al., 1994; McIntyre & Molfino, 1996). Alternatively, bi-spectral analysis of North Atlantic data including an IRD record, show sub-orbital frequencies result from non-linear interactions within the high latitude climate system and are indirectly forced by local insolation (Wara et al., 2000). Further investigation into the origin of sub-orbital variability and its occurrence in paleo-records outside of the Atlantic is needed.

In this study we investigate the evolution of the sub-Arctic Pacific cryosphere to further our understanding of how the system responds to external forces (i.e., insolation) and internal forces (i.e., feedbacks) at both orbital and sub-orbital

timescales. The Integrated Ocean Drilling Program (IODP) Expedition 323 to the Bering Sea presents the opportunity to study the evolution of the sub-Arctic Pacific cryosphere which is not as well characterized as the North Atlantic region. In this study we present an orbitally resolved 255 kyr early Pleistocene record (~1.87-1.61 Ma) of Ice Rafted Debris (IRD) flux from Site U1341 in the Bering Sea. Our results suggest the IRD flux record primarily reflects sea ice transport and has significant cyclicity at precession and half-precession frequencies.

Background

Bering Sea modern oceanography

The Bering Sea is a semi-enclosed marginal sea that connects the Pacific and Arctic oceans. It is characterized by a broad continental shelf in the northeast that extends roughly 500 km to the shelf break (defined 180 m; Stabeno et al., 2001) and abyssal basins in the southwest (Figure 2). Generally, surface currents have a cyclonic circulation pattern in the Aleutian Basin, which includes the eastward Aleutian North Slope Current (ANSC), the northwest flowing Bering Slope Current, and the southwest flowing Kamchatka current (Figure 2). Pacific waters flow into the Bering Sea through the Aleutian Island chain and Bering Sea waters flow northward through the Bering Strait into the Chukchi Sea (Figure 2; Woodgate & Aagard, 2005).
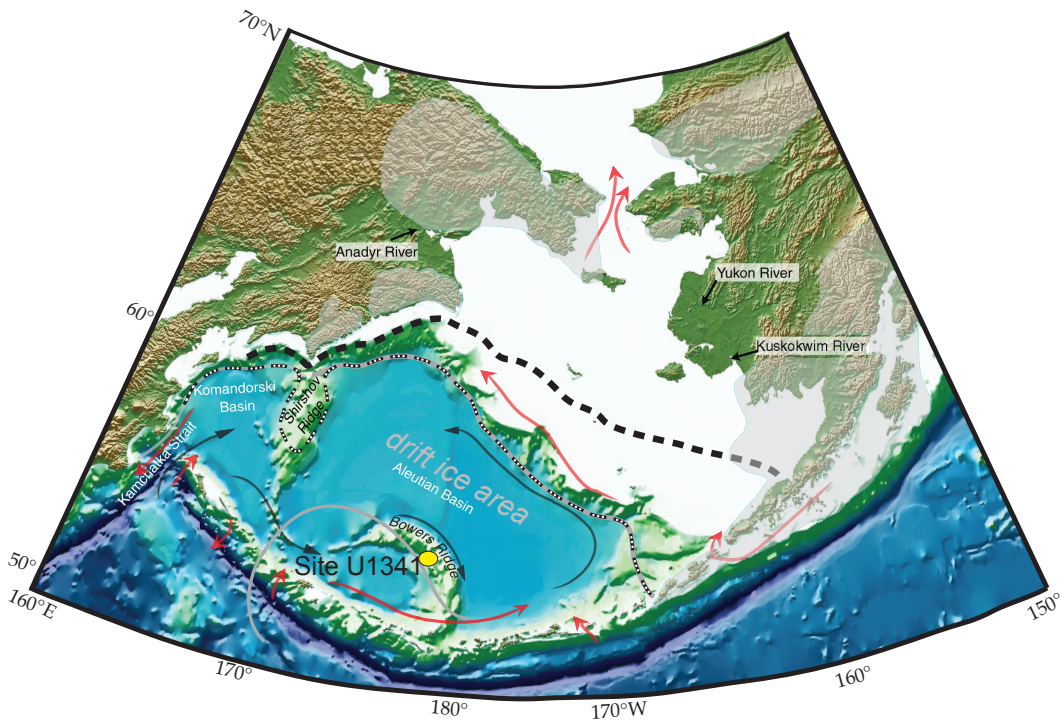
Figure 2

Figure 2. Map of Bering Sea. Study location, IODP Site U1341 (yellow circle). Last Glacial Maximum estimated seasonal sea ice extent (grey dashed-dot line) and boundaries of sea ice drift area (between grey line) based on Tanaka and Takahashi (2005). Estimate of maximum glacial extent (grey shading; Kaufman et al., 2004). Modern sea ice edge (black dashed line; Fetterer et al., 2016), surface currents (red arrows) and intermediate water circulation (black arrows). Base map modified from Takahashi et al (2011).

Sea ice the Bering Sea

Seasonal sea ice is a critical component of the Bering Sea ecosystem and studies of the modern instrumental record show the seasonal ice extent is highly variable on interannual and decadal timescales (e.g., Frey et al., 2015; Stabeno et al., 2012; Wendler et al., 2014). During the fall and winter sea ice forms on the northeastern continental shelf and is advected southward by prevailing winds (Stringer & Groves, 1991). Sea ice reaches its maximum extent in March and melts

during the spring (Figure 2; Stringer & Groves, 1991). Sea ice formation is largely

controlled by wind velocity and cloud cover while the maximum extent and

persistence of the ice edge is controlled by thermodynamic processes (Pease, 1980).

Interannual variability in the maximum extent of the sea ice edge is affected by the

location of winter storm tracks, which are strongly influenced by the position of the

Aleutian low-pressure cell (Rodionov et al., 2005, 2007). Typically, light sea ice

years are dominated by storms moving north-northeast up the coast of the Siberian

Peninsula (Overland & Pease, 1982; Rodionov et al., 2007). But the variability in

winter/spring sea ice extent has also been associated with the negative Pacific

Decadal Oscillation mode, the positive Arctic Oscillation mode, La Nina conditions

in the tropical Pacific, and a weak East Asian Winter Monsoon (Frey et al., 2015; Li

& Wang, 2013; Niebauer, 1988; Stabeno et al., 2012). Sea ice variability in the

greater Pacific-Arctic region exhibits heterogenous trends and the winter/spring

Bering Sea ice maximum has been decoupled from the Arctic summer minimum in

recent years (Stabeno et al., 2012).

Bering Sea paleo-data indicates sea ice has exceeded its modern extent.

Micropaleontological evidence from the Last Glacial Maximum (LGM) shows

periods of perennial sea ice and a sea ice margin that extended well beyond the

modern maximum (Caissie et al., 2010; Sancetta & Robinson, 1983; Sancetta et al.,

1985). Furthermore, there is evidence of extensive sea ice drift across the Aleutian

Basin to Bowers Ridge during periods of the deglaciation and Holocene (Gorbarenko

et al., 2010), the LGM (Katsuki & Takahashi, 2005), and as far back as 2.0 million

years ago (Ma) on the western slope of Bowers Ridge (Onodera et al., 2013) and 2.56

Ma on the eastern slope of Bowers Ridge (Stroynowski et al., 2015). We highlight

that sea ice rafting is recorded during warm interglacial periods on Umnak Plateau

throughout Marine Isotope Stage (MIS) 5 (Vaughn & Caissie, 2017) as well as

throughout MIS 11 on the Bering Slope and Bowers Ridge (Caissie et al., 2016;

Stroynowski et al., 2015; Teraishi et al., 2013).

Glacial history of the Bering Sea region

Glaciation of the land adjacent to the Bering Sea was not as extensive as other

North Pacific regions such as the southwest of Alaska and the Kamchatka Peninsula.

The presence of ice-rafted drop-stones in sediments of the northwest (ODP 881) and

northeast (ODP 887) Pacific suggest glaciation of the Kamchatka Peninsula and

southeastern Alaska respectively began sometime in the late Miocene (Lagoe et al.,

1993; Krissek, 1995; McKelvey, 1995). The interior of Alaska did not glaciate until

about 3.3 Ma, based on geochemical and micropaleontological evidence of meltwater

reaching Site U1341 on Bowers Ridge (Horikawa et al., 2015). This timing is

supported by the presence of drop-stones on the Umnak Plateau and Bowers Ridge in

sediment of late Pliocene age (Creager & Scholl,1973; Takahashi et al., 2011).

Overall, the Pleistocene glacial history of the sub-Arctic Pacific shows regional

complexity (St. John & Krissek, 1999) and appears to suggest the least glaciated area

was the land immediately adjacent to the Bering Sea.

Currently, Alaskan mountain glaciers cover 75,000 km^2 (Molnia, 2007), but there is evidence for more extensive glacial coverage (727,800 km^2) during the late Pleistocene (Figure 2; Kaufman & Manley, 2004). Late Pleistocene glaciation primarily occurred in the mountains surrounding the Gulf of Alaska, which would not result in iceberg calving within the Bering Sea. There is evidence for tidewater glaciers on the Seward Peninsula (Calkin et al., 2001), the Ahklun Mountains (Briner & Kaufman, 2000; Manley et al., 2001), and the Pribilof Islands (Hopkins & Einarsson, 1966), which could calve icebergs into the Bering Sea (Figure 2). The Siberian Chukotka Peninsula also has evidence of glacial advances stemming from the Koryak mountains into the Gulf of Anadyr (Gualtieri et al., 2000; Heiser & Roush, 2001) and a glacier that spanned the Anadyr Strait terminating on St. Lawrence Island (Brigham-Grette et al., 2001), all of which could have calved icebergs into the Bering Sea depending on the sea level. The exposed continental shelf (Beringia) and Yukon lowlands remained ice free (Elias & Brigham-Grette, 2013). Maximum glaciation on the land surrounding the Bering Sea likely occurred during MIS 4 or early MIS 3, which is asynchronous with peak glacial expansion elsewhere in the Northern Hemisphere (Barr & Clark, 2012; Briner & Kaufman, 2008). The limited glaciation of the region has long been attributed to its isolation from a source of moisture during glacial periods (e.g., Hopkins, 1982). The history of the early Pleistocene cryosphere (i.e., sea ice and icesheets) in the Bering Sea is not well documented and is the focus of this study.

Ice Rafted Debris (IRD) overview

Ice rafted debris (IRD) are defined as coarse grain particles transported to the open marine environment by ice (i.e., sea ice and icebergs) (Bischof, 2000). IRD in high latitude deep-sea sediment is one of the most direct pieces of evidence for the occurrence of sea ice and icebergs. The process of sediment entrainment into icebergs is distinct from sea ice. Icebergs originate from alpine glaciers and incorporate sediments through the erosion of rock as the glacier flows seaward whereas sea ice incorporates sediments from the coastal and near shore environments. Therefore, we expect material transported by icebergs to be distinct from material transported by sea ice.

Sediment entrainment into continental ice (i.e., glaciers and ice sheets) is complex and dependent on the thermal regime of the ice, a review of the topic can be found in Jaeger and Koppes (2016). Generally, most sediment is incorporated into the bottom of ice sheets and glaciers as they flow. Mechanisms of basal sediment incorporation include regelation into subglacial sediment, freeze-on from conductive cooling of ice, and folding or thrusting of sediment into ice during glacial surges (Alley et al., 1997; Knight, 1997; Lovell et al., 2015; Waller et al., 2000). The physics of these mechanisms commonly exclude the regelation of material smaller than medium silt size (Alley et al., 1997), a key fact this study will use to distinguish between continental ice and sea ice. Sediments entrained in continental ice can be transported into the marine environment by icebergs. Sediments thawed from glacier ice are poorly sorted and the surface texture of grains indicate mechanical breakage and

physical weathering (Dowdeswell, 1986; Dowdeswell & Dowdeswell, 1989; Dunhill, 1998).

In the Arctic Ocean sediment entrained in sea ice is dominated by silt and clay with sand and coarser material making up a lower percentage (e.g., 27%; Reimnitz et al., 1993) of total sediment (Kempema et al., 1989). This is due to the selective entrainment of fine grain particles during suspension freezing, a common mechanism of sea ice formation (Dethleff & Kuhlmann, 2009; Dethleff, 2005; Reimnitz et al., 1998). Coarser material is introduced into pack ice through the incorporation of anchor ice (Darby et al., 2011). Anchor ice forms at estimated depths of 0-30 meters and entrains benthic flora, fauna, and sediments (Dethleff, 2005; Reimnitz et al., 1986; Reimnitz et al., 1987; Reimnitz et al., 1992). Overall, these Arctic Ocean studies indicate sea ice primarily contain silt and clay sized sediment. This characterization will be used to distinguish between material transported by sea ice versus iceberg.

Although the presence of IRD is the most direct evidence of ice that can be derived from deep-sea sediments, there are some caveats to the method. The common interpretation for variations in the flux of iceberg rafted debris is the changing stability of continental ice sheets (e.g., Patterson et al., 2014), but this straightforward interpretation has been called into question (St. John & Krissek, 1999) because the deposition of IRD is also affected by independent factors influencing iceberg melt (Andrews, 2000). With respect to sea ice rafted debris, it is challenging to distinguish between a change in sea ice extent versus an increase in sea ice drift over a given

location. Notwithstanding, it is most important to differentiate between iceberg and sea ice rafted sediments because they represent different response rates to distinct components of the climate system. Overall, iceberg rafted sediments are expected to have signs of physical weathering and be poorly sorted with little fine grain material. Whereas sea ice rafted sediments are expected to have signs of chemical weathering, to include coastal sediment, and to be dominated by fine-grain material.

Material and Methods

Site location and age model

IODP Expedition 323 Site U1341 is located on the western slope of Bowers Ridge (54° 1.9984 N, 179° 0.5171 E) at 2139.5 meters water depth (Figure 2). This study targeted a 255 kyr interval during the early Pleistocene that is equivalent to 173.2 to 197.8 meter compensation depth (mcd). The sediment lithology is classified as diatom ooze and diatom clay/silt that alternate at decimeter to meter scale. Core images were carefully reviewed and there are no sedimentary structures that would suggest slumping or soft sediment deformation impacted the material used in this study. Furthermore, no such sediment disturbance was reported in the expedition proceedings corresponding to Site U1341 during the study interval (Takahashi et al., 2011).

The age model used in this study builds off the age model from Iwasaki et al., (2016), which estimates the study interval has a linear sedimentation rate between 12.05 to 8.52 cm/kyr (Table 1; Ikenoue et al., 2015; Onodera et al., 2013). The

average sedimentation rate applied in this study was determined by the average

spectral misfit (ASM) function from the Astrochon v.0.7 R package (Meyers et al.,

2015, 2012). The ASM function was applied to a 600 kyr record (2.0-1.4 Ma) of

shipboard Natural Gamma Radiation (NGR) data (temporal sample resolution: 1 kyr;

Takahashi et al., 2011). The ASM function was given eleven target frequencies and

an upper sedimentation rate of 12 cm/kyr (Iwasaki et al., 2016). The ASM algorithm

determined the study interval has an average sedimentation rate of 9.66 cm/kyr with

an ASM metric of 0.0014 (p=0.0004) and a match of six target frequencies. We are

confident the study interval represents about 255 kyr of time, but we consider the age

model to be floating because there are no microfossil datums within the study interval

and thus the absolute ages reported have significant uncertainty. Analysis presented in

this study is therefore limited to data collected from Site U1341 cores and no direct

comparisons to the benthic $\delta^{18}O$ stack or insolation curves were made.

Table 1.

Event	Depth ccsf-a (m)	Depth error (m)	Age (Ma)	Age error (Ma)	Reference
First occurance of *P. curvitrostris*	170.27	1.82	1.580	0	Onodera et al., (2013) in Iwasaki et al., 2016
Last common occurance of *N. koizumii*	218.75	1.51	2.06	0.05	Onodera et al., (2013) in Iwasaki et al., 2016

Table 1. Age model Expedition 323 Site U1341. Age model based on biostratigraphy of diatom datum events nearest to study interval.

Natural Gamma Radiation (NGR) and clay mineral abundance

NGR data was collected onboard IODP Expedition 323 following standard

protocols (Takahashi et al., 2011). Site U1341 NGR data between 173.2 to 197.8 mcd

has a sample resolution of 10 cm (n=247, temporal sample resolution: ~1 kyr). The source of NGR in deep-sea marine sediments is thought to be clay minerals.

Smear slide analysis was performed on 21 samples that represent the full range of NGR values present over the study interval (5.6-24.1 counts/sec). Smear slide analysis was used to estimate the relative percent abundance of all sedimentary components (Drake et al., 2014; Marsaglia et al., 2013). To reduce possible bias during smear slide analysis samples were given coded sample identifiers and randomized. The clay mineral abundance data was used in bivariate analysis with paired NGR data to verify the interpretation of NGR as a proxy for clay minerals.

Ice Rafted Debris flux

The IRD flux was measured in 119 samples (average temporal sample resolution: 2 kyr). Sediment samples were freeze dried, shaken in deionized water for 12 hours, wet sieved at 63 μm, and oven dried at temperatures no greater than 50°C. IRD was defined as mineral and lithic fragments greater than 250 μm (St John & Krissek, 1999). Samples were sieved at 250 μm and the IRD within the greater than 250 μm fraction was visually identified and counted with a binocular microscope. Great care was taken to identify and exclude pyroclastic material, biogenic particles, and authigenic minerals from the IRD counts. If necessary quantitative splits of the greater than 250 μm fraction were made and grains were identified and counted from the split, which was then extrapolated to the entire sample.

The flux of IRD (IRD grains cm^{-2} kyr^{-1}) was calculated with equation (1), using a linear sedimentation rate (LSR) of 9.66 cm/ kyr. The dry bulk density ($\rho_{dry\ bulk}$) was calculated with equation (2), using the shipboard gamma ray attenuation wet bulk density data (ρ_{GRA}), a pore fluid density ($\rho_{pore\ fluid}$) of 1.024 g cm^{-3}, and a grain density (ρ_{grain}) for each core, which is an average of the discreet shipboard measurements made on each core-section (Takahashi et al., 2011).

$$\text{IRD flux} = \frac{\text{\# IRD grains}}{\text{grams of sediment}} * \rho_{\text{dry bulk}} * \text{LSR} \qquad (1)$$

$$\rho_{\text{dry bulk}} = \left(\frac{\rho_{\text{GRA}} - \rho_{\text{pore fluid}}}{\rho_{\text{pore fluid}} - 1} \right) * \rho_{\text{grain}} \qquad (2)$$

Characterization of coarse fraction

Further analysis of the IRD and non-IRD components of the coarse fraction (>250 µm) was performed on a subset of samples (n=30). The expectation that sea ice rafted material would include both coarse grain and fine grain material while iceberg rafted debris would be dominated by coarse grain material (see section *IRD overview)* guided the subsampling strategy. The subsamples were selected to isolate end members that represented above and below average IRD flux (105 IRD grains/cm²/ kyr) and NGR values (11 counts/sec) and samples with opposing extremes (i.e., high IRD flux and low NGR values) were also specifically targeted (Figure 1). In these 30 samples the presence of glauconite and detrital plant matter and the composition of

the IRD was quantified. The glauconite and detrital plant matter data are presented as present (greater than 5 grains counted), rare (0-5 grains counted), or absent. IRD composition was measured as the relative proportions of quartz, feldspars, and lithic fragments (Pettijohn, 1975) and all IRD grains were identified and counted by binocular microscope. The composition of IRD was assessed with ternary diagrams. Comparisons of the IRD composition were made between samples categorized as the above or below average IRD and NGR values as well as combinations of the two variables (i.e., high IRD flux - low NGR samples versus low IRD flux – high NGR samples), as well as the amount of authigenic glauconite in a sample. These comparisons were statistically tested using Wilcoxon rank-sum tests. These comparisons were intended to help distinguish between samples dominated by material transported by iceberg versus sea ice.

Spectral analysis

Spectral estimates were calculated with the UCLA SSA-MTM Toolkit v4.4 software (Ghil et al., 2002). We used Singular Spectrum Analysis (SSA) and the multivariate equivalent, the Multichannel Singular Spectrum Analysis (M-SSA), because they use data-adaptive filters and are ideal for the detection of non-linear signals and weak oscillations (Ghil et al., 2002; Vautard et al., 1992). SSA and M-SSA involve embedding the data into a matrix of dimension M, deconstruction into an eigenvalue and eigenvectors that are then reconstructed by grouping the eigenelements and diagonalizing (see Ghil et al., 2002, 2015 for a comprehensive

review). The resulting empirical orthogonal functions (EOFs) and associated principal components (PCs) represent the trend, oscillations, and noise that can be analyzed separately or in combination as reconstructed components (RCs). The embedding dimension M is not a fixed value and is a tradeoff between spectral resolution and statistical confidence. The reported SSA and M-SSA results use M=21, which is equivalent to a window width of 42 kyr. The sensitivity to the choice of M was assessed by varying M between N/5 to N/10 (where N = total number of data points; Vautard et al., 1992; Yiou et al., 1994) and the results remained stable (not shown).

To determine the significant eigenvalue(s) within the IRD flux record we applied Monte Carlo-SSA (Allen & Smith, 1996) and to determine the significant shared cyclicity within the IRD flux and NGR records we applied Monte-Carlo M-SSA (Allen & Robertson, 1996; Groth & Ghil, 2015). Significance was tested against AR(1) noise using an ensemble of 10,000 surrogate data simulations. The error bars plotted with the SSA spectra represent 99% of the variance associated with each EOF defined by the 10,000 red noise simulations. Eigenvalues outside of the 99% confidence interval are not likely to be due to the red noise process being tested against and are considered statistically significant.

The significant eigenvalues identified in the Monte-Carlo SSA and M-SSA tests were combined into reconstruction components (RCs) and their spectral content was then analyzed. This step is recommended by Ghil et al. (2002), who highlights that the assigned frequency in the SSA can be ambiguous or not unique due to possible anharmonicity of the EOF. Therefore, the RCs spectra was estimated by the

adaptively weighted Multi-Taper Method (MTM) with a significance test relative to a

robust red noise estimate with a 99% reshaping threshold (Mann & Lees, 1996). The

power spectra of the RCs reflect the isolated signal from the original record and is

less complex than the power spectra of the full time series because the 'noise' has

been removed. Significant frequencies are reported as a frequency band (spectral peak

± bandwidth) to account for the uncertainty in the spectral estimate. For the SSA the

IRD flux data was transformed (natural log), detrended, and linearly interpolated to 2

kyr resolution (N=128) before analysis. For the M-SSA the data was normalized to

unit variance and the NGR data resolution was reduced to match the IRD flux record.

The bandwidth of the spectral analysis was 0.0156.

Results

IRD flux

The IRD flux record shows variable but continuous flux to Site U1341 with no

long-term trend (Figure 1). The average flux is 105 grains/cm^2/kyr with a range

between 3 to 1051 grains/cm^2/kyr (Figure 1). To review, the SSA will deconvolve the

data into eigenvalues and the Monte Carlo test produces the confidence intervals

estimated by a red noise process; the SSA spectra plot (Figure 3a) show the

eigenvalues of the data and confidence intervals estimated from red noise, with

significant eigenvalues plotting above of the confidence interval. The significant

eigenvalues were combined into reconstruction components (RC; Figure 3b) and their

spectra were then estimated by MTM analysis (Figure 3c). We found the 7th and 8th

eigenvalues are statistically significant (Figure 3a). The RC-7,8 represents 16% of the variance in the IRD flux record (Figure 3b). MTM analysis of RC-7,8 showed two frequency bands are significant, one around the orbital precession frequencies (1/32 – 1/21 cycles/kyr) and the other at sub-orbital half-precession (1/11.5 – 1/9.8 cycles/kyr) frequencies (Figure 3c). Surprisingly, the IRD flux record has no obvious obliquity-paced cycles in the raw data (Figure 1e, 1g) or in the results of our spectral analysis (Figure 3).
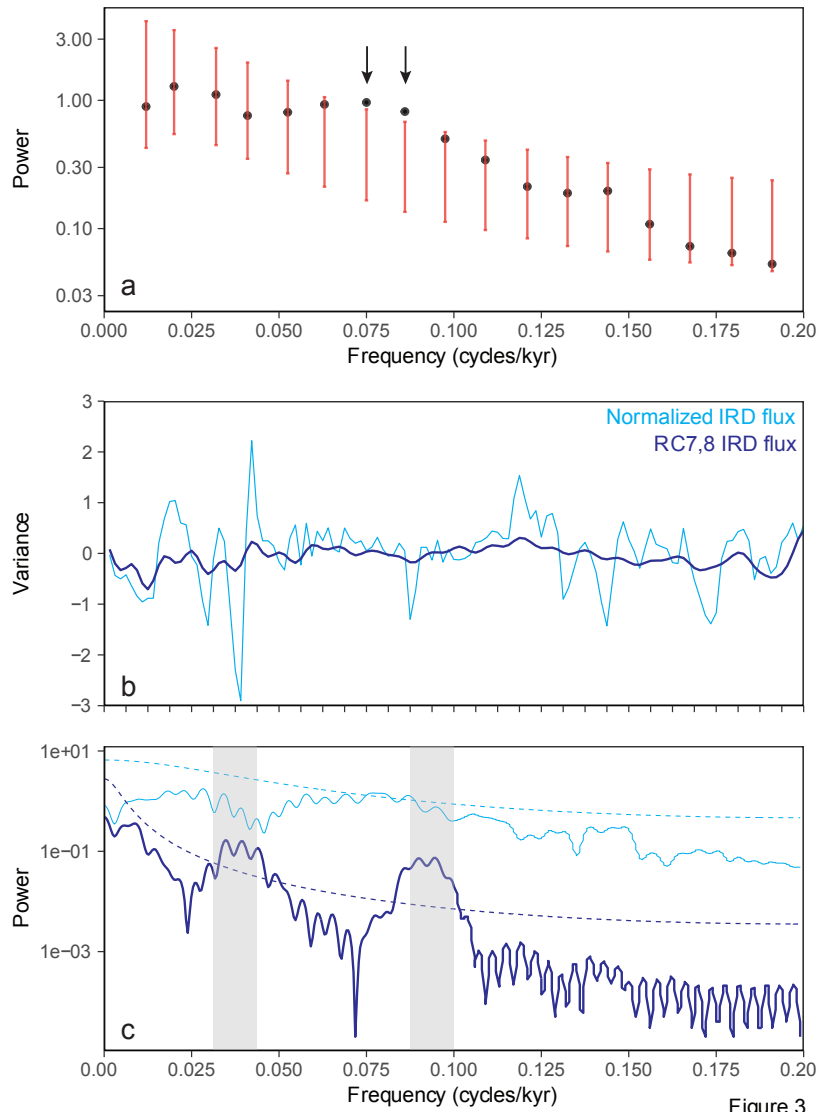
Figure 3. Spectral properties of Site U1341 IRD flux. (a) Monte-Carlo SSA (M=21) with the estimated variance of eigenvalues (black circles) plotted against frequency (cycles/kyr) and the significant eigenvalues 7 and 8 indicated by arrows. Error bars represent the 99% confidence interval constructed from AR(1) surrogate data (ensemble of 10,000). (b) Reconstructed components (RC) 7, 8 (light blue) and normalized IRD flux data (dark blue). (c) Adaptively weighted MTM power spectrum RC-7,8 (dark blue), IRD flux data (light blue), with 99% confidence interval (dashed lines) based on robust estimate of red noise. Grey bars mark the significant frequency band at 99% levels from the MTM analysis of RC-7,8, the near precession frequencies (1/32 – 1/21 cycles/kyr) and the sub-orbital frequencies (1/11.5 – 1/9.8 cycles/kyr).

67

NGR: a proxy for clay mineral abundance

Bivariate analysis between the relative percent abundance of clay minerals and the paired NGR measurements shows a significant positive correlation ($R^2=0.66$, p-value<0.001; Figure 4). The subset of samples (n=21) assessed have a relative percent abundance of clay minerals ranging from 2% to 18%, which is like the range of NGR values (6.6 – 20 g/cm^3) present throughout the 255 kyr study interval. The significant correlation confirms the NGR record is a proxy for clay mineral abundance at Site U1341.
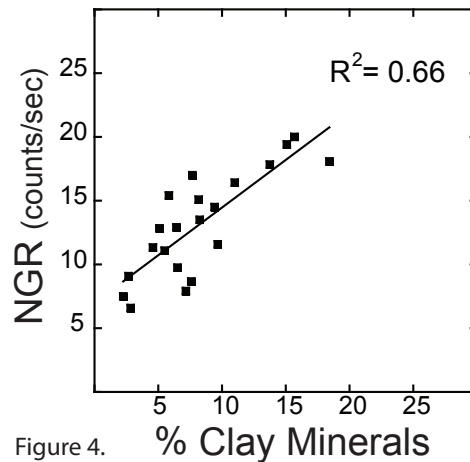
Figure 4.

Figure 4. Calibration of shipboard NGR data. There is a significant positive correlation between NGR (counts/sec) and the percent relative abundance of clay minerals measured through smear slide analysis. Shipboard NGR is therefore used as a proxy of clay mineral abundance.

Composition of coarse fraction

The composition of IRD (n=30) are very similar throughout the record with no significant difference between the composition of samples categorized based on multiple variables (e.g., IRD flux, NGR value; Figure 5). On average the composition of IRD have a larger percentage of feldspar (52%; range 74-26%) and lithic grains

(39%; range 61-18%) relative to quartz (9%; 4-15%) (Table 2). No significant

(p>0.01) difference in the percent of feldspar was found between samples with or

without glauconite present and samples with above or below average NGR values or

IRD flux compositions (Figure 5).
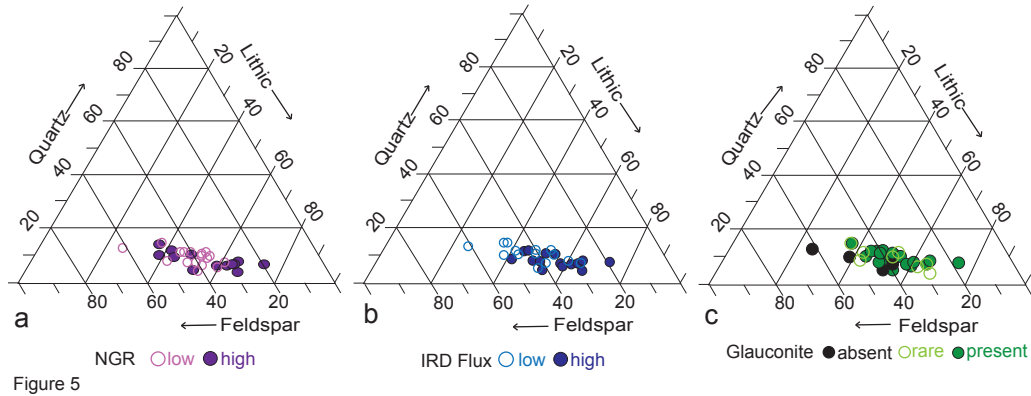
Figure 5

Figure 5. Ternary diagrams of the relative proportions of quartz, feldspar, and lithic fragments in the IRD fraction (n=30). IRD composition is not statistically distinct when comparing samples with (a) above or below average NGR values (11 counts/sec), (b) above or below average flux of IRD (106 IRD grains/cm^2/ kyr), or (c) presence of authigenic glauconite.

In the non-IRD coarse fraction (>250μm) we found there is a persistent presence

of authigenic glauconite and detrital plant matter (Figure 1f). We found authigenic

glauconite was present (>5 grains per sample) in 60% of subsamples and rare (1-5

grains per sample) in 27% of subsamples (Figure 1f). Detrital plant matter was

present in 47% of subsamples and rare in 8% of subsamples (Figure 1f).

Table 2.

Sample ID	IRD Flux (grains/cm^2/kyr)	NGR (counts/sec)	% of IRD-Quartz	% of IRD-Lithic grains	% of IRD-Feldspar	Glauconite grains	Detrital plant matter
U1341C-19H_6_2-4cm	20.30	5.68	7	54	39	0	50
U1341C-19H_5_62-64cm	46.16	12.91	10	39	51	0	25
U1341C-19H_6_62-64cm	158.70	18.48	7	65	29	4	5
U1341C-19H_7_2-4cm	47.74	10.97	12	54	35	4	14
U1341C-19H_6_92-94cm	120.82	11.67	9	43	49	3	67
U1341A-19H_2_32-34cm	152.33	13.51	4	67	29	4	11
U1341A-19H_3_2-4cm	1051.89	12.72	6	63	31	3	16
U1341A-19H_3_62-64cm	90.01	10.11	15	38	47	10	0
U1341A-19H_2_2-4cm	12.66	6.95	13	26	61	0	0
U1341A-19H_4_2-4cm	136.56	8.64	10	53	37	3	4
U1341A-19H_4_92-94cm	163.68	9.88	8	52	40	8	0
U1341A-19H_4_122-124cm	141.57	9.73	4	55	41	7	18
U1341A-19H_3_122-124cm	43.99	14.17	5	53	42	0	3
U1341A-19H_5_32-34cm	75.07	13.96	12	42	46	2	1
U1341C-20H_4_82-84cm	68.73	17.87	11	49	40	11	2
U1341C-20H_4_112-114cm	101.23	17.00	7	65	28	9	7
U1341C-20H_5_82-84cm	118.03	10.30	8	49	43	18	13
U1341C-20H_6_82-84cm	104.07	7.53	8	61	31	10	0
U1341A-20H_1_117-119cm	184.34	9.06	6	60	34	8	8
U1341A-20H_2_27-29cm	123.30	14.72	8	65	27	7	50+
U1341A-20H_1_147-149cm	347.30	12.73	7	59	34	17	5
U1341A-20H_2_87-89cm	234.46	11.93	10	56	34	13	50+
U1341A-20H_2_147-149cm	21.97	7.32	12	49	40	5	4
U1341A-20H_4_62-64cm	154.37	18.02	8	74	18	9	0
U1341A-20H_3_88-90cm	80.85	8.38	10	55	35	9	0
U1341A-20H_4_7-9cm	16.96	15.64	14	37	49	1	0
U1341A-20H_4_122-124cm	48.01	14.08	10	44	46	7	3
U1341B-21H_2_2-4cm	150.69	9.28	11	52	36	15	0
U1341B-21H_3_62-64cm	123.91	8.91	12	45	43	11	8
U1341B-21H_4_92-94cm	150.00	8.73	12	46	42	8	3

Table 2. Composition of coarse fraction.

Shared cyclicity between IRD flux and NGR records

Our results indicate that the IRD flux and NGR records have shared cyclicity near precession and half-precession band frequencies (Figure 6). The 8th and 9th eigenvalues plot outside of the 99% confidence intervals of red noise and are statistically significant (Figure 6a). The RC-8,9 represents 11% of the variance of the IRD flux and NGR records (Figure 6b, 6c). MTM spectral estimates of RC-8,9 for the IRD flux and NGR records show significant power near the precession band (1/19.9 – 1/15.2 cycles/kyr) above 99% and 95% levels respectively and half-precession band (1/12.5– 1/10.5 cycles/kyr) frequencies at the 99% level for both records (Figure 6d).
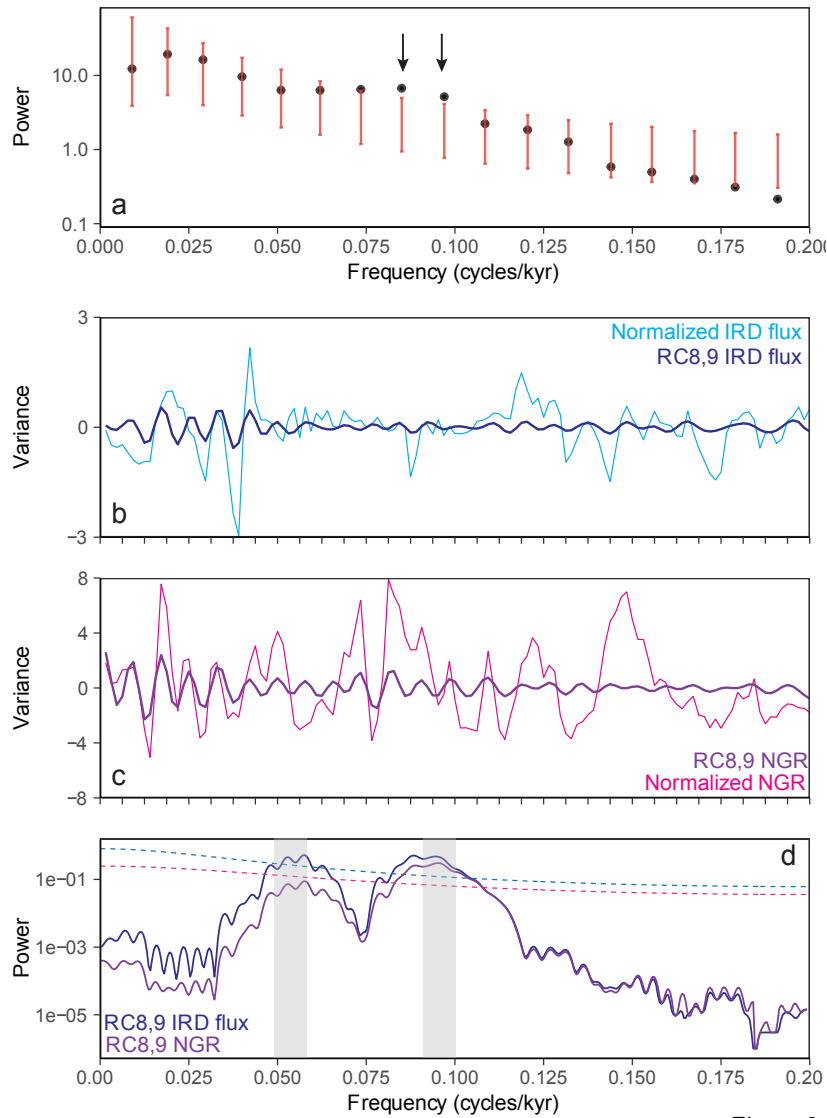
Figure 6. Shared spectral properties of Site U1341 IRD flux and NGR from study interval (a) M-SSA spectra (M=21), estimated variance of data modes (black circles; representative of eigenvalues) plotted against frequency (cycles/kyr), and the significant data modes 8 and 9 indicated with arrows. Error bars represent the 99% confidence interval constructed from AR(1) surrogate data (ensemble of 10,000). (b) Reconstructed components (RC) 8,9 of IRD flux (light blue) compared to normalized data (dark blue). (c) RC-8,9 of NGR (purple) compared to normalized data (pink). (d) Adaptively weighted MTM power spectrum RC-8,9 of IRD flux (blue) and NGR (purple, pink) with 99% confidence interval (dashed lines) based on robust estimate of red noise. Grey bars mark the significant frequency bands, the near precession frequencies (1/32 – 1/21 cycles/kyr) and the sub-orbital (1/11.5 – 1/9.8 cycles/kyr) frequencies.

Discussion

Site U1341 IRD is a proxy for sea-ice

The Site U1341 IRD flux record is interpreted as dominantly sea ice rafted debris, based on the composition of IRD and key components of the non-IRD coarse fraction, as well as the coherent cyclicity of the IRD flux and clay mineral records. Material entrained in sea ice is expected to be distinct from material entrained in icebergs (see section *IRD overview*), but we found the IRD composition was relatively constant throughout our record (Figure 5), suggesting one dominant transport mechanism for IRD to Bowers Ridge within the interval studied. An alternative explanation for the similar composition of the IRD would be the consist synchronous transport by both sea ice and icebergs, but the high-frequency variability of the record suggests sea ice is the dominant transport mechanism. There is a lack of evidence for the presence of large marine based glaciers in the Bering Sea during interglacial periods (see section *Glacial history of the Bering Sea)*, but there is evidence that sea ice is persist throughout interglacial intervals (Caissie et al., 2016; Vaughn & Caissie, 2017). Furthermore, we propose the dominant transport mechanism is sea ice because of the recurrent presence of authigenic glauconite and detrital plant matter in the coarse grain fraction, which suggests material was entrained from the continental shelf (Figure 1f; Cloud; 1955; Lisitzin, 2002; McRae, 1972). Authigenic glauconite in non-tropical regions precipitate in areas with low sedimentation rates at depths between 30-500m (McRae, 1972), which aptly describe parts of the Bering Sea continental shelf. With eustatic sea level low stands of -60 m

during the study interval it is reasonable that these areas could have become sites of sea ice production (Miller et al., 2020). Finally, the shared cyclicity between IRD and clay minerals (Figure 6) suggests that the dominant transportation mechanisms for IRD was sea ice, because iceberg rafted debris is not expected to contain significant amounts of fine grain material (e.g., Alley et al., 1997). This study cannot present direct evidence to support or refute the presence of iceberg rafted debris in the Bering Sea, but the interpretation of our record as dominantly sea ice rafted debris is supported by micropaleontological studies at Bowers Ridge (Katsuki & Takahashi, 2005; Onodera et al., 2013; Stroynowski et al., 2015) and provenance analysis of sediments from across the NW Pacific (Nechaev et al., 1994) that conclude there was sea ice drift over Bowers Ridge. In summary, the similar composition of IRD (Figure 5) and the shared cyclicity between the IRD and clay mineral records (Figure 6) suggest the IRD was transported by one mechanism to Bowers Ridge. The persistent presence of authigenic glauconite and plant debris (Figure 1) indicate sediment was entrained and transported from continental shelf. From these findings we conclude that the Site U1341 IRD flux record dominantly reflects sea ice transport, which will influence how we interpret the cyclicity of the record.

IRD cyclicity

This study shows sea ice in the Bering Sea has significant variability at sub-orbital half-precession frequencies (~1/12 -1/10 cycles/kyr) as well as precession band frequencies between ~1.87-1.61 Ma and we strive to understand the origin of

these signals to clarify what is forcing the Bering Sea cryosphere. Cautious of the limitations in the current Site U1341 age model (see *Site location and age model)* we do not find it appropriate to run linear cross-spectral analysis or non-linear cross-bispectral analysis, which would allow us to test the presence of a statistical relationship between our IRD flux record and records that are possibly forcing the system (i.e., insolation). In-lieu of this statistical analysis, we present a discussion on the plausible scenarios that could explain the cyclicity found in our record. The presence of precession band variability is unlike many early Pleistocene paleo-archives that exhibit strong obliquity cyclicity and we review how the presence of precession band variability could be a direct response to the intensity of local summer insolation. While the presence of sub-orbital half-precession variability suggests a non-linear response (Rial & Anaclerio, 2000) and we evaluate possible explanations including a non-linear response to high latitude insolation, non-linear interactions within the sub-Arctic Pacific climate, or the possibility that it has a non-local origin.

The absence of the 40 kyr frequency signals that the sea ice system in the Bering Sea may be sensitive to local not global forcing. Early Pleistocene proxy records such as the $\delta^{18}O$ records (e.g., Lisiecki & Raymo, 2004, Figure 1h) and the eustatic sea level curve (Miller et al., 2020) have a strong obliquity signal. The obliquity signal is also present in the Nordic Sea record of ice rafting (Jansen et al., 2000) as well as proxy records of the North Atlantic (e.g., Naafs et al., 2012; Lawrence et al., 2010), North Pacific (Asahi et al., 2014; Francke et al., 2013; Maslin et al., 1995), and low-latitude SST records (Venti et al., 2013; Herbert et al., 2010). The high latitude South

Atlantic (ODP 1090) is an exception with a strong precession signal in the SST record attributed to a sensitivity to southern hemisphere isolation (Martinez-Garcia et al., 2010).

The precession band frequencies observed in the SSA spectra of RC-7,8 of the IRD flux record could be a direct linear response to high latitude insolation (Figure 3). The intensity of high latitude summer insolation (i.e., mean daily insolation received on June 21 at 65°N) is primarily forced by precession and secondarily by obliquity (Figure 1j; Laskar et al., 2004). This would imply the IRD flux record has an antiphase relationship with the intensity of summer insolation forcing, where the minimum in June 21 65°N insolation corresponds to a maximum in sea ice. During this insolation minimum the reduced summer insolation leads to cooler SSTs in early fall resulting in early freeze up and overall maximum sea ice production. Conversely summer insolation maximum would correspond to a minimum in sea ice because increased sensible heating of the ocean would increase fall SSTs, delay sea ice freeze-up and reduce sea ice production and persistence. If sea ice is sensitive to local insolation forcing a strong coherence between the IRD flux record and daily summer insolation on June 21 65°N should be found in cross-spectral analysis. But the lack of spectral power at precession frequencies in the MTM spectra of the raw IRD flux data and the presence of precession alongside half-precession frequencies (1/12-1/10 cycles/kyr) in the SSA spectra may indicate there is not a direct linear response from cryosphere system (Figure 3).

Furthermore, the spectral power of the precession band frequencies is weaker than expected for a fundamental frequency in the SSA spectra (Figure 3c). This could be explained by a transfer of spectral power due to a non-liner asymmetric response to insolation, so called 'clipping' or 'truncation' as described by Clemens and Tiedemann (1997). This would imply that IRD flux is more sensitive to the minima of the insolation cycle more than the maxima. For example, if the cold phase of the insolation cycle resulted in a sea ice maximum and the warm phase resulted in ice free conditions with no seasonal sea ice. This scenario is supported by the presence of significant half precession frequencies (1/12-1/10) as well as eccentricity frequencies although the eccentricity frequencies are only significant at 90% confidence (Figure 3; Clemens & Tiedemann, 1997). This would imply that the sub-orbital frequencies result from a non-linear response to the intensity of local (i.e., high latitude) summer insolation.

An alternative non-linear response to local insolation would be a maximum sea ice response to both fall and spring insolation. Although these seasons do not represent the most significant changes in insolation, they are critical periods in the seasonal sea ice cycle. Sea ice would be sensitive to the minimum insolation during fall (March perihelion) and spring (September perihelion) associated with the freeze-up and melt periods respectively. This response to insolation would produce two sea ice maximums during a precession cycle and result in a spectrum with power around frequencies of half a precession cycle (1/12-1/10 cycles/kyr).

The sub-orbital cyclicity could also be a result of non-linear interactions within the sub-Arctic Pacific region in-line with to the results of Wara et al. (2000) for the late Pleistocene North Atlantic climate system. Hypothetically a significant response in sea ice could occur at both the maximum and minimum in summer insolation intensity generating significant spectral power at the half precession frequencies. This is an idealized thought experiment because mean daily insolation on June 21 at 65°N is not forced by the precession parameter alone, furthermore the length of the precession period varies through time and its amplitude is modulated by eccentricity (Laskar et al., 2004; Berger et al., 1978).

In this idealized thought experiment, we assume a significant sea ice response to the minimum in insolation on June 21 at 65°N (aphelion during June) and we speculate that the thermodynamic response to maximum insolation on June 21 at 65°N (perihelion during June) could be damped through negative feedbacks and result in a second significant sea ice response. There is a well-established temperature-vegetation relationship where increased summer temperatures drive vegetation growth and in turn decrease surface albedo in a positive feedback loop. There is also a tundra wintertime positive feedback on vegetation growth through a vegetation-snow-soil feedback (Strum et al., 2005). In this feedback tundra shrubs accumulate snow drift that insolates the winter soil and results in favorable spring growth conditions and is a positive feedback for vegetation (Strum et al., 2005). This positive vegetation-snow-soil feedback enhances a positive temperature-vegetation feedback. But, autumn melt events can result in a negative vegetation-snow-soil

feedback (Barrere et al., 2018). In this feedback autumn snowmelt events leave a layer of ice on soil that reduces the accumulation of snowdrift around tundra shrubs, resulting in less insolated soil and cooler spring soil temperatures that are unfavorable for vegetation growth (Barrere et al., 2018). This negative vegetation-snow-soil feedback could counteract a positive temperature-vegetation feedback. Other negative feedbacks on increased temperatures are an enhanced biological pump, due to increased riverine nutrient delivery caused by melting of perennial snowpack and glaciers, and enhanced surface albedo, due to increased cloud cover resulting from more evaporation (McGuire et al., 2006). In summary, the increased insolation received during periods of maximum insolation on June 21 at 65°N (June perihelion) could be offset by the cumulative effect of negative feedbacks such as an enhanced biological pump and increased surface albedo from cloud clover over ocean and reduced vegetation on land due to the negative vegetation-snow-soil feedback, resulting in favorable conditions for sea ice. This scenario is speculative but represents feasible non-linear interactions within the sub-Arctic Pacific that could result in two significant sea ice responses during one precession cycle, one at the minimum and another at maximum insolation on June 21 at 65°N, which would create half precession frequencies in the IRD flux record.

The cyclicity of the Bering Sea IRD flux record could originate from low latitudes where both precession and half-precession frequencies are found in proxy records (e.g., Clemens et al., 2008), climate models (e.g., Kutzbach & Guetter, 1986), and equatorial insolation (e.g., Berger & Loutre, 1997). To support this explanation, we

highlight paleo-monsoon records that report non-linear dynamics as well as studies

that link the East Asian Monsoon (EAM) system to Bering Sea sea ice suggesting an

atmospheric teleconnection exist between the two regions. Paleo-monsoon records

with half precession frequencies are recorded during the Pliocene (Clemens et al.,

2008), early Pleistocene (Ao et al., 2011), and late Pleistocene (Sun & Huang, 2006).

During the early Pleistocene eccentricity frequencies as well as heterodynes are

detected in a Chines Loess EAWM proxy record, which is symptomatic of a non-

linear response to precession forcing via a truncation mechanism (Sun et al., 2006;

Clemens & Tiedemann, 1997). This type of non-linear response also predicts spectral

power at sub-orbital frequencies (Clemens & Tiedemann, 1997) and although none

are reported by Sun et al. (2006) it is not clear if they are not present in the record or

if they are just not calculated and/or not reported. We speculate the low latitude non-

linear signal could be transmitted to the high latitude climate via atmospheric

teleconnections. A connection between the two regions has been suggested during the

Middle Pleistocene when the increase in pack-ice on the Bering Sea shelf corresponds

to periods of weak EAWM (Stroynowski et al., 2017). Similarly, analysis of the

modern instrumental records reveals the maximum sea ice extent in the Bering Sea

correlates to periods of weak EAWM (Li & Wang, 2013), presumably connected

through the dynamics of the winter Siberian high-pressure cell. This mechanistic

connection between the two regions can be indirectly inferred from the strong

correlation between a weak EAWM and the positive phase of the Arctic Oscillation

(AO) (e.g., He et al., 2017) and a positive AO and increased Bering Sea sea ice extent

(Frey et al., 2015). The transfer of low-latitude sub-orbital frequencies to high latitude climate has been previously modeled (Short et al., 1991) and demonstrated in proxy records from the Atlantic through higher order statistics (e.g., Hagelberg et al., 1994). We suggest the low latitude monsoon system is a possible source for the sub-orbital half-precession variability we detect in our high latitude IRD flux record, which would imply tropical climate plays a role in forcing the sub-Arctic Pacific cryosphere.

Finally, a North Atlantic proxy record of IRD ($\delta^{18}O$ of bulk carbonate) shows significant sub-orbital variability (from visual inspection of the evolutionary spectrum; Hodell et al., 2016) during the early Pleistocene. We speculate this high-frequency variability could be the result of non-linear interactions within the North Atlantic climate system, like those documented in the late Pleistocene by Wara et al. (2000). We further speculate that this signal could be transferred to the sub-Arctic Pacific, possibly through the mechanisms that currently link the winter sea ice variability and the North Atlantic Oscillation (NAO) presented by Ukita et al. (2007); where the dominant mode of sub-Arctic winter sea ice variability shows a double dipole (North Atlantic Labrador-Nordic Seas and North Pacific Bering-Okhotsk Seas) that are significantly correlated to each other (Labrador-Bering Seas and Nordic and Okhotsk Seas) and show a lagged correlation to the NAO (Ukita et al., 2007). Thus, North Atlantic sea ice anomalies (+ Labrador Sea and -Nordic Sea) are propagated eastward and result in lagged North Pacific sea ice anomalies (+Bering Sea and -Okhotsk Sea). The proposed origin of the sub-orbital variability detected by Hodell et al. (2016) and the possible mechanisms that could connect the North Atlantic and

Pacific regions are highly speculative, but the possible connection between sub-orbital variability in a North Atlantic proxy for IRD during the early Pleistocene and this Bering Sea record is worthy of further investigation.

Conclusion

Overall, this study documents a dynamic sea ice presence in the Bering Sea between ~1.87-1.6 Ma during the early Pleistocene and shows cyclicity at orbital precession band and sub-orbital half-precession frequencies within the Site U1341 IRD flux record (Figure 1, Figure 3). Since the IRD flux record does not appear to record the cyclicity of land-based ice we are unable to directly test the astronomical theories of the ice ages (e.g., Huybers 2006; Raymo & Huybers, 2008; Raymo et al 2006). We first suggest there is one dominant transport mechanism for IRD to Site U1341 because the IRD composition throughout the record is similar (Figure 5) and the IRD flux and clay mineral records shared cyclicity (Figure 6). We suggest the dominant transport mechanism for IRD is sea ice because there is a consistent presence of authigenic glauconite and detrital plant matter (Figure 1) that indicates the sediment was entrained on the continental shelf. Future research that couples IRD flux analysis with a method to independently determine sea ice such as sea ice diatom assemblages would help validate this interpretation.

We secondly outlined possible explanations for the precession and half-precession band frequencies detected in the IRD flux record. The most straightforward explanation for the precession band frequencies is a direct response to high latitude

summer insolation intensity, but the lack of spectral power at precession frequencies in the MTM spectra of the raw IRD flux data and the presence of precession alongside half-precession frequencies (1/12-1/10 cycles/kyr) in the SSA spectra suggest the precession signal is not a direct linear response to insolation (Figure 3). The relatively low power of precession band frequencies in the SSA spectra suggest the transfer of spectral power through a non-linear interaction such as truncation or clipping (Figure 3; Clemens & Tiedemann, 1997). However, the observed frequencies could also result from a sensitivity to maximums in local spring and fall insolation or from non-linear interactions within the sub-Arctic Pacific climate. Alternatively, the cyclicity could be a non-local signal transmitted via atmospheric teleconnection from low-latitudes or the North Atlantic.

The lack of obliquity frequencies in the IRD flux record during a period dominated by 40 kyr glacial cycles, suggests that local, rather than global, processes influenced the variability in sea ice in the Bering Sea. This favors the scenarios where the sub-orbital frequencies have a local high latitude source. But the transmission of a non-local signal via atmospheric teleconnections implies a sea ice system that is very sensitive to atmospheric conditions, which is consistent with our understanding of what influences modern seasonal sea ice dynamics (Sasaki & Minobe, 2005; Rodionov et al., 2007). Overall, the tentative explanations for the IRD cyclicity found in this study require further investigation to determine a more definitive answer. Future work must improve the age model at Site U1341, perhaps a stratigraphy generated by the $\delta^{18}O$ of diatoms could provide the age control needed to preform

linear cross spectral and non-linear cross-bispectral analysis between the proposed

forcing records and the Site U1341 IRD flux record allowing statistically rigorously

investigation of the origin of the cyclicity.

References

Allen, M. R., & Robertson, A. W. (1996). Distinguishing modulated oscillations from coloured noise in multivariate datasets. *Climate Dynamics*, *12*, 775–784. https://doi.org/https://doi.org/10.1007/s003820050142

Alley, R. B., Cuffey, K. M., Evenson, E. B., Strasser, J. C., Lawson, D. E., & Larson, G. (1997). How glaciers entrain and transport basal sediment: physical constraints. *Quaternary Science Reviews*, *16*, 1017–1038. https://doi.org/https://doi.org/10.1016/S0277-3791(97)00034-6

Andrews, J. T. (2000). Icebergs and iceberg rafted detritus (IRD) in the North Atlantic: facts and assumptions. *Oceanography*, *13*, 100–108. https://doi.org/https://doi.org/10.5670/oceanog.2000.19

Ao, H., Dekkers, M. J., Qin, L., & Xiao, G. (2011). An updated astronomical timescale for the Plio-Pleistocene deposits from South China Sea and new insights into Asian monsoon evolution. *Quaternary Science Reviews*, *30*(13–14), 1560–1575. https://doi.org/10.1016/j.quascirev.2011.04.009

Asahi, H., Kender, S., Ikehara, M., Sakamoto, T., Takahashi, K., Ravelo, a. C., … Leng, M. J. (2014). Orbital-scale benthic foraminiferal oxygen isotope stratigraphy at the northern Bering Sea Slope Site U1343 (IODP Expedition 323) and its Pleistocene paleoceanographic significance. *Deep-Sea Research Part II: Topical Studies in Oceanography*, 1–18. https://doi.org/10.1016/j.dsr2.2014.01.004

Ashkenazy, Y., & Tziperman, E. (2004). Are the 41 kyr glacial oscillations a linear response to Milankovitch forcing? *Quaternary Science Reviews*, *23*(18–19), 1879–1890. https://doi.org/10.1016/j.quascirev.2004.04.008

Barr, I. D., & Clark, C. D. (2012). Late Quaternary glaciations in Far NE Russia; combining moraines, topography and chronology to assess regional and global glaciation synchrony. *Quaternary Science Reviews*, *53*(C), 72–87. https://doi.org/10.1016/j.quascirev.2012.08.004

Barrere, M., Domine, F., Belke-Brea, M., & Sarrazin, D. (2018). Snowmelt events in autumn can reduce or cancel the soil warming effect of snow-vegetation interactions in the arctic. *Journal of Climate*, *31*(23), 9507–9518. https://doi.org/10.1175/JCLI-D-18-0135.1

Berger, A., & Loutre, M. F. (1997). Intertropical Latitudes and Precessional and Half-Precessional Cycles. *Science*, *278*(5342), 1476–1478. https://doi.org/10.1126/science.278.5342.1476

Berger, A., Loutre, M. F., Lema, D. G. G., Cyclotron, C., & Louvam-la-neuve, B. I. (1991). Insolation values for the climate of the last 10 million years. *Quaternary Science Reviews*, *10*(1988), 297–317. https://doi.org/10.1016/0277-3791(91)90033-Q

Berger, A., Loutre, M. F., & Mélice, J. L. (2006). Equatorial insolation: from precession harmonics to eccentricity frequencies. *Climate of the Past Discussions*, *2*(2), 519–533. https://doi.org/10.5194/cpd-2-519-2006

Billups, K., & Scheinwald, A. (2014). Origin of millennial-scale climate signals in the subtropical North Atlantic. *Paleoceanography*, *29*(6), 612–627. https://doi.org/10.1002/2014PA002641

Bischof, J. (2000). *Ice Drift, Ocean Circulation and Climate Change*. Norfolk, Virgina: Springer-Praxis Publishing Ltd.

Brigham-Grette, J. (2001). New perspectives on Beringian Quaternary paleogeography, stratigraphy, and glacial history. *Quaternary Science Reviews*, *20*(1–3), 15–24. https://doi.org/10.1016/S0277-3791(00)00134-7

Briner, J. P., & Kaufman, D. S. (2000). Late Pleistocene Glaciation of the Southwestern Ahklun Mountains, Alaska. *Quaternary Research*, *53*(1), 13–22. https://doi.org/10.1006/qres.1999.2088

Briner, J. P., & Kaufman, D. S. (2008). Late Pleistocene mountain glaciation in Alaska: key chronologies. *Journal of Quaternary Science*, *23*, 659–670. https://doi.org/10.1002/jqs

Caissie, B. E., Brigham-Grette, J., Cook, M. S., & Colmenero-Hidalgo, E. (2016). Bering Sea surface water conditions during Marine Isotope Stages 12 to 10 at Navarin Canyon (IODP Site U1345). *Climate of the Past*, *12*(9), 1739–1763. https://doi.org/10.5194/cp-12-1739-2016

Caissie, B. E., Brigham-Grette, J., Lawrence, K. T., Herbert, T. D., & Cook, M. S. (2010). Last Glacial Maximum to Holocene sea surface conditions at Umnak Plateau, Bering Sea, as inferred from diatom, alkenone, and stable isotope records. *Paleoceanography*, *25*(1), 1–16. https://doi.org/10.1029/2008PA001671

Calkin, P. E., Wiles, G. C., & Barclay, D. J. (2001). Holocene coastal glaciation of Alaska. *Quaternary Science Reviews*, *20*(1–3), 449–461. https://doi.org/10.1016/S0277-3791(00)00105-0

Clemens, S. C., Prell, W. L., Sun, Y., Liu, Z., & Chen, G. (2008). Southern

Hemisphere forcing of Pliocene δ18O and the evolution of Indo-Asian monsoons. *Paleoceanography*, *23*(4), 1–15. https://doi.org/10.1029/2008PA001638

Clemens, S., & Tiedemann, R. (1997). Eccentricity Forcing of Pliocene-early Pleistocene. *Nature*.385, 801-804. https://doi.org/10.1038/385801a0

Cloud Jr, P. E. (1955). Physical limits of glauconite formation. *Bulletin of the American Society of Petroleum Geologists*, *39*(4), 484–492. https://doi.org/10.1306/5CEAE166-16BB-11D7-8645000102C1865D

Creager, J. S., Scholl, D. W., & Supko, P. R. (1973). *Initial Reports of the Deep Sea Drilling Program, Volume 19*. Washington. https://doi.org/doi:10.2973/dsdp.proc.19.1973

Darby, D. A., Myers, W. B., Jakobsson, M., & Rigor, I. (2011). Modern dirty sea ice characteristics and sources: The role of anchor ice. *Journal of Geophysical Research: Oceans*, *116*(9), 1–18. https://doi.org/10.1029/2010JC006675

Dethleff, D. (2005). Entrainment and export of Laptev Sea ice sediments, Siberian Arctic. *Journal of Geophysical Research C: Oceans*, *110*(7), 1–17. https://doi.org/10.1029/2004JC002740

Dethleff, D., & Kuhlmann, G. (2009). Entrainment of fine-grained surface deposits into new ice in the southwestern Kara Sea, Siberian Arctic. *Continental Shelf Research*, *29*(4), 691–701. https://doi.org/10.1016/j.csr.2008.11.009

Dowdeswell, J. A. (1986). The distribution and character of sediments in a tidewater glacier, Southern Baffin Island. *Arctic and Alpine Research*, *18*, 45–56. Retrieved from http://www.jstor.org/stable/30065541

Dowdeswell, J. A., & Dowdeswell, E. K. (1989). Debris in Icebergs and Rates of Glaci-Marine Sedimentation: Observations from Spitsbergen and a Simple Model. *The Journal of Geology*, *97*(2), 221–231.

Drake, M. K., Aiello, I. W., & Ravelo, A. C. (2014). New Method for the Quantitative Analysis of Smear Slides in Pelagic and Hemi-Pelagic Sediments of the Bering Sea. *Fall Meeting, AGU*, *December 1*.

Dunhill, G. (1998). *Comparison of Sea-ice and Glacial-ice Rafted Debris: Grain Size, Surface Features, and Grain Shape*. U.S. Geological Survey. https://doi.org/10.3133/ofr98367

Elias, S., & Brigham-Grette, J. (2007). Late Pleistocene Glacial Events in Beringia.

Encyclopedia of Quaternary Science, (1), 191–201.
https://doi.org/10.1016/B978-0-444-53643-3.00116-3

Ferretti, P., Crowhurst, S. J., Naafs, B. D. A., & Barbante, C. (2015). The Marine
Isotope Stage 19 in the mid-latitude North Atlantic Ocean: Astronomical
signature and intra-interglacial variability. *Quaternary Science Reviews*, *108*,
95–110. https://doi.org/10.1016/j.quascirev.2014.10.024

Fetterer, F., Knowles, K., Meier, W., Savoie, M., & Windnagel, A. K. (2016). *Sea Ice
Index, Version 2 [Monthly Sea Ice Extent]*. Boulder, Colorado USA.
https://doi.org/http://dx.doi.org/10.7265/N5736NV7

Francke, A., Wennrich, V., Sauerbrey, M., Juschus, O., Melles, M., & Brigham-
Grette, J. (2013). Multivariate statistic and time series analyses of grain-Size
data in quaternary sediments of Lake El'gygytgyn, NE Russia. *Climate of the
Past*, *9*(6), 2459–2470. https://doi.org/10.5194/cp-9-2459-2013

Frey, K. E., Moore, G. W. K., Cooper, L. W., & Grebmeier, J. M. (2015). Divergent
patterns of recent sea ice cover across the Bering, Chukchi, and Beaufort seas of
the Pacific Arctic Region. *Progress in Oceanography*, *136*, 32–49.
https://doi.org/10.1016/j.pocean.2015.05.009

Ghil, M, Allen, M. R., Dettinger, M. D., Ide, K., Kondrashov, D., Mann, M. E., …
Yiou, P. (2002). Advanced spectral methods for climate time series. *Reviews of
Geophysics*, *40*(1), 3.1-3.41. https://doi.org/10.1029/2001RG000092

Ghil, Michael. (1994). Cryothermodynamics: the chaotic dynamics of paleoclimate.
Physica D: Nonlinear Phenomena, *77*(1–3), 130–159.
https://doi.org/10.1016/0167-2789(94)90131-7

Gildor, H., & Tziperman, E. (2000). Sea ice as the glacial cycles' climate switch Role
of seasonal and orbital forcing. *Paleoceanography*, *15*(6), 605–615.
https://doi.org/10.1029/1999PA000461

Gorbarenko, S. A., Wang, P., Wang, R., & Cheng, X. (2010). Orbital and suborbital
environmental changes in the southern Bering Sea during the last 50kyr.
Palaeogeography, Palaeoclimatology, Palaeoecology, *286*(1–2), 97–106.
https://doi.org/10.1016/j.palaeo.2009.12.014

Groth, A., & Ghil, M. (2015). Monte Carlo singular spectrum analysis (SSA)
revisited: Detecting oscillator clusters in multivariate datasets. *Journal of
Climate*, *28*(19), 7873–7893. https://doi.org/10.1175/JCLI-D-15-0100.1

Gualtieri, L., Glushkova, O., & Brigham-Grette, J. (2000). Evidence for restricted ice

extent during the last glacial maximum in the Koryak Mountains of Chukotka, far Eatern Russia. *Bulletin of the Geological Society of America*, *112*(7), 1106–1118. https://doi.org/10.1130/0016-7606(2000)112<1106:EFRIED>2.0.CO;2

Hagelberg, T. K., Bond, G., & DeMenocal, P. (1994). Milankovitch band forcing of sub-Milankovitch climate variability during the Pleistocene. *Paleoceanography*, *9*(4), 545–558. https://doi.org/10.1029/94PA00443

Hay, J. D., Imbrie, J., & Shackleton, N. J. (1976). Variations in the Earth's Orbit: Pacemaker of the Ice Ages. *Science*, *194*, 1121–1132. https://doi.org/10.1126/science.194.4270.1121

He, S., Gao, Y., Li, F., Wang, H., & He, Y. (2017). Impact of Arctic Oscillation on the East Asian climate: A review. *Earth-Science Reviews*, *164*, 48–62. https://doi.org/10.1016/j.earscirev.2016.10.014

Heiser, P. A., & Roush, J. J. (2001). Pleistocene glaciations in Chukotka, Russia; moraine mapping using satellite synthetic aperture radar (SAR) imagery. *Quaternary Science Reviews*, *20*(1–3), 393–404. https://doi.org/10.1016/S0277-3791(00)00109-8

Herbert, T. D., Peterson, L. C., Lawrence, K. T., & Liu, Z. (2010). Tropical ocean temperatures over the past 3.5 million years. *Science*, *328*(5985), 1530–1534. https://doi.org/10.1126/science.1185435

Hopkins, D. M. (1982). Aspects of the paleogeography of Beringia during the late Pleistocene. In *Paleoecology of Beringia* (pp. 3–28). Elsevier. https://doi.org/10.1016/b978-0-12-355860-2.50008-9

Hopkins, D. M., & Einarsson, T. (1966). Pleistocene Glaciation on St . George , Pribilof Islands. *Science*, *152*(3720), 343–345. https://doi.org/10.1126/science.152.3720.343

Horikawa, K., Martin, E. E., Basak, C., Onodera, J., Seki, O., Sakamoto, T., … Kawamura, K. (2015). Pliocene cooling enhanced by flow of low-salinity Bering Sea water to the Arctic Ocean. *Nature Communications*, *6*, 7587. https://doi.org/10.1038/ncomms8587

Huybers, P. (2006). Early Pleistocene glacial cycles and the integrated summer insolation forcing. *Science*, *313*(5786), 508–511. https://doi.org/10.1126/science.1125249

Huybers, P. (2011). Combined obliquity and precession pacing of late Pleistocene deglaciations. *Nature*, *480*(7376), 229–232. https://doi.org/10.1038/nature10626

Huybers, P., & Wunsch, C. (2005). Obliquity pacing of the late Pleistocene glacial terminations. *Nature*, *434*(7032), 491–494. https://doi.org/10.1038/nature03401

Ikenoue, T., Okazaki, Y., Takahashi, K., & Sakamoto, T. (2015). Bering sea radiolarian biostratigraphy and paleoceanography at IODP site U1341 during the last four million years. *Deep Sea Research Part II: Topical Studies in Oceanography*, 1–18. https://doi.org/10.1016/j.dsr2.2015.03.004

Imbrie, J., Berger, A., Boyle, E. A., Clemens, S. C., Duffy, A., Howard, W. R., … Lemaitre, G. (1993). On the structure and origin of major glaciation cycles 2. The 100,000 year cycle. *Paleoceanography*, *8*(6), 699–735. https://doi.org/10.1029/93PA02751

Iwasaki, S., Takahashi, K., Kanematsu, Y., Asahi, H., Onodera, J., & Ravelo, A. C. (2016). Paleoproductivity and paleoceanography of the last 4.3 Myrs at IODP Expedition 323 Site U1341 in the Bering Sea based on biogenic opal content. *Deep-Sea Research Part II: Topical Studies in Oceanography*, *125–126*, 145–154. https://doi.org/10.1016/j.dsr2.2015.04.005

Jaeger, J. M., & Koppes, M. N. (2016). The role of the cryosphere in source-to-sink systems. *Earth-Science Reviews*, *153*, 43–76. https://doi.org/10.1016/j.earscirev.2015.09.011

Jansen, E., Fronval, T., Rack, F., & Channell, J. E. T. (2000). Pliocene-Pleistocene ice rafting history and cyclicity in the Nordic Seas during the last 3.5 Myr. *Paleoceanography*, *15*(6), 709–721. https://doi.org/10.1029/1999PA000435

Katsuki, K., & Takahashi, K. (2005). Diatoms as paleoenvironmental proxies for seasonal productivity, sea-ice and surface circulation in the Bering Sea during the late Quaternary. *Deep-Sea Research Part II: Topical Studies in Oceanography*, *52*(16–18), 2110–2130. https://doi.org/10.1016/j.dsr2.2005.07.001

Kaufman, D. S., Briner, J. P., & Manley, W. F. (2004). Pleistocene maximum and Late Wisconsinan glacier extents across Alaska, USA. *Developments in Quaternary Sciences*, *2*, 9–27. https://doi.org/https://doi.org/10.1016/S1571-0866(04)80182-9

Kaufman, D. S., & Manley, W. F. (2004). Pleistocene Maximum and Late Wisconsinan glacier extents across Alaska, U. S. A. *Developments in Quaternary Sciences*, *2*, 9–27. https://doi.org/10.1016/S1571-0866(04)80182-9

Kempema, E. W., Reimnitz, E., & Barnes, P. W. (1989). Sea Ice Sediment

Entrainment and Rafting in the Arctic. *Journal of Sedimentary Petrology*, *59*(2), 308–317. https://doi.org/10.1306/212F8F80-2B24-11D7-8648000102C1865D

Knight, P. G. (1997). The basal ice layer of glaciers and ice sheets. *Quaternary Science Reviews*, *16*, 975–993. https://doi.org/0277-3791/97

Krissek, L. A. (1995). Late Cenozoic ice-rafting records from Leg 145 sites in the North Pacific: Late Miocene onset, late Pliocene intensification, and Pliocene-Pleistocene events. In D. K. Rea, I. A. Basov, D. W. Scholl, & J. F. Allan (Eds.), *Proc. ODP, Sci. Results, 145* (pp. 179–194). College Station, TX: Ocean Drilling Program. https://doi.org/10.2973/odp.proc.sr.145.118.1995

Kutzbach, J. E., & Guetter, P. J. (1986). The influence of changing orbital parameters and surface boundary conditions on climate simulatinos for the past 18000 years. *Journal of the Atmospheric Sciences*, *43*(16), 1726–1759. https://doi.org/10.1175/1520-0469(1986)043<1726:TIOCOP>2.0.CO;2

Lagoe, M. B., Eyles, C. H., Eyles, N., & Hale, C. (1993). Timing of late Cenozoic tidewater glaciation in the far North Pacific Timing of late Cenozoic tidewater glaciation in the far North Pacific. *Geological Society Of America Bulletin*, (12), 1542–1560. https://doi.org/10.1130/0016-7606(1993)105<1542

Laskar, J., Robutel, P., Joutel, F., Gastineau, M., Correia, a. C. M., & Levrard, B. (2004). A long-term numerical solution for the insolation quantities of the Earth. *Astronomy and Astrophysics*, *428*(1), 261–285. https://doi.org/10.1051/0004-6361:20041335

Lawrence, K. T., Sosdian, S., White, H. E., & Rosenthal, Y. (2010). North Atlantic climate evolution through the Plio-Pleistocene climate transitions. *Earth and Planetary Science Letters*, *300*(3–4), 329–342. https://doi.org/10.1016/j.epsl.2010.10.013

Le Treut, H., & Ghil, M. (1983). Orbital forcing, climatic interactions, and glaciation cycles. *Journal of Geophysical Research: Oceans*, *88*(C9), 5167–5190. https://doi.org/10.1029/JC088iC09p05167

Lee, S. Y., & Poulsen, C. J. (2009). Obliquity and precessional forcing of continental snow fall and melt: implications for orbital forcing of Pleistocene ice ages. *Quaternary Science Reviews*, *28*(25–26), 2663–2674. https://doi.org/10.1016/j.quascirev.2009.06.002

Li, F., & Wang, H. (2013). Relationship between Bering Sea ice cover and East Asian winter monsoon year-to-year variations. *Advances in Atmospheric Sciences*, *30*(1), 48–56. https://doi.org/10.1007/s00376-012-2071-2

Lisiecki, L. E., & Raymo, M. E. (2004). A Pliocene-Pleistocene stack of 57 globally distributed benthic δ 18 O records. *Paleoceanography*, (1). https://doi.org/10.1029/2004PA001071

Lisiecki, L. E., & Raymo, M. E. (2005). A Pliocene-Pleistocene stack of 57 globally distributed benthic 18O records. *Paleoceanography*, *20*(1), 1–17. https://doi.org/10.1029/2004PA001071

Lisitzin, A. (2002). Stages of lithogenesis in ice zones: Three types of sea ice sedimentation and two vertical levels of the process. In *Sea-ice and iceberg sedimentation in the ocean* (pp. 79–115). Berlin Heidelberg: Springer. https://doi.org/https://doi.org/10.1007/978-3-642-55905-1_6

Lovell, H., Fleming, E., Benn, D., Hubbard, B., Lukas, S., Rea, B. R., … Flink, A. E. (2015). Debris entrainment and landorm genesis during tidewater glacier surges. *Journal of Geophysical Research: Earth Surface*, *120*, 1574–1595. https://doi.org/10.1002/2015JF003509

Manley, W. F., Kaufman, D. S., & Briner, J. P. (2001). Pleistocene glacial history of the southern Ahklun Mountains, southwestern Alaska: Soil-development, morphometric, and radiocarbon constraints. *Quaternary Science Reviews*, *20*(1–3), 353–370. https://doi.org/10.1016/S0277-3791(00)00111-6

Marsaglia, K., Milliken, K., & Doran, L. (2013). *IODP Digital Reference for Smear Slides Analysis of Marine Mud. Part 1 : Methodology and Atlas of Siliciclastic and Volcanogenic Components*. IODP Technical Note 1. https://doi.org/10.2204/iodp.tn.1.2013

Martínez-Garcia, A., Rosell-Melé, A., McClymont, E. L., Gersonde, R., & Haug, G. H. (2010). Subpolar link to the emergence of the modern equatorial pacific cold tongue. *Science*, *328*(5985), 1550–1553. https://doi.org/10.1126/science.1184480

Maslin, M. A., Haug, G. H., Sarnthein, M., Tiedemann, R., Erlenkeuser, H., & Stax, R. (1995). Northwest Pacific Site 882: The Initiation of Northern Hemisphere Glaciation. In D.K. Rea, L. A. Basov, D. W. Scholl, & J. F. Allan (Eds.), *Proc. ODP, Sci. Results, 145* (pp. 315–329). College Station, TX: Ocean Drilling Program. 10.2973/odp.proc.sr.145.119.1995

McGuire, A. D., Chapin, F. S., Walsh, J. E., & Wirth, C. (2006). Integrated regional changes in arctic climate feedbacks: Implications for the global climate system. *Annual Review of Environment and Resources*, *31*, 61–91.

https://doi.org/10.1146/annurev.energy.31.020105.100253

McIntyre, A., & Molfino, B. (1996). Forcing of Atlantic Equatorial and Subpolar Millennial Cycles by Precession. *Science*, *274*(5294), 1867–1870. https://doi.org/10.1126/science.274.5294.1867

McIntyre, K., Delaney, M. L., & Ravelo, A. C. (2001). Millennial-scale climate change and oceanic processes in the late Pliocene and early Pleistocene. *Paleoceanography*, *16*(5), 535–543. https://doi.org/10.1029/2000PA000526

McKelvey, B., Chen, W., & Arculus, R. (1995). Provenance of Pliocene-Pleistocene ice-rafted debris, Leg 145, Northern Pacific Ocean. In D. K. Rea, I. A. Basov, D. W. Scholl, & J. F. Allan (Eds.), *Proc. ODP, Sci. Results, 145* (pp. 195–204). College Station, TX: Ocean Drilling Program. doi:10.2973/odp.proc.sr.145.120.1995

McRae, S. G. (1972). Glauconite. *Earth-Science Reviews*, *8*(4), 397–440. https://doi.org/10.1016/0012-8252(72)90063-3

Meyers, S. R. (2012). Seeing red in cyclic stratigraphy: Spectral noise estimation for astrochronology. *Paleoceanography*, *27*(3), 1–12. https://doi.org/10.1029/2012PA002307

Meyers, S. R. (2015). Testing and Time Scale Optimization. *Paleoceanography*, *30*, 1625–1640. https://doi.org/10.1002/2015PA002850

Milankovitch, M. K. (1941). Kanon der Erdbestrahlung und seine Anwendung auf das Eiszeitenproblem. *Royal Serbian Academy Special Publication*, *133*, 1–633. Retrieved from https://ci.nii.ac.jp/naid/10009278924

Miller, K. G., Browning, J. V., John Schmelz, W., Kopp, R. E., Mountain, G. S., & Wright, J. D. (2020). Cenozoic sea-level and cryospheric evolution from deep-sea geochemical and continental margin records. *Science Advances*, *6*(20). https://doi.org/10.1126/sciadv.aaz1346

Molnia, B. F. (2007). Late nineteenth to early twenty-first century behavior of Alaskan glaciers as indicators of changing regional climate. *Global and Planetary Change*, *56*(1–2), 23–56. https://doi.org/10.1016/j.gloplacha.2006.07.011

Naafs, B. D. A., Hefter, J., Acton, G., Haug, G. H., Martínez-Garcia, A., Pancost, R., & Stein, R. (2012). Strengthening of North American dust sources during the late Pliocene (2.7Ma). *Earth and Planetary Science Letters*, *317–318*, 8–19.

https://doi.org/10.1016/j.epsl.2011.11.026

Nechaev, V. P., Sorochinskaya, A. V., Tsoy, I. B., & Gorbarenko, S. A. (1994). Clastic components in Quaternary sediments of the northwest Pacific and their paleo-oceanic significance. *Marine Geology*, *118*(1–2), 119–137. https://doi.org/10.1016/0025-3227(94)90116-3

Niebauer, H. J. (1988). Interannual Variability in the Subarctic Bering Sea. *Journal Geophysical Research*, *93*, 5051–5068. https://doi.org/10.1029/JC093iC05p05051

Onodera, J., Takahashi, K., & Nagatomo, R. (2013). Diatoms, silicoflagellates, and ebridians at Site U1341 on the western slope of Bowers Ridge, IODP Expedition 323. *Deep Sea Research Part II: Topical Studies in Oceanography*, 1–10. https://doi.org/10.1016/j.dsr2.2013.03.025

Overland, J. E., & Pease, C. H. (1982). Cyclone Climatology of the Bering Sea and Its Relation to Sea Ice Extent. *Monthly Weather Review*, *110*(1), 5–13. https://doi.org/10.1175/1520-0493(1982)110<0005:CCOTBS>2.0.CO;2

Pease, C. H. (1980). Eastern Bering Sea Ice Processes. *Monthly Weather Review*, *108*(12), 2015–2023. https://doi.org/https://doi.org/10.1175/1520-0493(1980)108<2015:EBSIP>2.0.CO;2

Pettijohn, F. (1975). *Sedimentary Rocks*. Harper & Row.

Raymo, M. E., Lisiecki, L. E., & Nisancioglu, K. H. (2006). Plio-Pleistocene Ice Volume, Antarctic Climate, and the Global 18O Record. *Science*, *313*, 492–495. https://doi.org/10.1126/science.1123296

Raymo, Maureen E., & Huybers, P. (2008). Unlocking the mysteries of the ice ages. *Nature*, *451*, 284–285. https://doi.org/10.1038/nature06589

Raymo, Maureen E., & Nisancioglu, K. (2003). The 41 kyr world: Milankovitch's other unsolved mystery. *Paleoceanography*, *18*(1), 1–6. https://doi.org/10.1029/2002PA000791

Reimnitz, E., Cormick, M., Bischof, J., & Darby, D. A. (1998). Comparing sea-ice sediment load with Beaufort Sea shelf deposits is entrainment selective? *Journal of Sedimentary Research*, *68*, 777–787. https://doi.org/10.2110/jsr.68.777

Reimnitz, E., Kempema, E. W., & Barnes, P. W. (1986). *Anchor ice and bottom-freezing in high latitude marine sedimentary environments: observations from the Alaskan Beaufort Sea*. Menlo Park, CA. https://doi.org/10.3133/ofr86298

Reimnitz, E., Kempema, E. W., & Barnes, P. W. (1987). Anchor Ice, Seabed Freezing, and Sediment Dynamics in Shallow Arctic Seas. *Journal of Geophysical Research*, *92*, 671–678. https://doi.org/10.1029/JC092iC13p14671

Reimnitz, E., Marincovich Jr., L., McCormick, M., & Briggs, W. M. (1992). Suspension freezing of bottom sediment and biota in the Northwest Passage and implications for Arctic Ocean sedimentation. *Canadian Journal of Earth Sciences*, *29*(4), 693–703. https://doi.org/10.1139/e92-060

Reimnitz, E., Mccormick, M., Mcdougall, K., & Brouwers, E. (1993). Sediment Export by Ice Rafting from a Coastal Polynya, Arctic Alaska. *Arctic and Alpine Research*, *25*(2), 83–98.

Rial, J. A., & Anaclerio, C. A. (2000). Understanding nonlinear responses of the climate system to orbital forcing. *Quaternary Science Reviews*, *19*, 1709–1722. 10.1016/S0277-3791(00)00087-1

Ridgwell, A. J., Watson, A. J., & Raymo, M. E. (1999). Is the spectral signature of the 100 kyr glacial cycle consistent with a Milankovitch origin? *Paleoceanography*, *14*(4), 437–440. https://doi.org/10.1029/1999PA900018

Rodionov, S. N., Bond, N. a., & Overland, J. E. (2007). The Aleutian Low, storm tracks, and winter climate variability in the Bering Sea. *Deep-Sea Research Part II: Topical Studies in Oceanography*, *54*(23–26), 2560–2577. https://doi.org/10.1016/j.dsr2.2007.08.002

Rodionov, Sergei N., Overland, J. E., & Bond, N. A. (2005). The Aleutian low and winter climatic conditions in the Bering Sea. Part I: Classification. *Journal of Climate*, *18*(1), 160–177. https://doi.org/10.1175/JCLI3253.1

Sancetta, C., Heusser, L., Labeyrie, L., Naidu, A. S., & Robinson, S. W. (1985). Wisconsin—Holocene paleoenvironment of the Bering Sea: Evidence from diatoms, pollen, oxygen isotopes and clay minerals. *Marine Geology*, *62*(1–2), 55–68. https://doi.org/10.1016/0025-3227(84)90054-9

Sancetta, C., & Robinson, S. W. (1983). Diatom evidence on Wisconsin and Holocene events in the Bering Sea. *Quaternary Research*, *20*(2), 232–245. https://doi.org/10.1016/0033-5894(83)90079-0

Short, D. A., Mengel, J. G., Crowley, T. J., Hyde, W. T., & North, G. R. (1991). Filtering of milankovitch cycles by earth's geography. *Quaternary Research*, *35*(2), 157–173. https://doi.org/10.1016/0033-5894(91)90064-C

St John, K., & Krissek, L. A. (1999). Regional patterns of Pleistocene ice-rafted debris flux in the North Pacific. *Paleoceanography*, *14*(5), 653–662. https://doi.org/https://doi.org/10.1029/1999PA900030

Stabeno, P., Bond, N. A., Kachel, N. B., Salo, S. A., & Schumacher, J. D. (2001). On the temporal variability of the physical environment over the south-eastern Bering Sea. *Fisheries Oceanography*, *10*, 81–98. **10.1046/j.1365-2419.2001.00157.x**

Stabeno, P. J., Kachel, N. B., Moore, S. E., Napp, J. M., Sigler, M., Yamaguchi, A., & Zerbini, A. N. (2012). Comparison of warm and cold years on the southeastern Bering Sea shelf and some implications for the ecosystem. *Deep-Sea Research Part II: Topical Studies in Oceanography*, *65–70*, 31–45. https://doi.org/10.1016/j.dsr2.2012.02.020

Stringer, W. J., & Groves, J. E. (1991). Location and Areal Extent of Polynyas in the Bering and Chukchi Seas. *Arctic*, *44*, 164–171. Retrieved from http://www.jstor.org/stable/40510994

Stroynowski, Z., Abrantes, F., & Bruno, E. (2017). The response of the Bering Sea Gateway during the Mid-Pleistocene Transition. *Palaeogeography, Palaeoclimatology, Palaeoecology*, *485*, 974–985. https://doi.org/10.1016/j.palaeo.2017.08.023

Stroynowski, Z., Ravelo, A. C., & Andreasen, D. (2015). A Pliocene to recent history of the Bering Sea at Site U1340A, IODP Expedition 323. *Paleoceanography*, *30*(12), 1641–1656. https://doi.org/10.1002/2015PA002866

Strum, M., Schimel, J., Michaelson, G., Welker, J. M., Oberbauer, S. F., Liston, G. E., … Romanovsky, V. E. (2005). Winter biological processes could help convert Arctic tundra to shrubland. *BioScience*, *55*, 323–334. https://doi.org/10.1641/0006-3568(2005)055

Sun, J., & Huang, X. (2006). Half-precessional cycles recorded in Chinese loess: response to low-latitude insolation forcing during the Last Interglaciation. *Quaternary Science Reviews*, *25*(9–10), 1065–1072. https://doi.org/10.1016/j.quascirev.2005.08.004

Sun, Y., Clemens, S. C., An, Z., & Yu, Z. (2006). Astronomical timescale and palaeoclimatic implication of stacked 3.6-Myr monsoon records from the Chinese Loess Plateau. *Quaternary Science Reviews*, *25*, 33–48. https://doi.org/10.1016/j.quascirev.2005.07.005

Tabor, C. R., Poulsen, C. J., & Pollard, D. (2015). How obliquity cycles powered early Pleistocene global ice-volume variability. *Geophysical Research Letters*, *42*, 1871–1879. https://doi.org/10.1002/2015GL063322.

Takahashi, K., Ravelo, A. C., Alvarez Zarikian, C., & Expedition 323 Scientists. (2011). *Proc. IODP, 323*. Tokyo. https://doi.org/10.2204/ iodp.proc.323.2011

Teraishi, A., Suto, I., Onodera, J., & Takahashi, K. (2013). Diatom, silicoflagellate and ebridian biostratigraphy and paleoceanography in IODP 323 Hole U1343E at the Bering slope site. *Deep Sea Research Part II: Topical Studies in Oceanography*, 1–11. https://doi.org/10.1016/j.dsr2.2013.03.026

Ukita, J., Honda, M., Nakamura, H., Tachibana, Y., Cavalieri, D. J., Parkinson, C. L., … Yamamoto, K. (2007). Northern Hemisphere sea ice variability: Lag structure and its implications. *Tellus*, *Series A: Dynamic Meteorology and Oceanography*, *59*(2), 261–272. https://doi.org/10.1111/j.1600-0870.2006.00223.x

Vaughn, D. R., & Caissie, B. E. (2017). Effects of sea-level, sea-ice extent, and nutrient availability on primary production at the Umnak Plateau, Bering Sea (IODP Site U1339) during Marine Isotope Stage (MIS) 5. *Palaeogeography, Palaeoclimatology, Palaeoecology*, *485*, 283–292. https://doi.org/10.1016/j.palaeo.2017.06.020

Vautard, R., Yiou, P., & Ghil, M. (1992). Singular-spectrum analysis: A toolkit for short, noisy chaotic signals. *Physica D: Nonlinear Phenomena*, *58*(1–4), 95–126. https://doi.org/10.1016/0167-2789(92)90103-T

Venti, N. L., Billups, K., & Herbert, T. D. (2013). Increased sensitivity of the Plio-Pleistocene northwest Pacific to obliquity forcing. *Earth and Planetary Science Letters*, *384*, 121–131. https://doi.org/10.1016/j.epsl.2013.10.007

Waller, R. I., Hart, J. K., & Knight, P. G. (2000). The influence of tectonic deformation on facies variability in stratifed debris-rich basal ice. *Quaternary Science Reviews*, *19*, 775–786.10.1016/S0277-3791(99)00035-9

Wara, M. W., Ravelo, A. C., & Revenaugh, J. S. (2000). The pacemaker always rings twice. *Paleoceanography*, *15*(6), 616–624. https://doi.org/https://doi.org/10.1029/2000PA000500

Wendler, G., Chen, L., & Moore, B. (2014). Recent sea ice increase and temperature decrease in the Bering Sea area, Alaska. *Theoretical and Applied Climatology*, *117*(3–4), 393–398. https://doi.org/10.1007/s00704-013-1014-x

White, J. M., Ager, T. A., Adam, D. P., Leopold, E. B., Liu, G., Jetté, H., &

Schweger, C. E. (1997). An 18 million year record of vegetation and climate change in northwestern Canada and Alaska: Tectonic and global climatic correlates. *Palaeogeography, Palaeoclimatology, Palaeoecology*, *130*(1–4), 293–306. https://doi.org/10.1016/S0031-0182(96)00146-0

Woodgate, R. A., & Aagaard, K. (2005). Revising the Bering Strait freshwater flux into the Arctic Ocean. *Geophysical Research Letters*, *32*(2), 1–4. https://doi.org/10.1029/2004GL021747

Yiou, P., Ghil, M., Jouzel, J., Paillard, D., & Vautard, R. (1994). Nonlinear variability of the climatic system from singular and power spectra of Late Quaternary records. *Climate Dynamics*, *9*(8), 371–389. https://doi.org/10.1007/BF00207933

Chapter 4: Evolution of sea surface temperature in the West Pacific warm pool (Site U1488) over the last 10 Million years

Michelle K. Drake[1], Ana Christina Ravelo[1], Anna Joy Drury[2], Takuya Sagawa[3]

[1] Ocean Sciences Department, University of California, 1156 High Street, Santa Cruz, California, 95064, USA

[2] MARUM, University of Bremen, Leobenerstrasse, Bremen, 28359, Germany

[3] Institute of Science Engineering, Kanazawa University, Kakuma-Machi, Kanazawa, 920-1192, Japan

Abstract

The modern tropical Pacific mean state is characterized by a zonal asymmetry

between the eastern equatorial Pacific cold tongue and the western equatorial (WEP)

Pacific warm pool. It is well established that this mean state is not static and can

change on interannual as well as geologic timescales. The early Pliocene mean state,

the so-called El Padre, is characterized by a reduced zonal sea surface temperature

(SST) gradient, a deeper and/ or warmer thermocline, as well as shifts in temperature

and precipitation like modern El Niño teleconnections. However, because of the

scarcity in WEP warm pool data it has remained unclear if El Padre conditions were

unique to the early Pliocene or if they were also present during the late Miocene. Here

we show there is no long-term trend in the SSTs of the WEP warm pool over the last

9.7 million years, although there are temperature fluctuations of 1°C to 3°C. We

further demonstrate that the tropical Pacific zonal SST gradient was reduced between

9.7 to 4.4 Ma and propose that El Padre conditions were persistent throughout this

period. This work is the first to confirm the results of Wara et al. (2005) and our Site

U1488 record is the first continuous moderate resolution (25 kyr) Mg/Ca-temperature record for the WEP that extends into the late Miocene.

Introduction

The western equatorial Pacific (WEP) warm pool is a major source of heat and moisture for the atmosphere and has significant teleconnections to extratropical regions, therefore small changes in surface temperatures can have substantial influence on global climate (Palmer & Manfield, 1984; Taschetto et al., 2021). The warm pool, defined by sea surface temperatures (SST) that exceed 28°C, together with the cool SST of the eastern equatorial Pacific (EEP) characterize the zonal SST gradient of the modern tropical Pacific mean state. Other characteristics of the modern mean state include an asymmetry in the sea surface height and thermocline depth between the WEP and the EEP. The zonal asymmetry is sustained by the Bjerknes feedback, which is an atmosphere-ocean interaction where a strong zonal SST gradient drive easterly surface winds that lead to an asymmetry in the subsurface thermocline that is a positive feedback on the SST gradient through upwelling of cold thermocline waters in the EEP (Bjerknes, 1989). Another process that influences the tropical Pacific mean state is known as the 'ocean tunnel', where the subtropical surface temperatures are transferred to the EEP through the ventilated thermocline that is advected via the shallow subtropical cells (Burls et al., 2017; Gu & Philander, 2004). The tropical Pacific mean sate is not static and is known to change on interannual (e.g., El Niño) and geologic timescales with major implications for global climate. There is an ongoing debate about the 20th century trend in tropical Pacific

99

SSTs and zonal gradient (Deser et al., 2010; Tokinaga et al., 2012a), the result of which has implications for future climate change. This study looks to the geologic record to study the evolution of tropical Pacific conditions during periods considered possible analogues to future equilibrium climate states (Tierney et al., 2020). We focus on the early Pliocene and late Miocene because the boundary conditions are similar to modern, but paradoxically global temperatures were significantly warmer than today (Federov et al., 2006; LaRiviere et al., 2012). Surprisingly, during the early Pliocene the WEP warm pool temperatures remained near modern values (± 1-2°C), which is an important feature of the well documented mean state during this period referred to as a 'permanent El Niño-like' state or 'El Padre' conditions (Ford et al., 2015; Wara et al., 2005).

The early Pliocene tropical Pacific 'El Padre' mean state is characterized by a reduced zonal SST gradient across the tropical Pacific (Ravelo et al., 2014), driven by significantly warmer SSTs in the EEP cold tongue (Herbert et al., 2016; Lawrence et al., 2006; Liu and Herbert, 2004; Rousselle et al., 2013), but near modern temperatures in the WEP warm pool (Wara et al., 2005). Other features of El Padre are the latitudinal expansion of the Pacific warm pool (Brierley et al., 2009), a deeper and/or warmer thermocline across the tropical Pacific (Chaisson & Ravelo, 2000; Ford et al., 2015, 2012; Steph et al., 2010; Wara et al., 2005), and far-field changes to precipitation patterns (Burls et al., 2017; Molnar & Cane, 2007, 2002). It remains unknown if the distinct El Padre mean state was limited to the early Pliocene and this

100

study investigates if it was also a feature of the tropical Pacific during the late Miocene.

The late Miocene was a period of global warmth with a reduced meridional SST gradient (Herbert et al., 2016; LaRiviere et al., 2012), but our understanding of tropical Pacific temperature evolution is limited during this period by the dearth of data from the WEP warm pool. Although the late Miocene SST distribution is well constrained by the comprehensive compilation of continuous SST records from Herbert et al. (2016), the WEP warm pool was not included in this analysis due to the limitations of the alkenone paleothermometer. This paleothermometer reaches saturation at temperatures greater than 28°C to 30°C (Conte et al., 2006; Muller et al., 1998) and although alternative calibrations expand the temperature range of the paleothermometer (i.e., Tierney & Tingley, 2019b) the proxy remains less than ideal for warm regions like the WEP warm pool. Before this study, the only continuous temperature estimate of the WEP warm pool extending into the late Miocene was generated with the paleothermometer TEX_{86} (Zhang et al., 2014). The TEX_{86} proxy is an estimate of SST (Schouten et al., 2002; Kim et al., 2010), but this interpretation is complicated by data that correlate the proxy to subsurface temperatures under certain oceanographic conditions (Huguet et al., 2007; Pearson & Ingalls, 2013; Turich et al., 2007; Wuchter et al., 2005) as well studies demonstrating non-thermal factors influence the proxy (Schouten et al., 2013). In this study we use the Mg/Ca temperature proxy to examine the temperature evolution of the WEP warm pool and shed light on the conditions of the late Miocene. The Mg/Ca paleothermometer has

been successfully used in the WEP warm pool during the Pliocene and middle Miocene (e.g., Ford et al., 2015; Sosdian et al., 2020; Wara et al., 2005) although the proxy is not without issue. How to correct the Mg/Ca temperature data to account for the secular changes in the Mg/Ca ratio of seawater overtime has been debated and no standardize process has been agreed upon yet (e.g., Medina-Elizalde et al., 2008; O'Brien et al., 2014).

While each paleo-temperature proxy has limitations, it is critical to further our understanding of the long-term temperature trends in the WEP during past warm periods because it may help us understand possible consequences of anthropogenic warming, an area of ongoing debate (Coats & Karnauska, 2017; Seager et al., 2019; Xie et al., 2020), and has implications for global precipitation patterns (e.g., Taschetto et al., 2020). Furthermore, here is a discrepancy between late Miocene paleo-proxy data and paleoclimate model simulations, with models generally underestimating high latitude SSTs and overestimating tropical SSTs such as in the WEP warm pool (e.g., Burls et al., 2021). Therefore, it is critical to create good SST records from the WEP warm pool during the late Miocene because there is currently a dearth of data, and it is a region where there is a significant model-data discrepancy.

To evaluate the long-term evolution of WEP warm pool mixed-layer temperatures since the late Miocene we generate a Mg/Ca-derived temperature record from the recently drilled International Ocean Discovery Program (IODP) Expedition 363 Site U1488. We find there is no long-term trend in WEP warm pool surface temperatures over the last 9.7 million years (Myr). Using this new record, we also evaluate the

evolution of tropical Pacific zonal and meridional SST gradient and our analysis suggests the El Padre conditions of the early Pliocene were present during the late Miocene. This study presents the first continuous 9.7 Myr Mg/Ca-temperature record for the WEP warm pool.

Material and Methods

Site location and age model

IODP Expedition 363 Site U1488 (02°02.59'N, 141°45.29'E) is located on the top of the southern Eauripik Rise at 2604 meters water depth (Figure 1). The sediments at the site are classified as foraminifer-nannofossil ooze. Preservation of planktic foraminifers is good to very good throughout the core but are moderate to poor in the oldest samples ~9.69 Ma (Rosenthal et al., 2017). The appearance of the planktic foraminifers used in this study were mostly opaque or frosty. The age model includes shipboard and updated paleomagnetic datums (0-3 Ma) and calcareous nannofossil biostratigraphic datums in the older (>5 Ma) portion of the record (Table 1; Rosenthal et al., 2018). We tuned our planktic foraminifer carbon isotope data to the ODP site 1146 record using the start and end of the late Miocene carbon isotopic shift (LMCIS) as two tie points (Table 1; Holbourn et al., 2018).
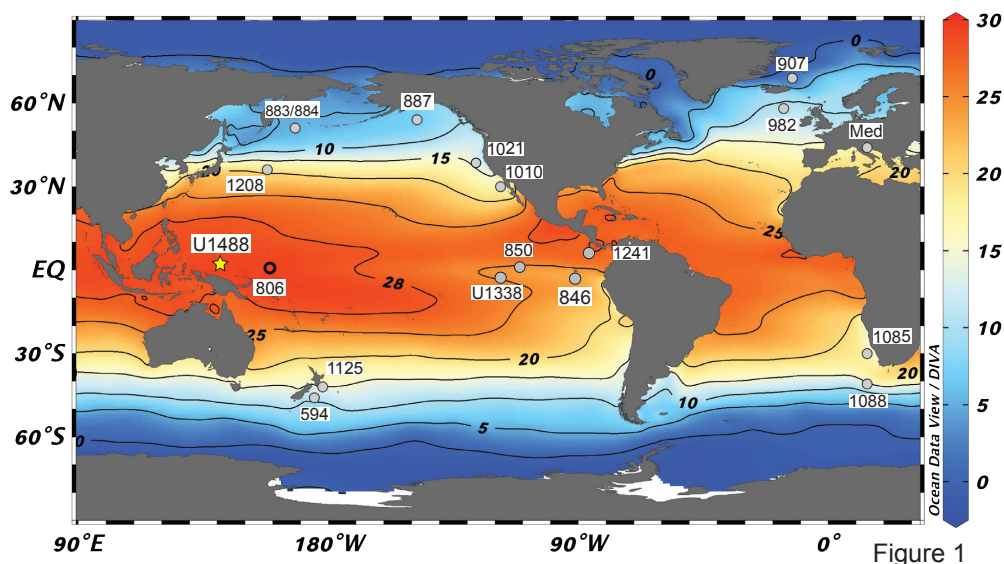
Figure 1. Map of study site and sites referenced. WEP warm pool site IODP Expedition 363 Site U1488 (2°N, 141°E) indicated with yellow star and ODP site 806 indicated with open circle. Previously published alkenone temperature records used in this study indicated with grey circle. Modern SST climatology (Locarnini et al., 2013). Map generated with Ocean Data View software, http://odv.awi.de. Site information and references can be found in Table 2.

Table 1. Age Model for IODP Exp 363 Site U1488		
Event	Depth ccsf-a (m)	Age (Ma)
Brunhes-Matayama	20.79	0.781
Upper Jaramillo	26.05	0.988
Lower Jaramillo	28.11	1.072
Upper Olduvai	43.51	1.778
Lower Olduvai	47.38	1.945
Matuyama/Gauss	65.84	2.581
Upper Keana	78.92	3.020
Lower Keana	82.19	3.116
Upper Mammoth	84.48	3.207
Gauss/Gilbert	94.46	3.596
T Ceratolithus armatus (mid)	144.94	5.080
B Ceratolithus armatus	163.40	5.350
T Discoaster quinqueramus	173.15	5.590
T Nicklithus amplificus	190.73	5.980
Tie Point ODP 1146 (end LMCIS)	216.56	6.675
Tie Point ODP 1146 (start LMCIS)	270.87	8.018
Bpa Reticulofenestra pseudoumbilicus	310.65	8.790
T D. bollii	325.13	9.295
T C. coalitus	337.92	9.690

Table 1. Age model, IODP Expedition 363 Site U1488.

Analysis of planktic foraminifera

We measured the minor element ratios (Mg/Ca, Mn/Ca, Sr/Ca) and paired carbon isotopes ($\delta^{13}C$) on the planktonic foraminifer species *Trilobatus trilobus* (previously *Globogerinoides sacculifer* without the final sac-like chamber; Spezzaferri et al., 2015). Data from *T*. *trilobus* represents conditions in the surface mixed-layer (upper ~150m; Bijma & Hemleben, 1994; Schmidt et al., 2016). Sediment samples were initially freeze dried, shaken in buffered de-ionized water for 8-12 hours, wet sieved at 63 μm, and oven dried at temperatures less than 50°C. An average of thirty *T*. *trilobus* specimen (355-425 μm) were carefully picked avoiding fragmented foraminifers, specimen with discoloration, or obvious signs of inorganic calcite growth. Prior to analysis foraminifer tests were gently broken and detrital material was carefully removed from inside the test before they were homogenized. Samples were then rinsed and ultrasonicated in milli-Q water and then methanol.

Elemental ratios

A total of 429 samples with a spatial resolution of 75 cm (average temporal resolution 25 kyr) were analyzed for minor element ratios (Mg/Ca, Mn/Ca, Sr/Ca). Samples were cleaned according to a modified "Boyle Method", including removal of fine particulates, oxidative, and reductive cleaning (Martin & Lea, 2002). Minor element ratios were analyzed at the University of California Santa Cruz (UCSC) plasma lab using a ThermoFisher iCAP 7000 Series, an inductively coupled plasma

optical emission spectrometer. The long-term reproducibility of the instrument was

monitored with an in-house liquid consistency standard 3.31 ±0.02 mmol/mol (1σ,

n=138) and two in-house foraminifer standards 3.73 ±0.13 mmol/mol (*T. trilobus*, 1σ,

n=29) and 2.35 ±0.18 mmol/mol (*Pulleniatina obliquiloculata*, 1σ, n=30).

The impact of diagenesis was monitored by the Mn/Ca (Figure 2) and Sr/Ca ratio

(not shown). We found no correlation between Mn/Ca and Mg/Ca suggesting Mn-

oxide coatings and/or Mn-Mg-Ca rich calcite overgrowths do not appear to have a

systematic influence on the Mg/Ca data (Figure 2).
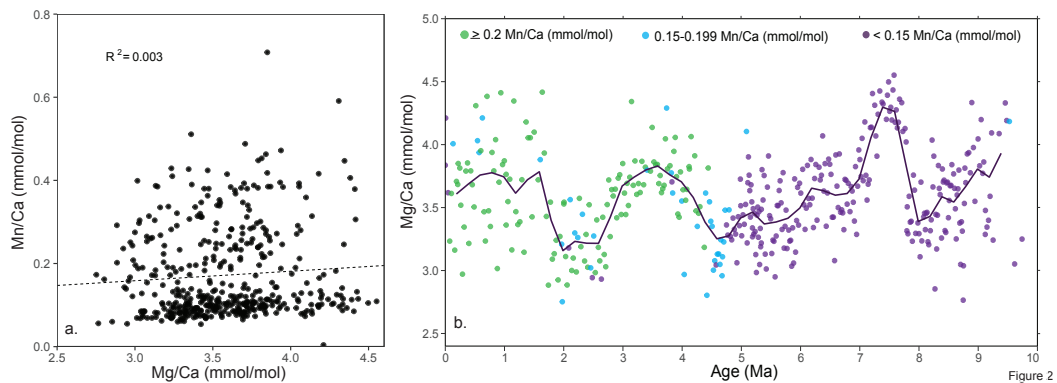
Figure 2. Relationship between Mn/Ca and Mg/Ca data at Site U1488. a) No
correlation between *T. trilobus* Mn/Ca (mmol/mol) and Mg/Ca (mmol/mol), adjusted
R^2 = 0.003. b) Multivariate timeseries of Mg/Ca and Mn/Ca values demonstrating no
systematic change in Mg/Ca with changes in Mn/Ca through time. Mn/Ca values less
than 0.15 mmol/mol in purple circles; Mn/Ca values between 0.15 – 0.199 mmol/mol
blue circles; Mn/Ca values greater than or equal to 0.20 mmol/mol green circles.

We applied the Gray and Evans (2019) temperature calibration to the Mg/Ca

data because it produced the best fit between paired clumped isotope and Mg/Ca

temperatures from Site U1488 (Meinicke et al., in review). A dissolution correction

was applied down core following the approach of Dyez and Ravelo (2013) using the

depth-dissolution relationship from Ontong Java Plateau core-tops (Dekens et al.,

2002). The Gray and Evans (2019) calibration includes a salinity correction based on

estimated whole ocean salinity changes scaled to a eustatic sea level curve (Miller et

al., 2011). No pH correction was applied for *T. sacculifer* (same species as *T.*

trilobus) because variable pH levels was not found to significantly affect the Mg/Ca

of this species (Gray & Evans, 2019). To account for the secular changes in Mg/Ca

ratio of seawater (Mg/Ca$_{sw}$) a temperature correction was calculated as the difference

between the estimated SST with variable Mg/Ca$_{sw}$ through time and the estimated

SST with modern Mg/Ca$_{sw}$ (5.2 mmol/mol) using the Evans et al. (2016) equations.

We used the Mg/Ca$_{sw}$ reconstruction published by Tierney et al. (2019b) (Figure 3).

This reconstruction resulted in Mg/Ca-SST estimates that best fit the independent

clumped isotope temperatures from Site U1488 samples (Meinicke et al., in-review).

An uncertainty envelope of the Mg/Ca-derived temperatures was estimated with a

monte-carlo simulation (ensemble of 1000) that propagated the Mg/Ca analytical

error of 1% (2σ), Mg/Ca salinity sensitivity error (3.6% ±0.01%, 2σ), Mg/Ca

temperature sensitivity error (6.1 ±0.01%, 2σ), and the variability in the Mg/Ca$_{sw}$

reconstruction (Gray & Evans, 2019; Tierney et al., 2019).
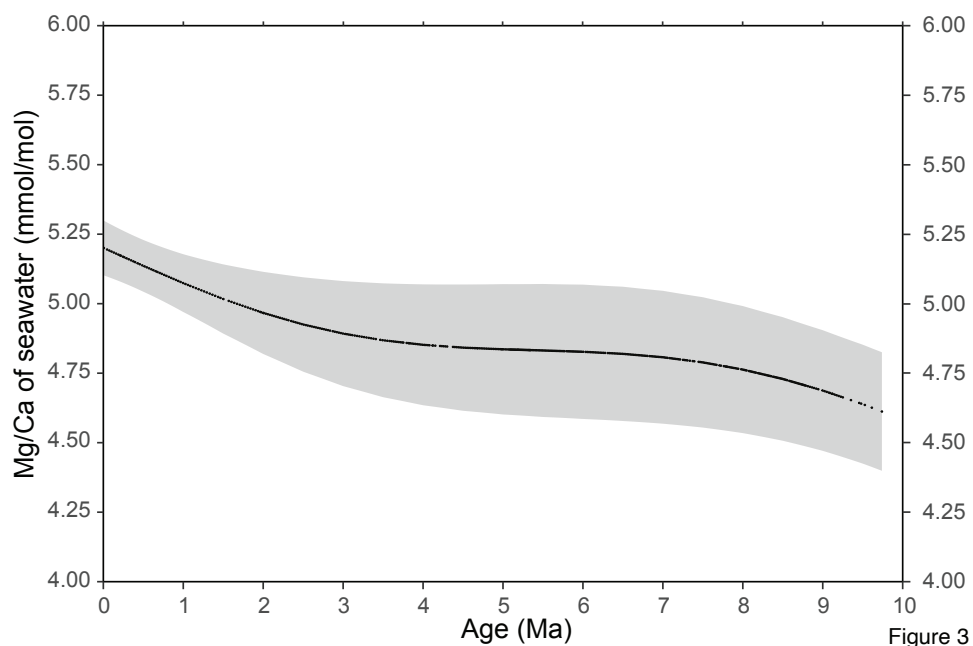
Figure 3

Figure 3. Mg/Ca of seawater reconstruction by Tierney et al. (2019).

Stable isotope analysis

A low-resolution planktonic foraminifer (*T. trilobus*) carbon isotope (δ^{13}C) record was reconstructed for age control. The Site U1488 δ^{13}C record shows the late Miocene carbon isotope shift and this feature was tuned to the high-resolution δ^{13}C record of site 1146 (Table 1; Holbourn et al., 2018). Samples were analyzed at the UCSC Stable Isotope Laboratory using a Kiel IV Carbonate Device and Thermo Scientific MAT253 isotope ratio mass spectrometer. Isotope values are reported in the per mil (‰) notation relative to Vienna Pee Dee Belemnite. Precision of the NBS-18 standard (NIST-8543) for δ^{13}C was 0.06 ‰ (n=30). Precision of the in-house Carrera Marble standard for δ^{13}C was 0.04‰ (n=72).

Estimate of temperature gradients

Continuous zonal and meridional temperature gradients were calculated using the newly generated Mg/Ca temperature data from Site U1488 and previously published $U^{k'}_{37}$ SST data (Figure 1, Table 2). The gradients were calculated with temperature anomalies to reduce the bias associated with the paleothermometry proxies.

The tropical Pacific zonal gradient is calculated with the Site U1488 Mg/Ca-derived anomaly record that represents the WEP warm pool and the published ODP site 846 $U^{k'}_{37}$-SST anomaly record that represents the EEP cold tongue (Figure 5b; Herbert et al., 2016; Lawrence et al., 2006; Liu & Herbert, 2004). Records in this calculation are a temperature anomaly relative to an average Holocene temperature (Table 2). ODP site 846 was chosen because it is located in the center of the modern EEP cold tongue (Figure 1), it has a high sample resolution, and the trend in the data is representative of the other EEP cold tongue records (Figure 5b; Herbert et al., 2016; Lawrence et al., 2006; Liu & Herbert, 2004; Rousselle et al., 2013; Zhang et al., 2014). The zonal gradient is calculated as the difference between the Site U1488 and ODP site 846, with the records smoothed to a 50 kyr resolution through binning and a 50% window. The calculation reflects how the zonal SST gradient has changed relative to the modern value, with negative values representing a more equitable temperature distribution across the tropical Pacific.

Table 2. Site Information used in the study						
Site	Latitude	Longitude	Modern SST for backtrack corrected location (C)*	Modern SST (C)**	Avg Holocene SST (C)	References
806	0.1ºN	159ºE		29.26		Zhang et al., 2014; Wara et al., 2005
850	1ºN	111ºW	24.96	24.50		Zhang et al., 2014
U1488	2ºN	141ºE		29.32	27.42	This Study; Meinicke et al., (in-review)
1010	30ºN	118ºW	17.3	17.80		LaRiviere et al., 2012
1085	30ºS	14ºE	17.33	18.28		Rommerskirchen et al., 2011
1208	36.1ºN	158.5ºE	18.7	22.19		LaRiviere et al., 2012
1021	39ºN	128ºW	14.3	14.87		LaRiviere et al., 2012
U1338	3ºS	118ºW		25.11		Rousselle et al., 2013
846	3ºS	91ºW	23.3	23.51	23.62	Liu and Herbert, 2004; Lawerence et al., 2006 ;Herbert et al., 2016
1088	41ºS	14ºE	13.8	13.78		Herbert et al., 2016
1125	42ºS	178ºW	14.45	14.89		Herbert et al., 2016
Med	44ºN	14ºE	19.2			Emeis et al., 2000, 2003; Cleaveland and Herbert 2009; Tzanova et al., 2015; Herbert et al., 2015 ; Herbert et al., 2016
594	46ºS	175ºE		15.10		Herbert et al., 2016
883/884	51ºN	168ºE	5.4	5.67		Herbert et al., 2016
887	54ºN	148ºW	7.2	7.21		Herbert et al., 2016
982	58ºN	16ºW	10.8	10.84		Lawrence, 2009; Herbert et al., 2016
907	69ºN	13ºW	1.77	1.86		Herbert et al., 2016
1241	6ºN	86ºW	27.7	27.87		Seki et al., 2012

*Levitus and Boyer, 1994 from Herbert et al., 2016
**Carton and Giese, 2008

Table 2. Site information for sites referenced in this study. Modern SST for the backtrack corrected location was used to calculate the SST anomalies for the meridional SST gradient (Levitus & Boyer, 1994; from Herbert et al., 2016). Modern SST used to estimate average global meridional temperature gradient and tropical Pacific zonal temperature gradient (Carton & Giese, 2008). Average Holocene temperatures were used to calculate the anomalies for zonal temperature gradient.

The meridional SST gradient calculation builds on the work of Herbert et al. (2016) using an average temperature stack that includes sites from latitudes greater than 30° north and south (>30° N/S stack) and a newly calculated tropical Pacific stack (Figure 1, Table 2). The data used in this calculation are anomalies relative to modern SST for the backtrack corrected location for each site taken from Herbert et al. (2016) except for Site U1488, which is reported as an anomaly to average Holocene temperature (Table 2). The tropical Pacific stack is calculated as an equally

weighted average between the WEP record (Site U1488; this study) and an average of published EEP $U^{k'}_{37}$ data from ODP sites 846, 850, 1241 and IODP Site U1338 (Table 2; Herbert et al., 2016; Lawrence et al., 2006; Liu & Herbert, 2004; Rousselle et al., 2013; Seki et al., 2012; Zhang et al., 2014). Sites included in the > 30° N/S stack include DSDP site 594, ODP sites 907, 982, 883/884, 887, 924, 1125, 1021, 1208, 2088, 1010, and 1085 (Table 2, Figure 1; Emeis et al., 2003, 2000; Herbert et al., 2016; LaRiviere et al., 2012; Lawrence et al., 2006; Liu & Herbert, 2003; Rommerskirchen et al., 2011; Rousselle et al., 2013; Seki et al., 2012; Tzanova et al., 2015; Zhang et al., 2014). The meridional gradient is calculated as the difference between the tropical Pacific stack and the >30° N/S stack, with all records smoothed to a 250 kyr resolution through binning and a 50% window.

Results

To determine the temperature evolution of the WEP warm pool over the last 9.7 Myr we generated a continuous ~25 kyr resolution Mg/Ca-derived temperature record at Site U1488. Our results indicate there is no significant long-term trend in the mixed-layer temperature (Figure 4a). We found a modest average temperature increase of 0.15°C/Myr. Site U1488 has an average Mg/Ca value of 3.58 ±0.72 mmol/mol (2σ) equivalent to 25.54 ±3.24°C (2σ) over the last 9.7 Myr (Figure 4a). This finding has implications for the tropical Pacific zonal temperature gradient, which we found to be reduced between ~9.7 to ~4.4 Ma, with an average gradient change of -5.5°C with respect to the modern zonal SST gradient (Figure 5c). To

assess possible mechanisms to sustain a reduced zonal temperature gradient we

calculated the meridional temperature gradient and found it has continuously

(although non-linearly) increased since the late Miocene (Figure 6). The inclusion of

WEP data into the tropical Pacific SST stack reduces the average late Miocene

temperature estimate by about 2°C, relative to the estimated temperature based on

only EEP data (Figure 6b). This result can be attributed to the lack of sustained late

Miocene warming in the WEP unlike the EEP (Figure 5). We found the late Miocene

meridional gradient was reduced by about 8°C (relative to the modern meridional

gradient) during the oldest portion of the record (Figure 6d).

Figure 4. Mg/Ca, SST, and sub-surface records of the WEP warm pool. A) Raw Mg/Ca data of *T. trilobus* from sites U1488 (purple, this study) and 806 (blue, Wara et al., 2005). B) Temperature estimates for WEP warm pool. Site U1488 *T. trilobus* Mg/Ca-derived mean temperature (200 kyr smooth of data) and uncertainty envelope of 95th to 5th percentile of the monte-carlo simulation (purple, ensemble of 1000, this study). Site U1488 average clumped isotope (Δ_{47}) derived temperatures of a 20 kyr interval (blue circles, Meinicke et al., in review). Site 806 TEX_{86} temperatures calibrated to integrated temperatures of 0-200m (turquoise upside-down triangle, Zhang et al., 2014). Site 806 *G. tumida* Mg/Ca-derived temperatures (green triangle, Ford et al., 2015). C) Site 806 oxygen isotopic gradient ($\Delta\delta^{18}O$) between subsurface foraminifer – surface plankton. $\Delta\delta^{18}O$ between subsurface - surface foraminifer (turquoise; Chaisson & Ravelo, 2000; LaRiviere et al., 2012; Nathan & Leckie et al., 2009; Wara et al., 2005). $\Delta\delta^{18}O$ between subsurface foraminifer – coccolith species (dark blue, Beltran et al., 2019). Solid lines are a 200 kyr smooth of data.
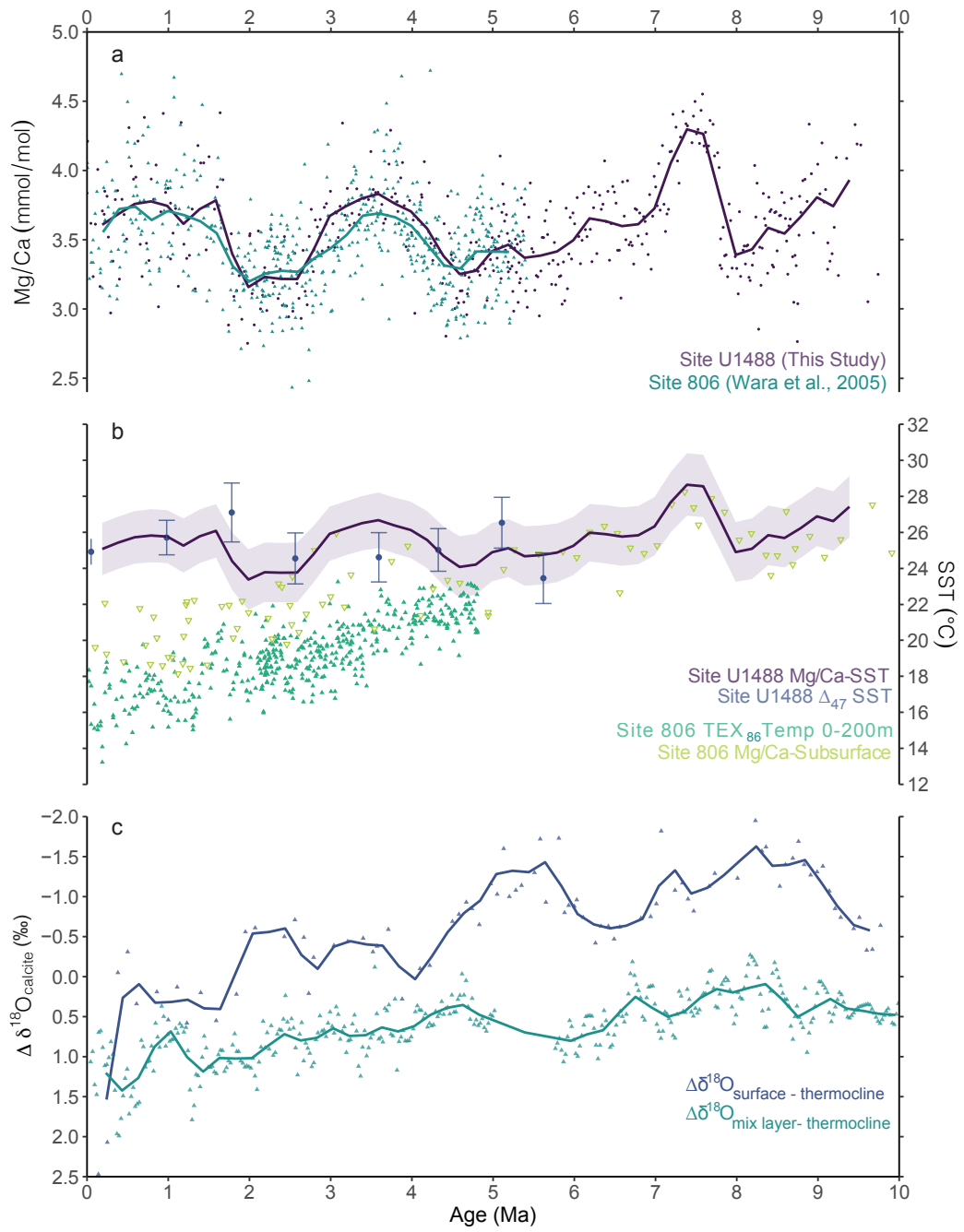
Figure 4
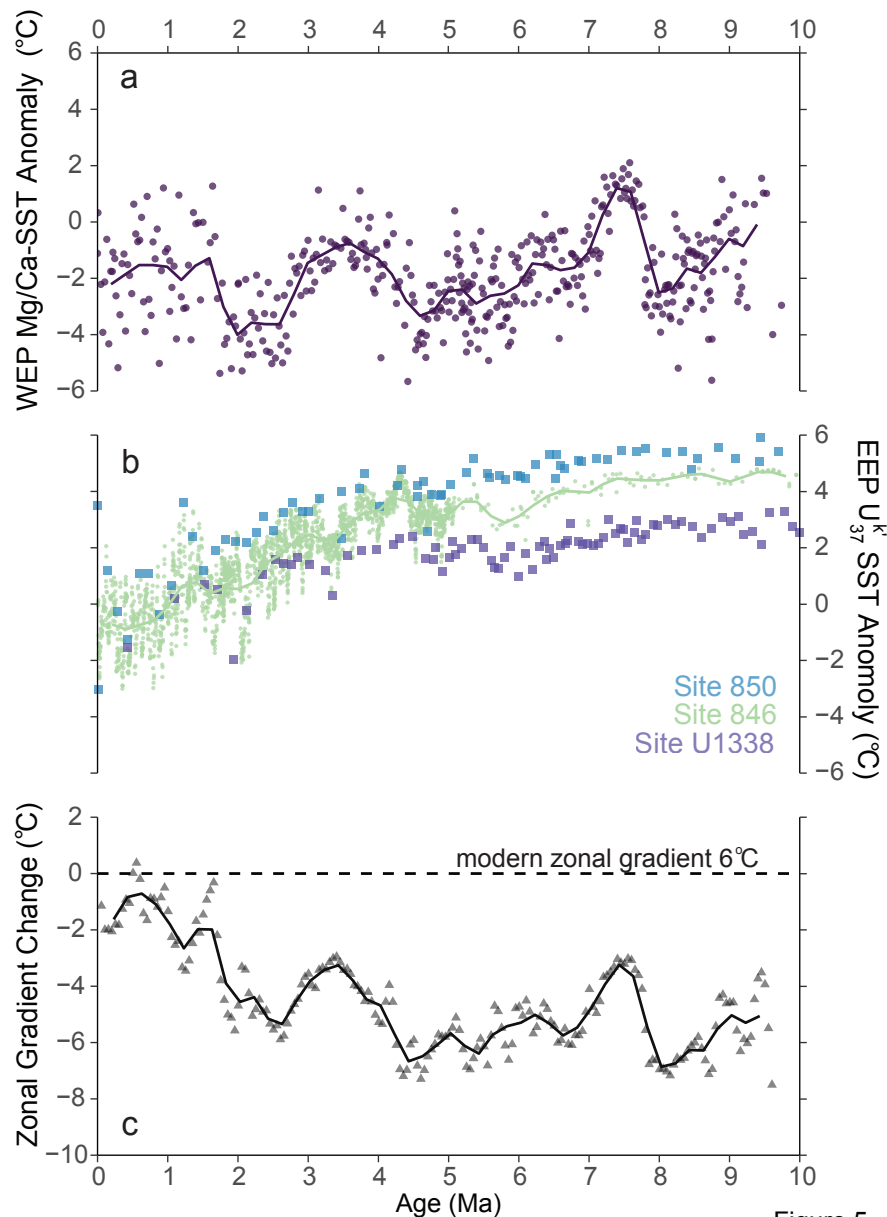
Figure 5. Evolution of tropical Pacific zonal SST gradient since late Miocene.
A) WEP warm pool Site U1488 Mg/Ca-temperature anomaly with respect to average
Holocene temperature (this study). B) EEP cold tongue $U^{k'}_{37}$-SST anomaly with
respect to average Holocene temperature for ODP 846 (green circle; Herbert et al.,
2016) and ODP 850 (blue square, Zhang et al., 2015). $U^{k'}_{37}$-SST anomaly with respect
to average modern temperature for IODP Site U1338 (purple square; Rousselle et al.,
2013). C) Tropical Pacific zonal SST gradient change (Site U1488 – Site 846). Solid
lines are a 200 kyr smooth of data.
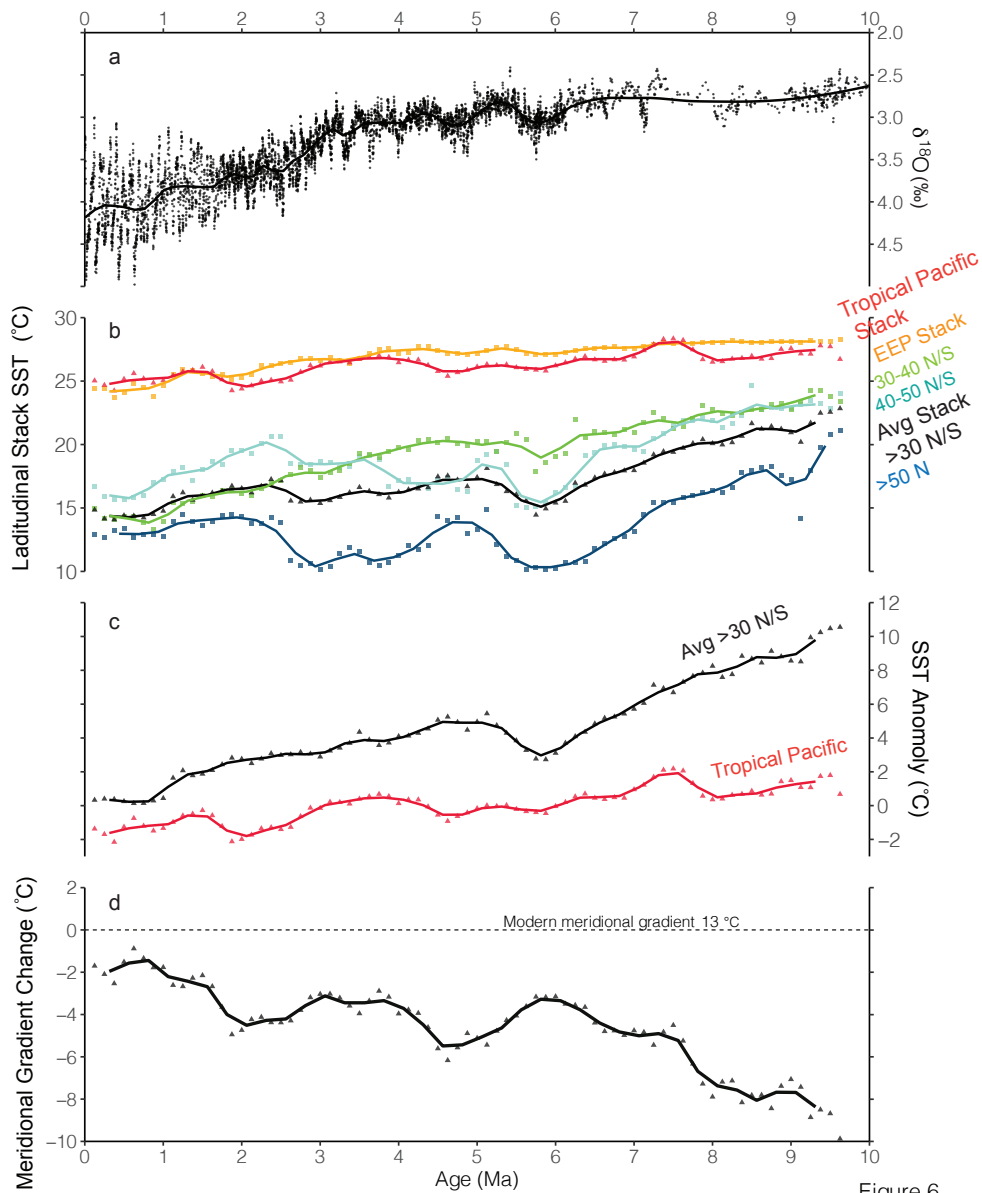
Figure 6. Evolution of meridional SST gradient since late Miocene. A) Benthic foraminifer oxygen isotope stack (δ^{18}O; Zachos et al., 2001). B) Average absolute temperature stacks by latitude. Tropical Pacific stack (red triangle; Site U1488 and EEP stack), EEP stack (orange; Sites 846, 850, U1338, 1241), 30°- 40° N/S (green; Sites 1085, 1010, 1208, 1021), 40°- 50° N/S (light blue; Sites 1088, 1125, 594, Mediterranean), >50°N (dark blue; Sites 907, 982, 887, 883/884), average of all sites >30° N/S (black triangle). C) Average temperature anomaly relative to modern for tropical Pacific stack (red triangle) and >30° N/S stack (black triangle). D) Meridional SST gradient change (tropical pacific stack - >30° N/S stack). Solid lines are a 500 kyr smooth of data. Site information and references in Table 2.

Although our main finding is that temperatures at Site U1488 have no long-term trend, there are temperature fluctuations around the long-term mean, with a range of 4.55 to 2.75 mmol/mol or 29.6 ±2.3°C to 21.3 ±2.5°C (Figure 4). The most prominent feature identified in this sample set is the warming event from 7.8 to 7.2 Ma with a rapid warming of +0.81mmol/mol or 3.22°C over less than 50 kyr. The event has sustained warm temperatures over 568 kyr (7.78-7.19 Ma) with average temperature of 28.5°C or 4.28 mmol/mol (Figure 4). During the late Miocene cooling event (LMC; 7.5-5.4Ma) the record shows very gradual ~1.41°C cooling, there are pronounced oscillations in temperature during the Pliocene and Pleistocene (Figure 4). During the middle Pliocene (~4.5-4.0 Ma) Site U1488 mixed-layer temperatures underwent transient warming with an increase of ~1.65°C (+0.38 mmol/mol). From 2.8 to 2.7 Ma average mixed-layer temperatures cooled by about 2.65°C (-0.56 mmol/mol). Finally, from 1.78 to 1.57 Ma mixed-layer temperatures increased about 2.04°C (-0.52 mmol/mol; Figure 4).

Discussion

Long-term trends late Miocene to present

Evolution of western equatorial Pacific warm pool temperatures

We find that over the last ~10 Myr the WEP warm pool mixed-layer temperatures have transient fluctuations, but do not show a significant long-term trend (Figure 4b). Our findings from Site U1488 are in excellent agreement with the 5

Myr Mg/Ca-temperature record from site 806 (Figure 4a; Wara et al., 2005). Taken together we suggest that the long-term temperature trend of the WEP warm pool since the early Pliocene is not forced by CO_2, which over the last 5 Myr displays a general decreasing trend (Dyez et al., 2018; Pagani et al., 2010; Seki et al., 2010; Zhang et al., 2013). This conclusion does not agree with some studies that suggest the long-term SST trend in the WEP warm pool is forced by CO_2, but this may be due to the use of Mg/Ca_{sw} reconstructions that are back-calculated from biomarker paleo-temperature records that may overestimate Mg/Ca SST corrections leading to very warm Pliocene temperatures (e.g., O'Brien et al., 2014), as well as studies that only focus at the mid-Piacenzian warm period (Tierney et al., 2019a) opposed to the long-term trend since the warmer early Pliocene period as this study does. The role of CO_2 forcing on warm pool temperatures during the Late Miocene is not clear because CO_2 reconstructions are highly variable. CO_2 estimates range from stable near pre-industrial levels ~350-200 ppm (Pagani et al., 2005) or stable near modern values ~300-550 ppm (Sosdian et al., 2018), or high CO_2 levels from 9 to 11 Ma (~450-800ppm) that decline through the latest Miocene to pre-industrial levels (Bolton et al., 2016; Mejia et al., 2017; Tanner et al., 20202). The long-term stability of mixed-layer temperatures at Site U1488 suggest CO_2 is not a major forcing, but this assertion is tentative given the variable CO_2 estimates.

We present a comparison of our Site U1488 Mg/Ca-temperature record with the site 806 TEX_{86}-temperature record (Zhang et al., 2014) that demonstrates there is agreement between these paleo-temperature proxies during the warm late Miocene

and early Pliocene, but not during the more recent portion of the record (Figure 4). To

draw this conclusion, we consider what depths the two temperature proxies represent,

which informs what temperature calibration should be applied to the data. The Site

U1488 *T. trilobus* Mg/Ca record reflects mixed-layer temperatures and therefore the

data are calibrated to calcification temperatures not SSTs (Gray & Evans, 2019;

Meinicke et al., in-review). The TEX_{86} proxy can reflect either surface or subsurface

temperatures depending on the oceanographic conditions (Schouten et al., 2013); and

studies from both the EEP cold tongue and the EEP warm pool have interpreted

TEX_{86} data as a subsurface temperature (e.g., Beltran et al., 2019; Hertzberg et al.,

2016; Seki et al., 2012). Furthermore, recent work has demonstrated that the TEX_{86}

signal has a significant correlation to integrated surface to shallow subsurface (200-

500m) temperatures (Ho & Lapepple, 2016; Zhang & Liu, 2018). Following this new

research, we applied the 0-200 m calibration of Zhang and Liu (2018) to the site 806

TEX_{86} data of Zhang et al., (2014) (Figure 4b).

To interpret the WEP temperature records we first must consider the evolution

of the WEP thermocline. The oxygen isotopic difference ($\Delta\delta^{18}O$) between a

subsurface and surface species is used as a proxy for thermocline temperature and/ or

depth. Site 806 $\Delta\delta^{18}O$ between subsurface and surface foraminifers shows a gradual

increase in $\Delta\delta^{18}O$ that is interpreted as a shoaling and/ or cooling of the thermocline

(Figure 4c; Chaisson & Ravelo, 2000; LaRiviere et al., 2012; Nathan & Leckie, 2009;

119

Wara et al., 2005). Similar data using site 806 $\Delta\delta^{18}O$ between subsurface foraminifers

and a coccolith species also has a long-term increase in $\Delta\delta^{18}O$, with a distinct

shoaling and/or cooling step between 5 to 4 Ma (Figure 4c; Beltran et al., 2019).

During the late Miocene and early Pliocene when the WEP thermocline is deep and/

or warm (Figure 4c) the U1488 Mg/Ca-temperatures and 806 TEX_{86}-temperatures

agree within error (Figure 4b). The temperature records begin to diverge after about 5

Ma (Figure 4b) coincident with the further shoaling and/ or cooling of the

thermocline (Figure 4c; Beltran et al., 2019; Chaisson & Ravelo, 2000; Ford et al.,

2015; Wara et al., 2005). The site 806 TEX_{86} temperatures (Zhang et al., 2014) fall

between the mixed-layer temperatures of Site U1488, recorded by both the Mg/Ca

(this study) and clumped isotope (Meinicke et al., in-review) proxies, and the

thermocline temperatures based on site 806 Mg/Ca of *G. tumida* (Figure 4b; Ford et

al., 2015). This observation suggests the TEX_{86} temperatures are influenced by

subsurface cooling in the later portion of the record, which supports the findings of

Ford et al. (2015). The subsurface cooling must occur below the calcification depth of

T. trilobus because the Site U1488 temperature estimates remain stable without a

significant long-term trend. In summary we show that during the late Miocene and

early Pliocene both TEX_{86} and Mg/Ca temperature proxies record long-term stable

warmth in the mixed-layer (Figure 4b), which we attribute to a deeper and/ or warmer

thermocline (Figure 4c). We suggest the divergence between the two proxies after

about 5 Ma is due to the shoaling and/ or cooling of the thermocline that influences

the TEX$_{86}$ signal (Figure 4). Overall, the new Site U1488 record shows there is no significant long-term trend in WEP warm pool mixed-layer temperatures, which has implications for the long-term tropical Pacific zonal temperature gradient.

Zonal SST gradient equatorial Pacific

The results of this study show the tropical Pacific zonal temperature gradient was reduced during the late Miocene and early Pliocene (Figure 5). Although the El Padre conditions of the early Pliocene tropical Pacific mean state are well established (e.g., Ford et al., 2015; Wara et al., 2005) the magnitude of the zonal gradient reduction during the Pliocene is debated. Some studies suggest a very moderate reduction in the Pliocene gradient (Tierney et al., 2019a; Zhang et al., 2014), but our results are consistent with studies that suggest a larger reduction in the zonal gradient (Fedorov et al., 2015; Wara et al., 2005; Wycech et al., 2019). This study is the first to validate the early Pliocene reduced zonal temperature gradient reported by Wara et al. (2005). Additionally, we find a reduced zonal temperature gradient during the late Miocene, which is consistent with 'El Niño-like' conditions present in the EEP warm pool (Site 1241) during the Pliocene warm period and before 7 Ma (Seki et al., 2012). The zonal SST gradient presented in this study suggests El Padre conditions also characterize the late Miocene tropical Pacific. We further investigate if expected subsurface conditions and far-field changes in precipitation, typical of the early Pliocene El Padre mean state, are also found during the late Miocene.

121

El Padre subsurface conditions differ from the modern conditions with a deeper and/or warmer thermocline (Ford et al., 2015, 2012; Steph et al., 2010; Wara et al., 2005). Site 806 data do show the late Miocene tropical Pacific thermocline is warmer and/ or deeper than modern subsurface conditions (Figure 4c; See *Absolute temperature of the WEP warm pool;* Beltran et al., 2019; Chaisson & Ravelo, 2000; LaRiviere et al., 2012; Nathan & Leckie, 2009; Wara et al., 2005). Site U1488 subsurface data has not yet been generated for the late Miocene, but the Plio-Pleistocene data (Mg/Ca of *G. tumida*; Meinicke et al., in-review) show a similar cooling trend to the one found at site 806 (Figure 4b; Ford et al., 2015). Therefore, both surface and subsurface conditions support the assertion that the tropical Pacific El Padre mean state was a persistent feature during the late Miocene (Figure 4, Figure 5).

Finally, the El Padre mean state is also characterized by a shift in far-field continental precipitation and temperature, with a pattern similar to modern El Niño teleconnections (Goldner et al., 2011; Molnar & Cane, 2007, 2002). Comparable late Miocene shifts are hard to confirm because data is limited but we summarize the currently available evidence. The northern and western regions of North America have warmer than average winters during modern El Niño events (Molnar & Cane, 2002; Taschetto et al., 2020) and throughout the late Miocene Alaskan and western North American winter temperatures are warmer than modern (Retallack, 2004; Retallack et al., 2002; White et al., 1997; Wolfe, 1994a, 1994b). A study from Southeast North America reports cooler and wetter climate during the Messinian

period (Shunk et al., 2006), which aligns with expected changes. Like modern El Niño conditions, drier winters in northeastern South America are inferred from the reduction in tropical rainforest coverage relative to modern (Pound et al., 2012, 2011). Regional tectonic and climatic shifts during the late Miocene in India as well as southeast and central Asia (Baldwin et al., 2012; Holbourn et al., 2018; Wang et al., 2014) confound possible patterns of El Niño-like teleconnections, but evidence from the Americas suggest an El Niño-like teleconnection pattern is present during the late Miocene. Taken together with the reduced zonal temperature gradient presented in this study and the published subsurface data we posit that El Padre conditions were present during the late Miocene. Mechanisms to sustain the El Padre mean state during the early Pliocene are associated with changes in the meridional temperature gradient (e.g., Fedorov et al., 2015), therefore we next evaluate the meridional gradient during the late Miocene.

Meridional SST gradient

There is currently a large (13°C) meridional SST gradient (Carton & Giese, 2008), which is a key driver of oceanic and atmospheric heat transport and thus global climate. This gradient was reduced during the early Pliocene (Brierley et al. 2009; Fedorov et al., 2015) and further reduced during the late Miocene, except for during the LMC (Herbert et al., 2016; LaRiviere et al., 2012). A good estimate of tropical SST is needed to calculate the meridional temperature gradient and this study contributes a regional record that greatly improves the characterization of the tropical

Pacific during the Late Miocene (Figure 6). WEP warm pool temperature data was previously excluded because alkenone temperature estimates from the region are near to or exceed the saturation index of the paleothermometer (Mueller et al., 1998; Zhang et al., 2014). The new estimate of the tropical Pacific SST stack uses two paleo-temperature proxies, our Mg/Ca-based temperature record and $U^{k'}_{37}$-temperature records of the EEP (Figure 6). Internal consistency of using one paleothermometer to characterize long-term trends in temperature must be weighed against the inclusion of climatically significant regions such as the WEP warm pool (Wycech et al. 2019). In this section we discuss the evolution of the meridional SST gradient over the last 9.7 Myr.

The non-linear increase of the meridional temperature gradient has periods of reversal (e.g., early Pliocene warm period) and three stepwise increases (Figure 6). The first steep increase in the meridional gradient begins about 8.5 Ma and culminates in the LMC from 7 to 5.4 Ma (Figure 6; Herbert et al., 2016). The LMC has a globally synchronous pattern (Figure 6b) suggesting a common forcing mechanism drove this change. The second stepwise increase in the gradient at 4.5 Ma is driven by cooling in northern hemisphere high-latitudes (>50°N) and subtropical latitudes between 30° to 40° N/S (Figure 6b). The asynchronous cooling suggests that regional forcing and climate feedbacks play an important role in these shifts. The final increase in the gradient begins around 1.8 Ma and is driven by SST cooling globally observed with the exception of the WEP warm pool (Figure 6b) and is associated with the reorganization of tropical Pacific to modern configuration (Ravelo

et al., 2004; Wara et al., 2005). The WEP warm pool does not appear to be sensitive to the climate forcing that drives this final cooling. Further discussion of these distinct events is presented in a later section (see *Prominent features in WEP warm pool temperature evolution)*. We focus our discussion on explanations for the late Miocene meridional temperature gradient changes because the Plio-Pleistocene changes are the focus of a recent study that uses high resolution SST records (Peterson et al., 2020).

The non-linear nature of the long-term meridional gradient increase suggests internal climate feedbacks play a role in the cooling of global sea-surface conditions over the last 9.7 Myr. We can look to the extensively studied early Pliocene warm period to try and understand possible mechanisms driving late Miocene climate dynamics. The early Pliocene climate was driven by modest CO_2 forcing coupled with dynamical reorganization of earth systems (Burls & Fedorov, 2014; Fedorov et al., 2010). The role of CO_2 forcing in the late Miocene is not currently well constrained (See *Absolute temperature of the WEP warm pool)* and therefore we focus on possible mechanisms for late Miocene warmth beyond CO_2 forcing. The boundary conditions during the late Miocene are similar to the Pliocene but differ with respect to paleogeography and vegetation cover, which may be key to understanding what is forcing the late Miocene climate system. Ongoing tectonic changes may influence atmospheric and oceanic circulation such as the restriction of the Indonesian and Central American Seaways (Montes et al., 2015; Baldwin et al., 2012; Coates et al., 2004) as well as the Himalayas and Andes reaching their final elevations (Garzione et al., 2017; Wang et al., 2014). The distribution of late Miocene

vegetation was different from the modern distribution with expansive forests at high

latitudes (Pound et al., 2012) and this period is also the culmination of the global rise

in grassland dominated ecosystems (Edwards et al., 2010; Stromberg, 2011).

Modeling suggest paleogeography and vegetation cover may be significant forcings

on late Miocene warmth (Knorr et al., 2011). Furthermore, coupled atmosphere-

ocean-vegetation modeling suggest that late Miocene paleogeography and vegetation

cover result in higher climate sensitivity than modern (Bradshaw et al., 2015), which

could explain late Miocene warmth with limited change in CO_2. Additional coupled

modeling studies as well as paleobotany reconstructions are needed to understand the

climate forcing during the late Miocene but paleogeography and/ or vegetation cover

appear to be significant factors. The new estimate of the meridional temperature

gradient (Figure 6) can inform possible mechanism(s) to sustain the reduced tropical

Pacific zonal temperature gradient (Figure 5).

Mechanism(s) to sustain the late Miocene reduced zonal SST gradient

Over the last 5 Myr the zonal and meridional SST gradients have shown a

strong one-to-one relationship and it is proposed that the reduced zonal SST gradient

during the early Pliocene is maintained by a reduced meridional gradient via the

'ocean tunnel' (Fedorov et al., 2015, Gu & Philander, 1997). We qualitatively

compare the newly calculated zonal and meridional SST gradients (Figure 5) and find

they have a similar trend over the last 5 Myr, confirming previous findings (e.g.,

Fedorov et al., 2015), but surprisingly during the late Miocene we find the gradients

126

are decoupled, with the continuous increase of the meridional gradient since 8.5 Ma (Figure 6) but a zonal gradient that remained reduced between 9.7 to 4.5 Ma (Figure 5). Possible explanations for the decoupling between the gradients include changes in the source waters of the tropical thermocline or a continental configuration that could not sustain a sloping tropical thermocline (Fedorov et al., 2015). There is currently no data to infer changes in thermocline source water and therefore it will not be discussed further, but we will consider if ocean gateways (i.e., Indonesian and Central American Seaway) influenced tropical Pacific surface temperatures during the late Miocene. There is also the possibility that the reduced zonal temperature gradient is sustained by a local forcing. Finally, despite the unexpected lack of response of tropical Pacific zonal SST gradient to the late Miocene meridional temperature gradient there is evidence of a subsurface reorganization (Beltran et al., 2019; Nathan & Leckie, 2009), which suggests a connection between the gradients was present during the late Miocene. We will first review the mechanisms attributed to sustaining the early Pliocene zonal SST gradient and discuss if they are applicable to the late Miocene.

A fundamental link is proposed between the tropical Pacific zonal SST gradient and the meridional SST gradient over the last 5 Myr, where extratropical conditions strongly influence the tropical Pacific surface conditions (Fedorov et al., 2015). The reduced zonal and meridional gradients in the early Pliocene (Brierly et al., 2009; Fedorov et al., 2013) have a near one-to-one relationship (Fedorov et al., 2015). This relationship is based a balanced ocean heat budget, where heat loss at

high latitudes is offset by heat gain in the low latitude upwelling regions (Boccaletti et al., 2004). Tropical upwelling regions are linked to the extratropical regions through the ventilated thermocline and the so-called 'ocean tunnel' (Boccaletti et al., 2004; Gu & Philander, 1997; Harper, 2000). The modern EEP has a shallow thermocline that reaches the surface during strong upwelling events (Fiedler & Talley, 2006). These thermocline waters are downwelled in subtropical regions and transported to the tropical Pacific through shallow wind driven sub-tropical cells (Philander & Gu, 1997). Thus, the surface conditions in these subtropical regions are 'mapped' onto the upper-ocean thermal structure of the tropical Pacific (Philander & Fedorov, 2003; Gu & Philander, 1997). Overall, a reduced zonal SST gradient in the tropical Pacific is sustained by reduced meridional gradient, where warm extratropical SST result in warm EEP SSTs (Fedorov et al., 2015).

Paleo-temperature reconstructions support the assertion that changes in the meridional gradient drive changes in the zonal gradient due to the ventilated thermocline or 'ocean tunnel'. Early Pliocene proxy records show a reduced meridional SST gradient relative to modern (Brierley et al., 2009; Fedorov et al., 2015). The reduced meridional temperature gradient is concurrent with a warmer and/ or deeper thermocline across the tropical Pacific (Ford et al., 2015), warmer SSTs in the EEP cold tongue (Figure 5b; Lawrence et al., 2006; Rousselle et al., 2013; Wara et al., 2005), and a reduced zonal SST gradient (Figure 5c; Wara et al., 2005). Conversely the increase in the meridional SST gradient around 4.5 Ma (Figure 6d; Brierley et al., 2009; Fedorov et al., 2015) is co-eval with EEP subsurface cooling

between 4.8 to 4.0 Ma (Steph et al., 2006; Ford et al., 2012). Subsurface temperatures begin to strongly influence surface temperature around 4 Ma, therefore it is suggested that shoaling of the thermocline is a precondition for cooling of EEP surface temperatures (Ford et al., 2015). Overall, the mid-Pliocene increase in the meridional gradient corresponds to cooling in tropical subsurface temperature followed by cooling in EEP SSTs and an increase in the tropical pacific zonal gradient.

Contrary to the Plio-Pleistocene relationship between the gradients, the late Miocene increase in the meridional temperature gradient does result in an increase in the zonal SST gradient. However, there is a simultaneous change in subsurface conditions. Prior to 8.5 Ma, warmer than modern SST are found globally and the tropical Pacific thermocline was deeper and/or warmer in both the WEP and EEP (Figure 4c; Beltran et al., 2019; Chaisson & Ravelo, 2000; LaRiviere et al., 2012; Nathan & Leckie, 2009; Wara et al., 2005; see *Zonal SST gradient of the tropical Pacific)*. The late Miocene maximum in the meridional gradient corresponding to the LMC (Figure 6; Herbert et al., 2016). During this period a shallower thermocline and a thin mixed-layer or 'La Nina-like' subsurface conditions were observed at WEP site 806 between 6.5 to 6.1 Ma (Nathan & Leckie, 2009). Furthermore, the thermocline between the WEP site 806 and EEP Site U1338 is asymmetrical between 6.5 to 5.3 Ma (Beltran et al., 2019). We speculate that during the LMC the subtropics remained relatively warm resulting in only minor changes in the tropical subsurface conditions and no major impact on the surface conditions; this speculation would imply the meridional gradient increase during the LMC is primarily driven by high-latitude

cooling (see *Global cooling event 7.0 to 5.4 Ma* for more discussion). Therefore, the transient shift in late Miocene tropical subsurface conditions indicates a link between the subtropical and tropical ocean and we speculate the tropical Pacific zonal gradient did not increase during the LMC due to subtropical warmth.

The decoupling of the zonal and meridional gradients could possibly be explained by the configuration of the Central American Seaway (CAS) during the late Miocene. An open CAS may hinder a sloping EEP thermocline and thus disconnect the influence of the meridional gradient on the zonal gradient (Fedorov et al., 2015). Although the CAS configuration has an influence on EEP upper ocean conditions it is not likely to be the primary driver of tropical Pacific SSTs considering there are climate shifts co-occurring during this period. Furthermore, the timing and configuration of the CAS closure is an area of active debate (i.e., Odea et al., 2016; Coates & Stallard, 2013) and currently cannot be definitively tied to the events of the late Miocene tropical SST changes. Recent geologic evidence suggests the flow of deep and intermediate water through the CAS was restricted by 15 Ma (Montes et al., 2015, 2012a; 2012b) or between 12.1 to 7.0 Ma (Coates et al., 2004). Whereas marine geochemical proxies suggest the sill shoaled between 11.2 to 9.0 Ma (Newkirk & Martin, 2009; Sepulchre et al., 2014;). However, the signal from the marine proxy data could be explained by events other than the tectonic closure of CAS (Molnar, 2008; Osbourne et al., 2014). Geologic evidence indicates transient shallow water passages across the isthmus were present until 10 Ma (Montes et al., 2015). But based on marine paleo-proxy data shallow water exchange between the Caribbean and

Pacific occurs until a divergence in surface salinity sometime between 4.7 to 3.5 Ma (e.g., Haug et al., 2001; Keigwin et al., 1982; Steph et al., 2006). An alternative explanation for the divergence in salinity between the two basins could be the demise of El Padre conditions (Mestas-Nunez & Molnar, 2012; Molnar, 2008). Studies, including this one acknowledge that the reconfiguration of the CAS must influence the oceanography of the region (e.g., Ford et al., 2012; Liu et al., 2019), but we contend that with the ongoing debate over the CAS during the late Miocene makes it challenging to draw conclusions about its influence on tropical SST at this time.

The other tropical ocean gateway that could influence the late Miocene tropical Pacific zonal gradient is the Indonesian seaway. Models have shown the restriction of this region could drive EEP SST cooling due to the reorganization of atmospheric circulation across the tropics (Brierly & Fedorov, 2016). The deep seaway passages closed during the early Miocene (Hall, 2017) and the seaway became further restricted between 12 to 4 Ma with the emergence of the New Guinea highlands (Baldwin et al., 2012). The proto-WEP warm pool formed between 11.7 to 11.4 Ma (Nathan & Leckie, 2009), but changes in regional circulation are not documented until 5 Ma (Karas et al., 2011; Molnar & Cane, 2001). Although restriction of this seaway effects tropical climate it does not appear to be the key driver of tropical SSTs during the late Miocene.

The late Miocene tropical Pacific conditions could be a result of local feedback mechanisms. Possible examples are atmospheric super-rotation or changes in walker circulation (Tierney et al., 2019; Tziperman & Farrell, 2009). These

mechanisms would alter tropical wind patterns, which is not likely because high surface productivity is recorded during the late Miocene EEP biogenic boom (Lyle, 2003; Lyle & Baldauf, 2015). Evaporative cooling or the cloud response to a warm world could reduce the zonal temperature gradient (Knutson & Manabe, 1995; Xie et al., 2010), but it is not clear how powerful these local forcings could be under late Miocene boundary conditions or if they could sustain surface conditions over millions of years. Although these local feedbacks are possible mechanisms, we do not favor this explanation.

In summary, our results show the zonal and meridional SST gradients have similar trends over the last 5 Myr but appear decoupled during the late Miocene, when the meridional gradient increases but the zonal gradient remains reduced (Figure 5, Figure 6). Although it is possible that the tropical Pacific zonal gradient did not increase during the late Miocene due to the configuration of either the Indonesian or Central American seaways or because of local feedback mechanisms we do not favor these explanations. We speculate that the late Miocene zonal SST gradient remains reduced through mechanisms similar to those proposed for the early Pliocene (Burls et al., 2014; Fedorov et al., 2015); and the apparent decoupling of zonal and meridional gradients suggests the zonal gradient is more sensitive to the temperature difference between the tropics-to-subtropics rather than the tropics-to-pole.

Prominent features of the WEP warm pool evolution

Warming event 7.5 Ma

We find the warming event (~3°C) between 7.8 to 7.2 Ma to be a robust

feature of the Site U1488 record (Figure 4). We first review the quality of the Mg/Ca

data before discussing the significance of this event. The data throughout this interval

was reproduced through replicate measurements demonstrating no analytical or

laboratory error resulted in erroneous Mg/Ca values (not shown). The Mn/Ca values

throughout this interval (average 0.1 mmol/mol; Figure 2) do not indicate there is a

warm bias from the presence of Mn-Fe oxide coatings or secondary Mn-Mg-Ca rich

calcite overgrowths (Pena et al., 2005, 2008; Boyle, 1983). The Sr/Ca values during

this interval (average 1.08 mmol/mol) may suggest there is some diagenesis, but we

do not think it has necessarily affected the Mg/Ca values. Planktic foraminifers record

the Sr/Ca of seawater (Sr/Ca$_{sw}$; Delaney et al., 1985) and the typical Sr/Ca range of

modern planktic foraminifers is 1.6-1.2 mmol/mol (Lear et al., 2003).

Reconstructions of Sr/Ca$_{sw}$ over the last 10 Myr suggest a 10-15% decrease around

7.5 Ma (Graham et al., 1982; Lear et al. 2003). The average Sr/Ca values during the

Site U1488 warm event decrease on average by 16.1% (not shown). Although

reduced Sr/Ca values have been associated with diagenetic overgrowths (Kozdon et

al., 2013; Regenberg et al., 2007) it is not always associated with co-eval warm bias

in the Mg/Ca data (Kozdon et al., 2013). Therefore, it is not certain that the additional

1.1% reduction in Site U1488 Sr/Ca can be attributed to diagenesis or how this

possible diagenesis would affect the Mg/Ca data. Changes in regional salinity could impact the Mg/Ca-SST estimate (e.g., Hönish et al., 2013). We calculate on average increase of 1 PSU would result in a 0.8°C change in the U1488 record (4.7% increase in Mg/Ca per salinity unit; Hönish et al., 2013). Therefore, an increase in 1 PSU during the event would mean an average warming of +2.2°C instead of +3°C through the event. In summary we do not find conclusive evidence of diagenetic overgrowths that would cause warm bias in the Mg/Ca data, but possible increases in the regional salinity could result in an overestimate of warming. Therefore, we consider the warming at ~7.5 Ma to be a robust signal but acknowledge the +3°C warming is a maximum estimate for the event.

Warming around 7.5 Ma is present records from the WEP, but it is not found in other late Miocene data, suggesting the event is driven by a local forcing. The site 806 TEX$_{86}$ temperature record appears to warm at ~7.5 Ma but sample resolution is low (~125 kyr) so the record may not capture the full extent of the signal (Figure 4b; Zhang et al., 2014). The warming event is not present in records from the Arabian Sea (ODP 722), northwest Pacific (ODP 1208, 883/884), northeast Pacific (ODP 1010, 1021, 887), southwest Pacific (DSDP 594, ODP 1125), or the North Atlantic (ODP 982, 906), which suggests the warming event is likely a local WEP phenomenon. This warming could be related to regional atmospheric circulation changes due to the final rise in the New Guinea highlands from 2 km around 8 Ma to 4 km by 6 Ma (Baldwin et al., 2012) or local changes in radiative forcing due to either clouds or aerosols.

134

This WEP warming event appears as an increase in the zonal temperature gradient but could be attributed to the underestimate of EEP warming (Figure 5c). From 7.8 to 7.2 Ma and for much of the late Miocene EEP temperatures are near the alkenone paleothermometer's saturation point (Conte et al., 2006; Muller et al., 1998), it is understood that the records reflect a minimum amount of warming (Herbert et al., 2016). Therefore, we suggest this feature of the tropical Pacific zonal SST gradient not be over interpreted (Figure 5c). The warming event also increases the meridional SST gradient but is not a prominent feature relative to the steep increase in the gradient associated with the LMC (Figure 6d).

Global cooling event 7.0 to 5.4 Ma

The late Miocene cooling event (LMC; 7.0 - 5.4 Ma) is a global cooling of SSTs to near modern values (Herbert et al., 2016), but the response of the WEP warm pool during the LMC has not yet been assessed. This study finds a very gradual ~1.4°C cooling at Site U1488 during the LMC, which aligns with the global pattern (Herbert et al., 2016). During the LMC the average SST of sites >30° N/S dropped from about +8°C to +3°C with respect to modern, with the largest cooling occurring in northern hemisphere high-latitude sites (Figure 6). Noticeably, the tropical Pacific stack lacks major cooling (Figure 6). Site U1338 in the EEP cold tongue shows cooling, with the $U^{k'}_{37}$-SST data decreasing by 1.2°C between 6.8-6.0 Ma (Rousselle et al., 2013) and Mg/Ca-SST data showing cooler temperatures around 6.5 Ma (Drury et al., 2018). Site 846 shows a little over 1°C of cooling (Figure 5b; Herbert et al.,

135

2016). During this period EEP cooling is roughly equivalent in magnitude to the WEP

cooling resulting in no significant change in the long-term trend of the tropical Pacific

zonal SST gradient (Figure 5c). Asymmetry in the $\delta^{18}O$ of planktic foraminifers

between sites 806 and U1338 is observed between 6.5 to 5.7 Ma, suggesting an

increase in the zonal SST gradient (Drury et al., 2018). Data from this study do not

disagree with this interpretation, with above average temperatures between 6.5 to 6.0

Ma at Site U1488 and an increased zonal SST gradient relative to the early Pliocene,

but from the perspective of the long-term trend the increase is relatively small and

transient (Figure3, Figure 5). Therefore, across the LMC event we find EEP cooling

is roughly equivalent in magnitude to the WEP cooling and results in no major

change in the long-term trend of the zonal gradient (Figure 5c).

This study confirms the global cooling pattern of the LMC (Herbert et al.,

2016), which suggests a common forcing mechanism for the event. It is proposed that

the global decline in SST was initially forced by a small decline in CO_2 (Herbert et

al., 2016). The data from Site U1488 does not refute this mechanism and although the

WEP warm pool is sensitive to CO_2 forcing at shorter timescales (i.e., Ford & Ravelo,

2019; Medina-Elizalde & Lea, 2010; Sosdian et al., 2020), it is our assertion that the

long-term trend in WEP warm pool temperatures is not forced by CO_2. Furthermore,

the late Miocene CO_2 levels are currently not well defined due the limited temporal

resolution of records and conflicting trends between paleo-proxies (see *Absolute*

temperatures of WEP warm pool; Bolton et al., 2016; Mejia et al., 2017; Pagani et al.,

2005; Sosdian et al., 2018; Tanner et al., 2020). It is possible Site U1488 responded to

CO_2 forcing during the LMC but based on available paleo-CO_2 estimates the forcing associated with the LMC event remains unresolved.

We calculate that the meridional gradient greatly increases during the late Miocene (Figure 6c), but this trend appears to be driven primarily by cooling in sites greater than 40°N/S (Figure 6b). Together with the relatively steady tropical Pacific zonal gradient (Figure 5c) we speculate that high latitude cooling may bias the magnitude of meridional SST gradient change during this period. We emphasize that although the late Miocene SST cooling pattern is global, the magnitude of cooling is variable. There is relatively gradual cooling at sites within the 30°N/S latitude band (ODP 1010, 1021, 1208: LaRiviere et al., 2012; ODP 1085: Rommerskirchen et al., 2011) and very gradual cooling in tropical oceans including the new data we present for the WEP warm pool (Figure 6b).

Here we consider the implications of a more modest cooling in the 30° to 40° N/S subtropical regions and the tropical Pacific. If these key sub-tropical regions do not cool enough this could explain why the EEP cold tongue does not develop, and a reduced zonal gradient can persist throughout the late Miocene. If the LMC is forced by a decline in CO_2 as suggested by Herbert et al. (2016) it is possible high-latitude cooling was largely amplified by positive ice-albedo feedbacks due to the emergent Greenland (Larsen et al., 1994), Kamchatka (Krissek, 1995), and Alaskan (Lagoe et al. 1993) glaciers. Hypothetically the effects of cooling could be dampened in key sub-tropical regions (i.e., where waters subduct into the ventilated thermocline) by reduced sub-tropical cloud albedo (Burls et al., 2014; Fedorov et al., 2015). We

speculate it is possible the tropical Pacific zonal gradient did not develop during the LMC because subtropical (30°-40° N/S) SSTs remained significantly warm. Corroborating evidence from subtropical downwelling regions is necessary to confirm this assertion.

WEP during the emergence of the EEP cold tongue ~4.5 Ma

We find that during the middle Pliocene the WEP warm pool underwent transient warming (Figure 4). Between ~4.5 to 4.0 Ma mixed-layer temperatures at Site U1488 increased by about 1.65°C and a slightly lower amplitude warming is observed at ODP 806 (Figure 4a; Wara et al., 2005). This WEP warming is concurrent with the development of the EEP cold tongue (Site U1338) between 4.4 to 3.6 Ma (Rousselle et al., 2013). This period marks the initial increase in the tropical Pacific zonal SST gradient (Figure 5c), which is preceded by the increase of the meridional temperature gradient (Figure 6d). The increase in the meridional gradient is driven by the onset of long-term permanent cooling between 30° to 40° N/S (Figure 6b). Cooling at ODP 1088 (31°S; Rommerskirchen et al., 2011) and ODP 1010 (31°N; LaRiviere et al., 2012) begins around 4.5 Ma and is followed by cooling at ODP 1021 at 4 Ma (39°N; LaRiviere et al., 2012). There is also cooling in the northern hemisphere high latitudes although it is transient and sites between 40°S to 50°S have stable temperature trends (Herbert et al., 2016). The cooling of EEP SSTs has been linked to the cooling and shoaling of EEP subsurface temperatures (Ford et al., 2012), suggesting there is likely a connection via the ventilated thermocline (Ford

et al., 2015). The WEP warm pool and the southern hemisphere mid-latitudes are not sensitive to the forcing.

Intensification of Northern Hemisphere glaciation

The WEP warm pool records transient cooling during the intensification of Northern Hemisphere Glaciation (NHG). We find steep cooling (-2.65°C) at Site U1488 between 2.8 to 2.7 Ma whereas the cooling at ODP 806 is more gradual and of a slightly smaller in magnitude (Figure 4a; Wara et al., 2005). This corresponds to a transient reduction in both the zonal and meridional temperature gradients (Figure 5c, Figure 6d). During this period the average latitudinal SST stacks do not have a coherent pattern of change (Figure 6b), indicating regional forcings play an important role. These long-term trends generally agree with the analysis of high-resolution temperature records that show a teleconnection between SSTs in the northern hemisphere high-latitudes and tropical upwelling regions, which the southern hemisphere and WEP warm pool are not sensitive to (Peterson et al. 2020).

Establish modern tropical mean state ~1.8 Ma

The final reorganization of tropical Pacific climate into its modern configuration occurs around 1.8 Ma (Ravelo et al., 2004; Wara et al., 2005). The WEP warm pool warms by about 2°C from 1.78 to 1.57 Ma at both Site U1488 and ODP 806 (Figure 4a; Wara et al., 2005). This coincides with the final increase in the tropical Pacific zonal gradient (Figure 5c) and the meridional gradient (Figure 6d). A

139

possible driver of this warming is the final expansion of the polar ocean that led to a contraction of warm pool (Martinez-Garcia et al., 2010). This final meridional gradient step is driven by the initiation of a permanent cooling trend in sites between 40°S to 50°S and the continued gradual cooling of all northern hemisphere sites (Figure 6b). Analysis of high-resolution SST records finds synchronous hemispheric cooling and an increase in coherence of all temperature records at the obliquity periodicity, which is attributed to CO_2 – biological pump feedback due to dust fertilization of the South Atlantic (Peterson et al., 2020).

Conclusions

This study presents the first late Miocene to modern Mg/Ca-derived temperature record from IODP Expedition 363 Site U1488. We find there is no significant long-term trend in WEP warm pool surface temperatures over the last 9.7 Myr (Figure 4). This finding suggests long-term temperature trends in the WEP warm pool are not forced by changing CO_2 concentrations.

This study shows the tropical Pacific zonal SST gradient is reduced from 9.7 to 4.4 Ma (Figure 5). We propose that tropical Pacific El Padre conditions were present from the late Miocene through the early Pliocene, based on the new zonal gradient data together with evidence of a deeper and/ or warmer tropical Pacific thermocline and evidence for far-field temperature and precipitation changes that resemble modern El Niño teleconnections during the late Miocene. Long-term continuous tropical Pacific subsurface temperature records and more continental

precipitation estimates from western and southeast North America, northeast South America, and Australia among other regions would further validate this assertion.

To investigate possible mechanisms that sustain a reduced zonal gradient during the late Miocene we make a qualitative comparison of the long-term trends in the newly calculated tropical Pacific zonal SST gradient and the meridional SST gradient. We find the gradients have parallel trends over the last 5 Myr, but are decoupled during Late Miocene (Figure 5, Figure 6). We speculate that the late Miocene increase in the meridional SST gradient may be dominated by high-latitude northern hemisphere cooling. We speculate that relatively warm subtropical temperatures (30°-40° N/S) during the late Miocene explain why the EEP cold tongue did not develop, and the tropical Pacific zonal SST gradient remained reduced during this period. Generating SST records in key subtropical regions of the southern hemisphere would help verify this speculative explanation.

Although we find the long-term WEP warm pool temperature trend remained stable there are temperature fluctuations. Newly documented warming event around 7.5 Ma at Site U1488 appears to be a feature of the WEP warm pool and is likely due to local forcing. The WEP warm pool shows very gradual cooling (avg -1.4°C) during late Miocene cooling event (7-5.4 Ma). Transient warming (+1.65°C) around 4.5 Ma, is later followed by transient cooling of -2.65°C during the intensification of northern hemisphere glaciation (2.8-2.7 Ma) and a final warming (+2.04°C) between 1.78 to 1.57 Ma. The Site U1488 temperature oscillations (±1.5-2.5°C) around a stable long-term mean temperature beginning around 4.5 Ma and are nearly synchronous with

those observed at ODP site 806 (Wara et al., 2005). The pacing of these oscillations is close to the long eccentricity periodicity (~2.4 Ma), which is typically associated with changes in global carbon cycle (De Vleeschouwer et al., 2020), but the connection between the global carbon cycle and WEP warm pool temperatures is not clear. The forcing for the WEP warm pool temperature oscillations remains unknown and requires further study.

References

Baldwin, S. L., Fitzgerald, P. G., & Webb, L. E. (2012). Tectonics of the new Guinea region. *Annual Review of Earth and Planetary Sciences*, *40*, 495–520. https://doi.org/10.1146/annurev-earth-040809-152540

Barker, S., Greaves, M., & Elderfield, H. (2003). A study of cleaning procedures used for foraminiferal Mg/Ca paleothermometry. *Geochemistry, Geophysics, Geosystems*, *4*(9), 1–20. https://doi.org/10.1029/2003GC000559

Beltran, C., Rousselle, G., de Rafélis, M., Sicre, M. A., Labourdette, N., & Schouten, S. (2019). Evolution of the zonal gradients across the equatorial Pacific during the Miocene–Pleistocene. *Journal of Sedimentary Research*, *89*(3), 242–252. https://doi.org/10.2110/jsr.2019.15

Bijma, J., & Hemleben, C. (1994). Population dynamics of the planktic foraminifer Globigerinoides sacculifer (Brady) from the central Red Sea. *Deep-Sea Research I*, *41*(3), 485–510. https://doi.org/10.1016/0967-0637(94)90092-2

Bjerknes, J. (1969). Atmospheric teleconnections from the equatorial Pacific. *Monthly Weather Review*, *97*(3), 163–172. https://doi.org/10.1175/1520-0493(1969)097<0163:ATFTEP>2.3.CO;2

Boccaletti, G., Pacanowski, R. C., George, S., Philander, H., & Fedorov, A. V. (2004). The Thermal Structure of the Upper Ocean. *Journal of Physical Oceanography*, *34*(4), 888–902. https://doi.org/10.1175/1520-0485(2004)034<0888:TTSOTU>2.0.CO;2

Bolton, C. T., Hernández-Sánchez, M. T., Fuertes, M. Á., González-Lemos, S., Abrevaya, L., Mendez-Vicente, A., … Stoll, H. M. (2016). Decrease in coccolithophore calcification and CO2 since the middle Miocene. *Nature Communications*, *7*, 1–13. https://doi.org/10.1038/ncomms10284

Boyle, E. A. (1983). Manganese carbonate overgrowths on foraminifera tests. *Geochimica et Cosmochimica Acta*, *47*(10), 1815–1819. https://doi.org/10.1016/0016-7037(83)90029-7

Bradshaw, C. D., Lunt, D. J., Flecker, R., & Davies-Barnard, T. (2015). Disentangling the roles of late Miocene palaeogeography and vegetation - Implications for climate sensitivity. *Palaeogeography, Palaeoclimatology, Palaeoecology*, *417*, 17–34. https://doi.org/10.1016/j.palaeo.2014.10.003

Brierley, C. M., Fedorov, A. V., Liu, Z., Herbert, T. D., Lawrence, K. T., & LaRiviere, J. P. (2009). Greatly Expanded Tropical Warm Pool and Weakened

Hadley Circulation in the Early Pliocene. *Science*, *323*(5922), 1714–1718. https://doi.org/10.1126/science.1167625

Brierley, Chris M., & Fedorov, A. V. (2016). Comparing the impacts of Miocene–Pliocene changes in inter-ocean gateways on climate: Central American Seaway, Bering Strait, and Indonesia. *Earth and Planetary Science Letters*, *444*, 116–130. https://doi.org/10.1016/j.epsl.2016.03.010

Brierley, Christopher M., & Fedorov, A. V. (2010). Relative importance of meridional and zonal sea surface temperature gradients for the onset of the ice ages and Pliocene-Pleistocene climate evolution. *Paleoceanography*, *25*(2), 1–16. https://doi.org/10.1029/2009PA001809

Burls, N. J., & Fedorov, A. V. (2014). What controls the mean east-west sea surface temperature gradient in the equatorial pacific: The role of cloud albedo. *Journal of Climate*, *27*(7), 2757–2778. https://doi.org/10.1175/JCLI-D-13-00255.1

Burls, Natalie J., & Fedorov, A. V. (2017). Wetter subtropics in a warmer world: Contrasting past and future hydrological cycles. *Proceedings of the National Academy of Sciences*, *114*(49), 12888–12893. https://doi.org/10.1073/pnas.1703421114

Cane, M. a, & Molnar, P. (2001). Closing of the Indonesian seaway as a precursor to east African aridification around 3-4 million years ago. *Nature*, *411*, 157–162. https://doi.org/10.1038/35075500

Carton, J. A., & Giese, B. S. (2008). A reanalysis of ocean climate using Simple Ocean Data Assimilation (SODA). *Monthly Weather Review*, *136*(8), 2999–3017. https://doi.org/10.1175/2007MWR1978.1

Chaisson, W. P., & Ravelo, A. C. (2000). Pliocene development of the east-west hydrographic gradient in the equatorial Pacific. *Paleoceanography*, *15*(5), 497–505. https://doi.org/10.1029/1999PA000442

Coates, A. G., Collins, L. S., Aubury, M. P., & Berggren, W. A. (2004). The geology of the Darien, Panama, and the late Miocene-Pliocene collision of the Panama arc with northwestern South America. *Bulletin of the Geological Society of America*, *116*(11–12), 1327–1344. https://doi.org/10.1130/B25275.1

Coates, A. G., & Stallard, R. F. (2013). How old is the Isthmus of Panamaδ. *Bulletin of Marine Science*, *89*(4), 801–813. https://doi.org/10.5343/bms.2012.1076

Coats, S., & Karnauskas, K. B. (2017). Are Simulated and Observed Twentieth Century Tropical Pacific Sea Surface Temperature Trends Significant Relative

to Internal Variability? *Geophysical Research Letters*, *44*(19), 9928–9937. https://doi.org/10.1002/2017GL074622

Conte, M. H., Sicre, M. A., Rühlemann, C., Weber, J. C., Schulte, S., Schulz-Bull, D., & Blanz, T. (2006). Global temperature calibration of the alkenone unsaturation index (U 37k) in surface waters and comparison with surface sediments. *Geochemistry, Geophysics, Geosystems*, *7*(2). https://doi.org/10.1029/2005GC001054

De Vleeschouwer, D., Drury, A. J., Vahlenkamp, M., Rochholz, F., Liebrand, D., & Pälike, H. (2020). High-latitude biomes and rock weathering mediate climate–carbon cycle feedbacks on eccentricity timescales. *Nature Communications*, *11*(1), 1–10. https://doi.org/10.1038/s41467-020-18733-w

Dekens, P. S., Lea, D. W., Pak, D. K., & Spero, H. J. (2002). Core top calibration of Mg/Ca in tropical foraminifera: Refining paleotemperature estimation. *Geochemistry, Geophysics, Geosystems*, *3*(4), 1–29. https://doi.org/10.1029/2001GC000200

Delaney, M. L., & Boyle, E. A. (1985). Li, Sr, Mg, and Na in foraminiferal calcite shells from laboratory culture, sediment traps, and sediment cores. *Deep Sea Research Part B*. *Oceanographic Literature Review*, *32*(12), 1025. https://doi.org/10.1016/0198-0254(85)93853-1

Deser, C., Phillips, A. S., & Alexander, M. A. (2010). Twentieth century tropical sea surface temperature trends revisited. *Geophysical Research Letters*, *37*(10), 1–6. https://doi.org/10.1029/2010GL043321

Drury, A. J., Lee, G. P., Gray, W. R., Lyle, M., Westerhold, T., Shevenell, A. E., & John, C. M. (2018). Deciphering the State of the Late Miocene to Early Pliocene Equatorial Pacific. *Paleoceanography and Paleoclimatology*, *33*(3), 246–263. https://doi.org/10.1002/2017PA003245

Dyez, K. A., Hönisch, B., & Schmidt, G. A. (2018). Early Pleistocene Obliquity-Scale pCO2 Variability at ~1.5 Million Years Ago. *Paleoceanography and Paleoclimatology*, *33*(11), 1270–1291. https://doi.org/10.1029/2018PA003349

Dyez, K. A., & Ravelo, A. C. (2014). Dynamical changes in the tropical Pacific warm pool and zonal SST gradient during the Pleistocene. *Geophysical Research Letters*, *871*, 7626–7633. https://doi.org/10.1002/2014GL061639

Edwards, E. J., Osborne, C. P., Strömberg, C. a E., Smith, S. a, Bond, W. J., Christin, P.-A., … Tipple, B. (2010). The origins of C4 grasslands: integrating evolutionary and ecosystem science. *Science*, (328), 587–591.

https://doi.org/10.1126/science.1177216

Emeis, K.-C., Schulz, H., Struck, U., Rossignol-Strick, M., Erlenkeuser, H., Howell, M. W., … Koizumi, I. (2003). Eastern Mediterranean surface water temperatures and δ ^{18}O composition during deposition of sapropels in the late Quaternary. *Paleoceanography*, *18*(1), n/a-n/a. https://doi.org/10.1029/2000PA000617

Emeis, K. C., Struck, U., Schulz, H. M., Rosenberg, R., Bernasconi, S., Erlenkeuser, H., … Martinez-Ruiz, F. (2000). Temperature and salinity variations of Mediterranean Sea surface waters over the last 16,000 years from records of planktonic stable oxygen isotopes and alkenone unsaturation ratios. *Palaeogeography, Palaeoclimatology, Palaeoecology*, *158*(3–4), 259–280. https://doi.org/10.1016/S0031-0182(00)00053-5

Fedorov, A. V., Dekens, P. S., McCarthy, M., Ravelo, A. C., DeMenocal, P. B., Barreiro, M., … Philander, S. G. (2006). The Pliocene Paradox (Mechanisms for a Permanent El Nino). *Science*, *312*, 1485–1489. https://doi.org/10.1126/science.1122666

Fedorov, Alexey V., Brierley, C. M., Lawrence, K. T., Liu, Z., Dekens, P. S., & Ravelo, A. C. (2013). Patterns and mechanisms of early Pliocene warmth. *Nature*, *496*(7443), 43–49. https://doi.org/10.1038/nature12003

Fedorov, Alexey V., Burls, N. J., Lawrence, K. T., & Peterson, L. C. (2015). Tightly linked zonal and meridional sea surface temperature gradients over the past five million years. *Nature Geoscience*, *8*(12), 975–980. https://doi.org/10.1038/ngeo2577

Fiedler, P. C., & Talley, L. D. (2006). Hydrography of the eastern tropical Pacific: A review. *Progress in Oceanography*, *69*(2–4), 143–180. https://doi.org/10.1016/j.pocean.2006.03.008

Ford, H. L., & Ravelo, A. C. (2019). Estimates of Pliocene Tropical Pacific Temperature Sensitivity to Radiative Greenhouse Gas Forcing. *Paleoceanography and Paleoclimatology*, *34*(1), 2–15. https://doi.org/10.1029/2018PA003461

Ford, H. L., Ravelo, A. C., & Hovan, S. (2012). A deep Eastern Equatorial Pacific thermocline during the early Pliocene warm period. *Earth and Planetary Science Letters*, *355–356*, 152–161. https://doi.org/10.1016/j.epsl.2012.08.027

Ford, H. L., Ravelo, A. C., & Polissar, P. J. (2015). Reduced El Niño–Southern Oscillation during the Last Glacial Maximum. *Science*, *347*(6219), 255–258. https://doi.org/10.1126/science.1258437

Garzione, C. N., McQuarrie, N., Perez, N. D., Ehlers, T. A., Beck, S. L., Kar, N., … Horton, B. K. (2017). Tectonic Evolution of the Central Andean Plateau and Implications for the Growth of Plateaus. *Annual Review of Earth and Planetary Sciences*, *45*, 529–559. https://doi.org/10.1146/annurev-earth-063016-020612

Goldner, A., Huber, M., Diffenbaugh, N., & Caballero, R. (2011). Implications of the permanent El Niño teleconnection "blueprint" for past global and North American hydroclimatology. *Climate of the Past*, *7*(3), 723–743. https://doi.org/10.5194/cp-7-723-2011

Graham, D. W., Bender, M. L., Williams, D. F., & Keigwin, L. D. (1982). Strontium-calcium ratios in Cenozoic planktonic foraminifera. *Geochimica et Cosmochimica Acta*, *46*(7), 1281–1292. https://doi.org/10.1016/0016-7037(82)90012-6

Gray, W. R., & Evans, D. (2019). Nonthermal Influences on Mg/Ca in Planktonic Foraminifera: A Review of Culture Studies and Application to the Last Glacial Maximum. *Paleoceanography and Paleoclimatology*, *34*(3), 306–315. https://doi.org/10.1029/2018PA003517

Gu, D., & Philander, S. G. H. (1997). Interdecadal climate fluctuations that depend on exchanges between the tropics and extratropics. *Science*, *275*(5301), 805–807. https://doi.org/10.1126/science.275.5301.805

Hall, R. (2017). Southeast Asia: New Views of the Geology of the Malay Archipelago. *Annual Review of Earth and Planetary Sciences*, *45*, 331–358. https://doi.org/10.1146/annurev-earth-063016-020633

Harper, B. S., Atmospheric, P., & Sciences, O. (2000). Thermocline ventilation and pathways of tropical – subtropical water mass exchange. *Tellus*, *0870*(April), 330–345. https://doi.org/10.3402/tellusa.v52i3.12269

Haug, G. H., Tiedemann, R., Zahn, R., & Ravelo, A. C. (2001). Role of Panama uplift on oceanic freshwater balance. *Geology*, *29*(3), 207–210. https://doi.org/10.1130/0091-7613(2001)029<0207:ROPUOO>2.0.CO;2

Herbert, T. D., Lawrence, K. T., Tzanova, A., Peterson, L. C., Caballero-Gill, R., & Kelly, C. S. (2016). Late Miocene global cooling and the rise of modern ecosystems. *Nature Geoscience*, *9*(11), 843–847. https://doi.org/10.1038/ngeo2813

Hertzberg, J. E., Schmidt, M. W., Bianchi, T. S., Smith, R. K., Shields, M. R., & Marcantonio, F. (2016). Comparison of eastern tropical Pacific TEX86 and

Globigerinoides ruber Mg/Ca derived sea surface temperatures: Insights from the Holocene and Last Glacial Maximum. *Earth and Planetary Science Letters*, *434*, 320–332. https://doi.org/10.1016/j.epsl.2015.11.050

Ho, S. L., & Laepple, T. (2016). Flat meridional temperature gradient in the early Eocene in the subsurface rather than surface ocean. *Nature Geoscience*, *9*(8), 606–610. https://doi.org/10.1038/ngeo2763

Holbourn, A. E., Kuhnt, W., Clemens, S. C., Kochhann, K. G. D., Jöhnck, J., Lübbers, J., & Andersen, N. (2018). Late Miocene climate cooling and intensification of southeast Asian winter monsoon. *Nature Communications*, *9*, 1–13. https://doi.org/10.1038/s41467-018-03950-1

Hönisch, B., Allen, K. A., Lea, D. W., Spero, H. J., Eggins, S. M., Arbuszewski, J., … Elderfield, H. (2013). The influence of salinity on Mg/Ca in planktic foraminifers - Evidence from cultures, core-top sediments and complementary $\delta 18O$. *Geochimica et Cosmochimica Acta*, *121*, 196–213. https://doi.org/10.1016/j.gca.2013.07.028

Huguet, C., Schimmelmann, A., Thunell, R., Lourens, L. J., Damsté, J. S. S., & Schouten, S. (2007). A study of the TEX86 paleothermometer in the water column and sediments of the Santa Barbara Basin, California. *Paleoceanography*, *22*(3), 1–9. https://doi.org/10.1029/2006PA001310

Karas, C., Nürnberg, D., Tiedemann, R., & Garbe-Schönberg, D. (2011). Pliocene Indonesian Throughflow and Leeuwin Current dynamics: Implications for Indian Ocean polar heat flux. *Paleoceanography*, *26*(2), 1–9. https://doi.org/10.1029/2010PA001949

Keigwin, L. D. (1982). Isotopic paleoceanography of the Caribbean and East pacific: role of panama uplift in late neogene time. *Science*, *217*(4557), 350–353. https://doi.org/10.1126/science.217.4557.350.

Kim, J. H., van der Meer, J., Schouten, S., Helmke, P., Willmott, V., Sangiorgi, F., … Damsté, J. S. S. (2010). New indices and calibrations derived from the distribution of crenarchaeal isoprenoid tetraether lipids: Implications for past sea surface temperature reconstructions. *Geochimica et Cosmochimica Acta*, *74*(16), 4639–4654. https://doi.org/10.1016/j.gca.2010.05.027

Knorr, G., Butzin, M., Micheels, A., & Lohmann, G. (2011). A warm Miocene climate at low atmospheric CO2 levels. *Geophysical Research Letters*, *38*(20), 1–5. https://doi.org/10.1029/2011GL048873

Knutson, T., & Manabe, S. (1995). Time-Mean Response over the Tropical Pacific to

Increeased CO2 in a Coupled Ocean-Atmoshere Model. *Journal of Climate*, *8*(9), 2181–2199. https://doi.org/10.1175/1520-0442(1995)008<2181:TMROTT>2.0.CO;2

Kozdon, R., Kelly, D. C., Kitajima, K., Strickland, A., Fournelle, J. H., & Valley, J. W. (2013). In situ δ18O and Mg/Ca analyses of diagenetic and planktic foraminiferal calcite preserved in a deep-sea record of the Paleocene-Eocene thermal maximum. *Paleoceanography*, *28*(3), 517–528. https://doi.org/10.1002/palo.20048

Krissek, L. A. (1995). Late Cenozoic ice-rafting records from Leg 145 sites in the North Pacific: Late Miocene onset, late Pliocene intensification, and Pliocene-Pleistocene events. In D. K. Rea, I. A. Basov, D. W. Scholl, & J. F. Allan (Eds.), *Proc. ODP, Sci. Results, 145* (pp. 179–194). College Station, TX: Ocean Drilling Program. https://doi.org/10.2973/odp.proc.sr.145.118.1995

Lagoe, M. B., Eyles, C. H., Eyles, N., & Hale, C. (1993). Timing of late Cenozoic tidewater glaciation in the far North Pacific Timing of late Cenozoic tidewater glaciation in the far North Pacific. *Geological Society Of America Bulletin*, (12), 1542–1560. https://doi.org/10.1130/0016-7606(1993)105<1542

LaRiviere, J. P., Ravelo, A. C., Crimmins, A., Dekens, P. S., Ford, H. L., Lyle, M., & Wara, M. W. (2012). Late Miocene decoupling of oceanic warmth and atmospheric carbon dioxide forcing. *Nature*, *486*(7401), 97–100. https://doi.org/10.1038/nature11200

Larsen, H. C., Saunders, a D., Clift, P. D., Beget, J., Wei, W., & Spezzaferri, S. (1994). Seven million years of glaciation in greenland. *Science*, *264*(5161), 952–955. https://doi.org/10.1126/science.264.5161.952

Lawrence, K. T., Pearson, A., Castañeda, I. S., Ladlow, C., Peterson, L. C., & Lawrence, C. E. (2020). Comparison of Late Neogene Uk′37 and TEX86 Paleotemperature Records From the Eastern Equatorial Pacific at Orbital Resolution. *Paleoceanography and Paleoclimatology*, *35*(7), 1–7. https://doi.org/10.1029/2020PA003858

Lawrence, Kira T., Liu, Z., & Herbert, T. D. (2006). Evolution of the Eastern Tropical Pacific Through Plio-Pleistocene Glaciation. *Science*, *312*, 79–84. https://doi.org/10.1126/science.1120395

Lear, C. H., Elderfield, H., & Wilson, P. A. (2003). A Cenozoic seawater Sr/Ca record from benthic foraminiferal calcite and its application in determining global weathering fluxes. *Earth and Planetary Science Letters*, *208*(1–2), 69–84. https://doi.org/10.1016/S0012-821X(02)01156-1

Levitus, S., & Boyer, T. P. (1994). *World Ocean Atlast 1994*. United States.

Liu, J., Tian, J., Liu, Z., Herbert, T. D., Fedorov, A. V., & Lyle, M. (2019). Eastern equatorial Pacific cold tongue evolution since the late Miocene linked to extratropical climate. *Science Advances*, *5*(4), 1–8. https://doi.org/10.1126/sciadv.aau6060

Liu, Z., & Herbert, T. D. (2004). High-latitude influence on the eastern equatorial Pacific climate in the early Pleistocene epoch. *Nature*, *427*, 720–723. https://doi.org/10.1038/nature02338

Locarnini, R. A., Mishonov, A. V., Antonov, J. I., Boyer, T. P., Garcia, H. E., Baranova, O. K., … Seidov, D. (2013). World Ocean Atlas 2013. Vol. 1: Temperature. *S. Levitus, Ed.; A. Mishonov, Technical Ed.; NOAA Atlas NESDIS*. https://doi.org/10.7289/V55X26VD

Lyle, M. (2003). Neogene carbonate burial in the Pacific Ocean. *Paleoceanography*, *18*(3), 1059-undefined. https://doi.org/10.1029/2002PA000777

Lyle, M., & Baldauf, J. (2015). Biogenic sediment regimes in the Neogene equatorial Pacific, IODP Site U1338: Burial, production, and diatom community. *Palaeogeography, Palaeoclimatology, Palaeoecology*, *433*, 106–128. https://doi.org/10.1016/j.palaeo.2015.04.001

Martin, P. A., & Lea, D. W. (2002). A simple evaluation of cleaning procedures on fossil benthic foraminiferal Mg/Ca. *Geochemistry, Geophysics, Geosystems*, *3*(10), 1–8. https://doi.org/10.1029/2001GC000280

Martinez-Garcia, A., Rosell-Melé, A., McClymont, E. L., Gersonde, R., & Haug, G. H. (2010). Subpolar Link to the Emergence of the Modern Equatorial Pacific Cold Tongue. *Science*, *5985*, 1550–1553. https://doi.org/10.1126/science.1184480

Medina-Elizalde, M., & Lea, D. W. (2010). Late Pliocene equatorial Pacific. *Paleoceanography*, *25*(2), 1–10. https://doi.org/10.1029/2009PA001780

Medina-Elizalde, M., Lea, D. W., & Fantle, M. S. (2008). Implications of seawater Mg/Ca variability for Plio-Pleistocene tropical climate reconstruction. *Earth and Planetary Science Letters*, *269*(3–4), 584–594. https://doi.org/10.1016/j.epsl.2008.03.014

Mejía, L. M., Méndez-Vicente, A., Abrevaya, L., Lawrence, K. T., Ladlow, C., Bolton, C., … Stoll, H. (2017). A diatom record of CO2 decline since the late Miocene. *Earth and Planetary Science Letters*, *479*, 18–33.

https://doi.org/10.1016/j.epsl.2017.08.034

Mestas-Nuñez, A. M., & Molnar, P. (2014). A mechanism for freshening the Caribbean Sea in pre-Ice Age time. *Paleoceanography*, *29*(6), 508–517. https://doi.org/10.1002/2013PA002515

Miller, K. G., Mountain, G. S., Wright, J. D., & Browning, J. V. (2011). Sea level and ice volume variations from continental margin and deep-sea isotopic records. *Oceanography*, *24*(2), 40–53. https://doi.org/10.5670/oceanog.2011.26

Molnar, P. (2008). Closing of the Central American Seaway and the ice age: A critical review. *Paleoceanography*, *23*(2), 1–15. https://doi.org/10.1029/2007PA001574

Molnar, P., & Cane, M. (2002). El Niño's tropical climate and teleconnections as a blueprint for pre-Ice Age climates. *Paleoceanography*, *17*(2), 1021-undefined. https://doi.org/10.1029/2001PA000663

Molnar, P., & Cane, M. A. (2007). Early Pliocene (pre-Ice age) El Niño-like global climate: Which El Niño? *Geosphere*, *3*(5), 337–365. https://doi.org/10.1130/GES00103.1

Montes, C., Cardona, A., Jaramillo, C., Pardo, A., Silva, J. C., Valencia, V., … Niño, H. (2015). Middle Miocene closure of the Central American Seaway. *Science*, *348*(6231), 226–229. https://doi.org/10.1126/science.aaa2815

Montes, Camilo, Bayona, G., Cardona, A., Buchs, D. M., Silva, C. A., Morón, S., … Valencia, V. (2012). Arc-continent collision and orocline formation: Closing of the Central American seaway. *Journal of Geophysical Research: Solid Earth*, *117*(4), 1–25. https://doi.org/10.1029/2011JB008959

Montes, Camilo, Cardona, A., McFadden, R., Morón, S. E., Silva, C. A., Restrepo-Moreno, S., … Flores, J. A. (2012). Evidence for middle Eocene and younger land emergence in central Panama: Implications for Isthmus closure. *Bulletin of the Geological Society of America*, *124*(5–6), 780–799. https://doi.org/10.1130/B30528.1

Muller, P. J., Kirst, G., Ruhland, G., von Storch, I., & Rosell-Mele, A. (1998). Calibration of the alkenone paleotemperature index U-37(K ') based on core-tops from the eastern South Atlantic and the global ocean (60 degrees N-60 degrees S). *Geochimica Et Cosmochimica Acta*, *62*(10), 1757–1772. https://doi.org/10.1016/S0016-7037(98)00097-0

Nathan, S. a., & Leckie, R. M. (2009). Early history of the Western Pacific Warm

Pool during the middle to late Miocene (~13.2–5.8 Ma): Role of sea-level change and implications for equatorial circulation. *Palaeogeography, Palaeoclimatology, Palaeoecology*, *274*(3–4), 140–159. https://doi.org/10.1016/j.palaeo.2009.01.007

Newkirk, D. R., & Martin, E. E. (2009). Circulation through the Central American Seaway during the Miocene carbonate crash. *Geology*, *37*(1), 87–90. https://doi.org/10.1130/G25193A.1

O'Brien, C. L., Foster, G. L., Martínez-Botí, M. a., Abell, R., Rae, J. W. B., & Pancost, R. D. (2014). High sea surface temperatures in tropical warm pools during the Pliocene. *Nature Geoscience*, *7*(8), 606–611. https://doi.org/10.1038/ngeo2194

O'Dea, A., Lessios, H. A., Coates, A. G., Eytan, R. I., Restrepo-Moreno, S. A., Cione, A. L., … Jackson, J. B. C. (2016). Formation of the Isthmus of Panama. *Science Advances*, *2*(8), 1–12. https://doi.org/10.1126/sciadv.1600883

Osborne, A., Newkirk, D. R., Groeneveld, J., Martin, E. E., Tiedemann, R., & Frank, M. (2014). The seawater neodymium and lead isotope record of the final stages of Central American Seaway closure. *Paleoceanography*, *29*, 715–729. https://doi.org/10.1002/2014PA002676

Pagani, M., Liu, Z., Lariviere, J., & Ravelo, A. C. (2010). High Earth-system climate sensitivity determined from Pliocene carbon dioxide concentrations. *Nature Geoscience*, *3*(1), 27–30. https://doi.org/10.1038/ngeo724

Pagani, M., Zachos, J. C., Freeman, K. H., Tipple, B., & Bohaty, S. (2005). Marked decline in atmospheric carbon dioxide concentrations during the Paleogene. *Science*, *309*(5734), 600–603. https://doi.org/10.1126/science.1110063

Palmer, T. N., & Mansfield, D. A. (1984). Response of two atmospheric general circulation models to sea- surface temperature anomalies in the tropical East and West Pacific. *Nature*, *310*(5977), 483–485. https://doi.org/10.1038/310483a0

Pearson, A., & Ingalls, A. E. (2013). Assessing the use of archaeal lipids as marine environmental proxies. *Annual Review of Earth and Planetary Sciences*, *41*, 359–384. https://doi.org/10.1146/annurev-earth-050212-123947

Pena, L. D., Cacho, I., Calvo, E., Pelejero, C., Eggins, S., & Sadekov, A. (2008). Characterization of contaminant phases in foraminifera carbonates by electron microprobe mapping. *Geochemistry, Geophysics, Geosystems*, *9*(7). https://doi.org/10.1029/2008GC002018

Pena, L. D., Calvo, E., Cacho, I., Eggins, S., & Pelejero, C. (2005). Identification and removal of Mn-Mg-rich contaminant phases on foraminiferal tests: Implications for Mg/Ca past temperature reconstructions. *Geochemistry, Geophysics, Geosystems*, *6*(9). https://doi.org/10.1029/2005GC000930

Philander, S. G., & Fedorov, A. V. (2003). Role of tropics in changing the response to Milankovich forcing some three million years ago. *Paleoceanography*, *18*(2). https://doi.org/10.1029/2002PA000837

Pound, M. J., Haywood, A. M., Salzmann, U., & Riding, J. B. (2012). Global vegetation dynamics and latitudinal temperature gradients during the Mid to Late Miocene (15.97-5.33Ma). *Earth-Science Reviews*, *112*, 1–22. https://doi.org/10.1016/j.earscirev.2012.02.005

Pound, M. J., Haywood, A. M., Salzmann, U., Riding, J. B., Lunt, D. J., & Hunter, S. J. (2011). A Tortonian (Late Miocene, 11.61-7.25Ma) global vegetation reconstruction. *Palaeogeography, Palaeoclimatology, Palaeoecology*, *300*, 29–45. https://doi.org/10.1016/j.palaeo.2010.11.029

Ravelo, A. C., Andreasen, D. H., Lyle, M., Olivarez Lyle, A., & Wara, M. W. (2004). Regional climate shifts caused by gradual global cooling in the Pliocene epoch. *Nature*, *429*, 263–267. https://doi.org/10.1038/nature02567

Ravelo, A. C., Lawrence, K. T., Fedorov, A., & Ford, H. L. (2014). Comment on "A 12-million-year temperature history of the tropical Pacific Ocean." *Science*, *344*(6179), 84–87. https://doi.org/10.1126/science.1246172

Regenberg, M., Nürnberg, D., Schönfeld, J., & Reichart, G. J. (2007). Early diagenetic overprint in Caribbean sediment cores and its effect on the geochemical composition of planktonic foraminifera. *Biogeosciences*, *4*(6), 957–973. https://doi.org/10.5194/bg-4-957-2007

Retallack, G. J. (2004). Late Miocene climate and life on land in Oregon within a context of Neogene global change. *Palaeogeography, Palaeoclimatology, Palaeoecology*, *214*(1–2), 97–123. https://doi.org/10.1016/j.palaeo.2004.07.024

Retallack, G. J., Tanaka, S., & Tate, T. (2002). Late Miocene advent of tall grassland paleosols in Oregon. *Palaeogeography, Palaeoclimatology, Palaeoecology*, *183*(3–4), 329–354. https://doi.org/10.1016/S0031-0182(02)00250-X

Rommerskirchen, F., Condon, T., Mollenhauer, G., Dupont, L., & Schefuss, E. (2011). Miocene to Pliocene development of surface and subsurface temperatures in the Benguela Current system. *Paleoceanography*, *26*(3), 1–15. https://doi.org/10.1029/2010PA002074

Rosenthal, Y., Holbourn, A., Kullhanek, D. K., & Expedition 363 Scientists. (2017). *Expedition 363 Preliminary Report: Western Pacific Warm Pool*. International Ocean Discovery Program. https://doi.org/10.14379/iodp.pr.363.2017

Rousselle, G., Beltran, C., Sicre, M. A., Raffi, I., & De Rafélis, M. (2013). Changes in sea-surface conditions in the Equatorial Pacific during the middle Miocene-Pliocene as inferred from coccolith geochemistry. *Earth and Planetary Science Letters*, *361*, 412–421. https://doi.org/10.1016/j.epsl.2012.11.003

Schmidt, D. N., Caromel, A. G. M., Seki, O., Rae, J. W. B., & Renaud, S. (2016). Morphological response of planktic foraminifers to habitat modifications associated with the emergence of the Isthmus of Panama. *Marine Micropaleontology*, *128*, 28–38. https://doi.org/10.1016/j.marmicro.2016.08.003

Schouten, S., Hopmans, E. C., Schefub, E., & Sinninghe Damste, J. S. (2002). Distributional variations in marine crenarchaeotal membrane lipids: A new tool for reconstructing ancient sea water temperatures? *Earth and Planetary Science Letters*, *204*(1–2), 265–274. https://doi.org/10.1016/S0012-821X(02)00979-2

Schouten, S., Hopmans, E. C., & Sinninghe Damsté, J. S. (2013). The organic geochemistry of glycerol dialkyl glycerol tetraether lipids: A review. *Organic Geochemistry*, *54*, 19–61. https://doi.org/10.1016/j.orggeochem.2012.09.006

Seager, R., Cane, M., Henderson, N., Lee, D. E., Abernathey, R., & Zhang, H. (2019). Strengthening tropical Pacific zonal sea surface temperature gradient consistent with rising greenhouse gases. *Nature Climate Change*, *9*(7), 517–522. https://doi.org/10.1038/s41558-019-0505-x

Seki, O., Foster, G. L., Schmidt, D. N., Mackensen, A., Kawamura, K., & Pancost, R. D. (2010). Alkenone and boron-based Pliocene pCO2 records. *Earth and Planetary Science Letters*, *292*(1–2), 201–211. https://doi.org/10.1016/j.epsl.2010.01.037

Seki, O., Schmidt, D. N., Schouten, S., Hopmans, E. C., Sinninghe Damsté, J. S., & Pancost, R. D. (2012). Paleoceanographic changes in the Eastern Equatorial Pacific over the last 10 Myr. *Paleoceanography*, *27*(3), 1–14. https://doi.org/10.1029/2011PA002158

Sepulchre, P., Arsouze, T., Donnadieu, Y., Dutay, J. C., Jaramillo, C., Le Bras, J., … Waite, A. J. (2014). Consequences of shoaling of the Central American Seaway determined from modeling Nd isotopes. *Paleoceanography*, *29*(3), 176–189. https://doi.org/10.1002/2013PA002501

Shunk, A. J., Driese, S. G., & Clark, G. M. (2006). Latest Miocene to earliest Pliocene sedimentation and climate record derived from paleosinkhole fill deposits, Gray Fossil Site, northeastern Tennessee, U.S.A. *Palaeogeography, Palaeoclimatology, Palaeoecology*, *231*(3–4), 265–278. https://doi.org/10.1016/j.palaeo.2005.08.001

Sosdian, S. M., Babila, T. L., Greenop, R., Foster, G. L., & Lear, C. H. (2020). Ocean Carbon Storage across the middle Miocene: a new interpretation for the Monterey Event. *Nature Communications*, *11*(1), 1–11. https://doi.org/10.1038/s41467-019-13792-0

Sosdian, S. M., Greenop, R., Hain, M. P., Foster, G. L., Pearson, P. N., & Lear, C. H. (2018). Constraining the evolution of Neogene ocean carbonate chemistry using the boron isotope pH proxy. *Earth and Planetary Science Letters*, *498*, 362–376. https://doi.org/10.1016/j.epsl.2018.06.017

Spezzaferri, S., Kucera, M., Pearson, P. N., Wade, B. S., Rappo, S., Poole, C. R., … Stalder, C. (2015). Fossil and genetic evidence for the polyphyletic nature of the Planktonic foraminifera "Globigerinoides", and description of the new genus Trilobatus. *PLoS ONE*, *10*(5), 1–20. https://doi.org/10.1371/journal.pone.0128108

Steph, S., Tiedemann, R., Groeneveld, J., Sturm, A., & Nürnberg, D. (2006). Pliocene changes in tropical east Pacific upper ocean stratification: Response to tropical gateways? In R. Tiedemann, A. C. Mix, C. Richter, & W. F. Ruddiman (Eds.), *Proc. ODP, Sci. Results, 202* (pp. 1–51). College Station, TX: Ocean Drilling Program. https://doi.org/10.2973/odp.proc.sr.202.211.2006

Steph, S., Tiedemann, R., Prange, M., Groeneveld, J., Schulz, M., Timmermann, A., … Haug, G. H. (2010). Early Pliocene increase in thermohaline overturning: A precondition for the development of the modern equatorial Pacific cold tongue. *Paleoceanography*, *25*(2), 1–17. https://doi.org/10.1029/2008PA001645

Strömberg, C. A. E. (2011). Evolution of grasses and grassland ecosystems. *Annual Review of Earth and Planetary Sciences*, *39*, 517–544. https://doi.org/10.1146/annurev-earth-040809-152402

Tanner, T., Hernández-Almeida, I., Drury, A. J., Guitián, J., & Stoll, H. (2020). Decreasing Atmospheric CO2 During the Late Miocene Cooling. *Paleoceanography and Paleoclimatology*, *35*(12), 1–25. https://doi.org/10.1029/2020PA003925

Taschetto, A. S., Ummenhofer, C. C., Stuecker, M. F., Dommenget, D., Ashok, K., Rodrigues, R. R., & Yeh, S. (2020). ENSO Atmospheric Teleconnections. In M.

J. McPhaden, A. Santoso, & W. Cai (Eds.), *El Nino Southern Oscillation in a Changing Climate* (pp. 309–335). Wiley. https://doi.org/10.1002/9781119548164.ch14

Tierney, J. E., Haywood, A. M., Feng, R., Bhattacharya, T., & Otto-Bliesner, B. L. (2019). Pliocene Warmth Consistent With Greenhouse Gas Forcing. *Geophysical Research Letters*, *46*(15), 9136–9144. https://doi.org/10.1029/2019GL083802

Tierney, J. E., Malevich, S. B., Gray, W., Vetter, L., & Thirumalai, K. (2019). Bayesian calibration of the Mg/Ca paleothermometer in planktic foraminifera. *Paleoceanography and Paleoclimatology*. https://doi.org/10.1029/2019pa003744

Tierney, J. E., Poulsen, C. J., Montañez, I. P., Bhattacharya, T., Feng, R., Ford, H. L., … Zhang, Y. G. (2020). Past climates inform our future. *Science*, *370*(6517). https://doi.org/10.1126/science.aay3701

Tokinaga, H., Xie, S. P., Timmermann, A., McGregor, S., Ogata, T., Kubota, H., & Okumura, Y. M. (2012). Regional patterns of tropical indo-pacific climate change: Evidence of the walker circulation weakening. *Journal of Climate*, *25*(5), 1689–1710. https://doi.org/10.1175/JCLI-D-11-00263.1

Turich, C., Freeman, K. H., Bruns, M. A., Conte, M., Jones, A. D., & Wakeham, S. G. (2007). Lipids of marine Archaea: Patterns and provenance in the water-column and sediments. *Geochimica et Cosmochimica Acta*, *71*(13), 3272–3291. https://doi.org/10.1016/j.gca.2007.04.013

Tzanova, A., Herbert, T. D., & Peterson, L. (2015). Cooling Mediterranean Sea surface temperatures during the Late Miocene provide a climate context for evolutionary transitions in Africa and Eurasia. *Earth and Planetary Science Letters*, *419*, 71–80. https://doi.org/10.1016/j.epsl.2015.03.016

Tziperman, E., & Farrell, B. (2009). Pliocene equatorial temperature: Lessons from atmospheric superrotation. *Paleoceanography*, *24*(1), 1–6. https://doi.org/10.1029/2008PA001652

Wang, C., Dai, J., Zhao, X., Li, Y., Graham, S. A., He, D., … Meng, J. (2014). Outward-growth of the Tibetan Plateau during the Cenozoic: A review. *Tectonophysics*, *621*, 1–43. https://doi.org/10.1016/j.tecto.2014.01.036

Wara, M. W., Ravelo, A. C., & Delaney, M. L. (2005). Permanent El Niño-like Conditions during the Pliocene Warm Period. *Science*, *309*(5735), 758–761. https://doi.org/10.1126/science.1112596

White, J. M., Ager, T. A., Adam, D. P., Leopold, E. B., Liu, G., Jetté, H., & Schweger, C. E. (1997). An 18 million year record of vegetation and climate change in northwestern Canada and Alaska: Tectonic and global climatic correlates. *Palaeogeography, Palaeoclimatology, Palaeoecology*, *130*(1–4), 293–306. https://doi.org/10.1016/S0031-0182(96)00146-0

Wolfe, J. A. (1994a). An analysis of Neogene climates in Beringia. *Palaeogeography, Palaeoclimatology, Palaeoecology*, *108*(3–4), 207–216. https://doi.org/10.1016/0031-0182(94)90234-8

Wolfe, J. A. (1994b). Tertiary climatic changes at middle latitudes of western North America. *Palaeogeography, Palaeoclimatology, Palaeoecology*, *108*(3–4), 195–205. https://doi.org/10.1016/0031-0182(94)90233-X

Wuchter, C., Schouten, S., Wakeham, S. G., & Sinninghe Damsté, J. S. (2005). Temporal and spatial variation in tetraether membrane lipids of marine Crenarchaeota in particulate organic matter: Implications for TEX86 paleothermometry. *Paleoceanography*, *20*(3), 1–11. https://doi.org/10.1029/2004PA001110

Wycech, J. B., Gill, E., Rajagopalan, B., Marchitto, T. M., & Molnar, P. H. (2020). Multiproxy Reduced-Dimension Reconstruction of Pliocene Equatorial Pacific Sea Surface Temperatures. *Paleoceanography and Paleoclimatology*, *35*(1), 1–20. https://doi.org/10.1029/2019PA003685

Xie, S. P., Deser, C., Vecchi, G. A., Ma, J., Teng, H., & Wittenberg, A. T. (2010). Global warming pattern formation: Sea surface temperature and rainfall. *Journal of Climate*, *23*(4), 966–986. https://doi.org/10.1175/2009JCLI3329.1

Zhang, Y. G., & Liu, X. (2018). Export Depth of the TEX86 Signal. *Paleoceanography and Paleoclimatology*, *33*(7), 666–671. https://doi.org/10.1029/2018PA003337

Zhang, Y. G., Pagani, M., & Liu, Z. (2014). A 12-Million-Year Temperature History of the Tropical Pacific Ocean. *Science*, *344*(6179), 84–87. https://doi.org/10.1126/science.1246172

Zhang, Y. G., Pagani, M., Liu, Z., Bohaty, S. M., Deconto, R., & A, P. T. R. S. (2013). A 40-million-year history of atmospheric CO2. *Phil. Trans. R. Soc. B*, *371*(2001). https://doi.org/10.1098/rsta.2013.0096

References

Abrantes, F., Cermeno, P., Lopes, C., Romero, O., Matos, L., Van Iperen, J., … Magalhães, V. (2016). Diatoms Si uptake capacity drives carbon export in coastal upwelling systems. *Biogeosciences*, *13*(14), 4099–4109. https://doi.org/10.5194/bg-13-4099-2016

Abrantes, F., & Moita, M. T. (1999). Water column and recent sediment data on diatoms and coccolithophorids, off Portugal, confirm sediment record of upwelling events. *Oceanologica Acta*, *22*(3), 319–336. https://doi.org/10.1016/S0399-1784(99)80055-3

Aiello, I. W., & Christina Ravelo, A. (2012). Evolution of marine sedimentation in the bering sea since the pliocene. *Geosphere*, *8*(6), 1231–1253. https://doi.org/10.1130/GES00710.1

Allen, M. R., & Robertson, A. W. (1996). Distinguishing modulated oscillations from coloured noise in multivariate datasets. *Climate Dynamics*, *12*, 775–784. https://doi.org/https://doi.org/10.1007/s003820050142

Alley, R. B., Cuffey, K. M., Evenson, E. B., Strasser, J. C., Lawson, D. E., & Larson, G. (1997). How glaciers entrain and transport basal sediment: physical constraints. *Quaternary Science Reviews*, *16*, 1017–1038. https://doi.org/https://doi.org/10.1016/S0277-3791(97)00034-6

Andrews, J. T. (2000). Icebergs and iceberg rafted detritus (IRD) in the North Atlantic: facts and assumptions. *Oceanography*, *13*, 100–108. https://doi.org/https://doi.org/10.5670/oceanog.2000.19

Ao, H., Dekkers, M. J., Qin, L., & Xiao, G. (2011). An updated astronomical timescale for the Plio-Pleistocene deposits from South China Sea and new insights into Asian monsoon evolution. *Quaternary Science Reviews*, *30*(13–14), 1560–1575. https://doi.org/10.1016/j.quascirev.2011.04.009

Asahi, H., Kender, S., Ikehara, M., Sakamoto, T., Takahashi, K., Ravelo, a. C., … Leng, M. J. (2014). Orbital-scale benthic foraminiferal oxygen isotope stratigraphy at the northern Bering Sea Slope Site U1343 (IODP Expedition 323) and its Pleistocene paleoceanographic significance. *Deep-Sea Research Part II: Topical Studies in Oceanography*, 1–18. https://doi.org/10.1016/j.dsr2.2014.01.004

Ashkenazy, Y., & Tziperman, E. (2004). Are the 41 kyr glacial oscillations a linear response to Milankovitch forcing? *Quaternary Science Reviews*, *23*(18–19), 1879–1890. https://doi.org/10.1016/j.quascirev.2004.04.008

Baldwin, S. L., Fitzgerald, P. G., & Webb, L. E. (2012). Tectonics of the new Guinea region. *Annual Review of Earth and Planetary Sciences*, *40*, 495–520. https://doi.org/10.1146/annurev-earth-040809-152540

Barker, S., Greaves, M., & Elderfield, H. (2003). A study of cleaning procedures used for foraminiferal Mg/Ca paleothermometry. *Geochemistry, Geophysics, Geosystems*, *4*(9), 1–20. https://doi.org/10.1029/2003GC000559

Barr, I. D., & Clark, C. D. (2012). Late Quaternary glaciations in Far NE Russia; combining moraines, topography and chronology to assess regional and global glaciation synchrony. *Quaternary Science Reviews*, *53*(C), 72–87. https://doi.org/10.1016/j.quascirev.2012.08.004

Barrere, M., Domine, F., Belke-Brea, M., & Sarrazin, D. (2018). Snowmelt events in autumn can reduce or cancel the soil warming effect of snow-vegetation interactions in the arctic. *Journal of Climate*, *31*(23), 9507–9518. https://doi.org/10.1175/JCLI-D-18-0135.1

Beckman Coulter, I. (2003). LS 13 320 particle size analyzer manual. Miami, Florida. Retrieved from https://www.beckmancoulter.com/wsrportal/techdocs?docname=B05577AB.pdf

Behl, R J, & Smith, B. M. (1992). Silicification of deep-sea sediments and the oxygen isotope composition of diagentic rocks from the western Pacific, Pigafetta and East Mariana Basins, Leg 129. In R. L. Larson & Y. Lancelot (Eds.), *Proc. ODP, Sci. Results, 129* (pp. 81–117). College Station, TX: Ocean Drilling Program. https://doi.org/10.2973/odp.proc.sr.129.112.1992

Behl, Richard J. (1999). Since Bramlette (1946): The Miocene Monterey Formation of California revisited. *Geological Society of America Special Papers*, *338*(1946), 301–313. https://doi.org/10.1130/0-8137-2338-8.301

Beltran, C., Rousselle, G., de Rafélis, M., Sicre, M. A., Labourdette, N., & Schouten, S. (2019). Evolution of the zonal gradients across the equatorial Pacific during the Miocene–Pleistocene. *Journal of Sedimentary Research*, *89*(3), 242–252. https://doi.org/10.2110/jsr.2019.15

Bennett, R. H., Fischer, K. M., Lavoie, D. L., Bryant, W. R., & Rezak, R. (1989). Porometry and fabric of marine clay and carbonate sediments: determination of permeability. *Marine Geology*, *89*, 127–152. https://doi.org/10.1016/0025-3227(89)90030-3

Berger, A., & Loutre, M. F. (1997). Intertropical Latitudes and Precessional and Half-

Precessional Cycles. *Science*, *278*(5342), 1476–1478.
https://doi.org/10.1126/science.278.5342.1476

Berger, A., Loutre, M. F., Lema, D. G. G., Cyclotron, C., & Louvam-la-neuve, B. I.
(1991). Insolation values for the climate of the last 10 million years. *Quaternary
Science Reviews*, *10*(1988), 297–317. https://doi.org/10.1016/0277-
3791(91)90033-Q

Berger, A., Loutre, M. F., & Mélice, J. L. (2006). Equatorial insolation: from
precession harmonics to eccentricity frequencies. *Climate of the Past
Discussions*, *2*(2), 519–533. https://doi.org/10.5194/cpd-2-519-2006

Bijma, J., & Hemleben, C. (1994). Population dynamics of the planktic foraminifer
Globigerinoides sacculifer (Brady) from the central Red Sea. *Deep-Sea Research
I*, *41*(3), 485–510. https://doi.org/10.1016/0967-0637(94)90092-2

Billups, K., & Scheinwald, A. (2014). Origin of millennial-scale climate signals in the
subtropical North Atlantic. *Paleoceanography*, *29*(6), 612–627.
https://doi.org/10.1002/2014PA002641

Bischof, J. (2000). *Ice Drift, Ocean Circulation and Climate Change*. Norfolk,
Virgina: Springer-Praxis Publishing Ltd.

Bjerknes, J. (1969). Atmospheric teleconnections from the equatorial Pacific.
Monthly Weather Review, *97*(3), 163–172. https://doi.org/10.1175/1520-
0493(1969)097<0163:ATFTEP>2.3.CO;2

Boccaletti, G., Pacanowski, R. C., George, S., Philander, H., & Fedorov, A. V.
(2004). The Thermal Structure of the Upper Ocean. *Journal of Physical
Oceanography*, *34*(4), 888–902. https://doi.org/10.1175/1520-
0485(2004)034<0888:TTSOTU>2.0.CO;2

Bolton, C. T., Hernández-Sánchez, M. T., Fuertes, M. Á., González-Lemos, S.,
Abrevaya, L., Mendez-Vicente, A., … Stoll, H. M. (2016). Decrease in
coccolithophore calcification and CO2 since the middle Miocene. *Nature
Communications*, *7*, 1–13. https://doi.org/10.1038/ncomms10284

Boyce, R. E. (1976). Definitions and laboratory techniques of compressional sound
velocity parameters and wet-water content, wet-bulk density, and porosity
parameters by gravimetric and gamma ray attenuation techniques. In S. O.
Schlanger, E. D. Jackson, & E. Al. (Eds.), *Initial Report Deep Sea Drilling
Project, Volume 33* (pp. 931–958). Washington: U.S. Government Printing
Office. https://doi.org/10.1017/CBO9781107415324.004

Boyle, E. A. (1983). Manganese carbonate overgrowths on foraminifera tests. *Geochimica et Cosmochimica Acta*, *47*(10), 1815–1819. https://doi.org/10.1016/0016-7037(83)90029-7

Bradshaw, C. D., Lunt, D. J., Flecker, R., & Davies-Barnard, T. (2015). Disentangling the roles of late Miocene palaeogeography and vegetation - Implications for climate sensitivity. *Palaeogeography, Palaeoclimatology, Palaeoecology*, *417*, 17–34. https://doi.org/10.1016/j.palaeo.2014.10.003

Breitzke, M. (2006). Physical Properties of Marine Sediments. In H. D. Schulz & M. Zabel (Eds.), *Marine Geochemistry* (pp. 27–71). Berlin, Heidelberg: Springer. https://doi.org/10.1007/3-540-32144-6_2

Brierley, C. M., Fedorov, A. V., Liu, Z., Herbert, T. D., Lawrence, K. T., & LaRiviere, J. P. (2009). Greatly Expanded Tropical Warm Pool and Weakened Hadley Circulation in the Early Pliocene. *Science*, *323*(5922), 1714–1718. https://doi.org/10.1126/science.1167625

Brierley, C M, Fedorov, a V, Liu, Z., Herbert, T. D., Lawrence, K. T., & LaRiviere, J. P. (2009). Greatly Expanded Tropical Warm Pool and Weakened Hadley Circulation in the Early Pliocene. *Science*, *323*, 1714–1718. https://doi.org/10.1126/science.1167625

Brierley, Chris M., & Fedorov, A. V. (2016). Comparing the impacts of Miocene–Pliocene changes in inter-ocean gateways on climate: Central American Seaway, Bering Strait, and Indonesia. *Earth and Planetary Science Letters*, *444*, 116–130. https://doi.org/10.1016/j.epsl.2016.03.010

Brierley, Christopher M., & Fedorov, A. V. (2010). Relative importance of meridional and zonal sea surface temperature gradients for the onset of the ice ages and Pliocene-Pleistocene climate evolution. *Paleoceanography*, *25*(2), 1–16. https://doi.org/10.1029/2009PA001809

Brigham-Grette, J. (2001). New perspectives on Beringian Quaternary paleogeography, stratigraphy, and glacial history. *Quaternary Science Reviews*, *20*(1–3), 15–24. https://doi.org/10.1016/S0277-3791(00)00134-7

Briner, J. P., & Kaufman, D. S. (2000). Late Pleistocene Glaciation of the Southwestern Ahklun Mountains, Alaska. *Quaternary Research*, *53*(1), 13–22. https://doi.org/10.1006/qres.1999.2088

Briner, J. P., & Kaufman, D. S. (2008). Late Pleistocene mountain glaciation in Alaska: key chronologies. *Journal of Quaternary Science*, *23*, 659–670. https://doi.org/10.1002/jqs

Burls, N. J., Bradshaw, C. D., De Boer, A. M., Herold, N., Huber, M., Pound, M., … Zhang, Z. (2021). Simulating Miocene Warmth: Insights From an Opportunistic Multi-Model Ensemble (MioMIP1). *Paleoceanography and Paleoclimatology*, *36*(5). https://doi.org/10.1029/2020pa004054

Burls, N. J., & Fedorov, A. V. (2014). What controls the mean east-west sea surface temperature gradient in the equatorial pacific: The role of cloud albedo. *Journal of Climate*, *27*(7), 2757–2778. https://doi.org/10.1175/JCLI-D-13-00255.1

Burls, Natalie J., & Fedorov, A. V. (2017). Wetter subtropics in a warmer world: Contrasting past and future hydrological cycles. *Proceedings of the National Academy of Sciences*, *114*(49), 12888–12893. https://doi.org/10.1073/pnas.1703421114

Caissie, B. E., Brigham-Grette, J., Cook, M. S., & Colmenero-Hidalgo, E. (2016). Bering Sea surface water conditions during Marine Isotope Stages 12 to 10 at Navarin Canyon (IODP Site U1345). *Climate of the Past*, *12*(9), 1739–1763. https://doi.org/10.5194/cp-12-1739-2016

Caissie, B. E., Brigham-Grette, J., Lawrence, K. T., Herbert, T. D., & Cook, M. S. (2010). Last Glacial Maximum to Holocene sea surface conditions at Umnak Plateau, Bering Sea, as inferred from diatom, alkenone, and stable isotope records. *Paleoceanography*, *25*(1), 1–16. https://doi.org/10.1029/2008PA001671

Calkin, P. E., Wiles, G. C., & Barclay, D. J. (2001). Holocene coastal glaciation of Alaska. *Quaternary Science Reviews*, *20*(1–3), 449–461. https://doi.org/10.1016/S0277-3791(00)00105-0

Calvert, S. E. (1966). Origin of Diatom-Rich, Varved Sediments from the Gulf of California. *Journal of Geology*, *74*(5), 546–565. https://doi.org/www.jstor.org/stable/30059298

Calvert, S. E. (1983). Sedimentary Geochemistry of Silicon. In S. R. Aston (Ed.), *Silicon Geochemistry and Biogeochemistry* (pp. 143–186). London: Academic Press Inc.

Cane, M. a, & Molnar, P. (2001). Closing of the Indonesian seaway as a precursor to east African aridification around 3-4 million years ago. *Nature*, *411*, 157–162. https://doi.org/10.1038/35075500

Carton, J. A., & Giese, B. S. (2008). A reanalysis of ocean climate using Simple Ocean Data Assimilation (SODA). *Monthly Weather Review*, *136*(8), 2999–3017. https://doi.org/10.1175/2007MWR1978.1

162

Chaisson, W. P., & Ravelo, A. C. (2000). Pliocene development of the east-west hydrographic gradient in the equatorial Pacific. *Paleoceanography*, *15*(5), 497–505. https://doi.org/10.1029/1999PA000442

Clemens, S. C., Prell, W. L., Sun, Y., Liu, Z., & Chen, G. (2008). Southern Hemisphere forcing of Pliocene δ18O and the evolution of Indo-Asian monsoons. *Paleoceanography*, *23*(4), 1–15. https://doi.org/10.1029/2008PA001638

Clemens, S., & Tiedemann, R. (1997). Eccentricity Forcing of Pliocene-early Pleistocene. *Nature*, *385*, 801–804. https://doi.org/10.1038/385801a0

Cloud Jr, P. E. (1955). Physical limits of glauconite formation. *Bulletin of the American Society of Petroleum Geologists*, *39*(4), 484–492. https://doi.org/10.1306/5CEAE166-16BB-11D7-8645000102C1865D

Coates, A. G., Collins, L. S., Aubury, M. P., & Berggren, W. A. (2004). The geology of the Darien, Panama, and the late Miocene-Pliocene collision of the Panama arc with northwestern South America. *Bulletin of the Geological Society of America*, *116*(11–12), 1327–1344. https://doi.org/10.1130/B25275.1

Coates, A. G., & Stallard, R. F. (2013). How old is the Isthmus of Panamaδ. *Bulletin of Marine Science*, *89*(4), 801–813. https://doi.org/10.5343/bms.2012.1076

Coats, S., & Karnauskas, K. B. (2017). Are Simulated and Observed Twentieth Century Tropical Pacific Sea Surface Temperature Trends Significant Relative to Internal Variability? *Geophysical Research Letters*, *44*(19), 9928–9937. https://doi.org/10.1002/2017GL074622

Conte, M. H., Sicre, M. A., Rühlemann, C., Weber, J. C., Schulte, S., Schulz-Bull, D., & Blanz, T. (2006). Global temperature calibration of the alkenone unsaturation index (U 37k) in surface waters and comparison with surface sediments. *Geochemistry, Geophysics, Geosystems*, *7*(2). https://doi.org/10.1029/2005GC001054

Cook, M. S., Ravelo, A. C., Mix, A., Nesbitt, I. M., & Miller, N. V. (2016). Tracing subarctic Pacific water masses with benthic foraminiferal stable isotopes during the LGM and late Pleistocene. *Deep Sea Research Part II: Topical Studies in Oceanography*, *126*, 84–95. https://doi.org/10.1016/j.dsr2.2016.02.006

Creager, J. S., Scholl, D. W., & Supko, P. R. (1973). *Initial Reports of the Deep Sea Drilling Program, Volume 19*. Washington. https://doi.org/doi:10.2973/dsdp.proc.19.1973

Darby, D. A., Myers, W. B., Jakobsson, M., & Rigor, I. (2011). Modern dirty sea ice characteristics and sources: The role of anchor ice. *Journal of Geophysical Research: Oceans*, *116*(9), 1–18. https://doi.org/10.1029/2010JC006675

De Vleeschouwer, D., Drury, A. J., Vahlenkamp, M., Rochholz, F., Liebrand, D., & Pälike, H. (2020). High-latitude biomes and rock weathering mediate climate–carbon cycle feedbacks on eccentricity timescales. *Nature Communications*, *11*(1), 1–10. https://doi.org/10.1038/s41467-020-18733-w

Dekens, P. S., Lea, D. W., Pak, D. K., & Spero, H. J. (2002). Core top calibration of Mg/Ca in tropical foraminifera: Refining paleotemperature estimation. *Geochemistry, Geophysics, Geosystems*, *3*(4), 1–29. https://doi.org/10.1029/2001GC000200

Delaney, M. L., & Boyle, E. A. (1985). Li, Sr, Mg, and Na in foraminiferal calcite shells from laboratory culture, sediment traps, and sediment cores. *Deep Sea Research Part B. Oceanographic Literature Review*, *32*(12), 1025. https://doi.org/10.1016/0198-0254(85)93853-1

Deser, C., Phillips, A. S., & Alexander, M. A. (2010). Twentieth century tropical sea surface temperature trends revisited. *Geophysical Research Letters*, *37*(10), 1–6. https://doi.org/10.1029/2010GL043321

Dethleff, D. (2005). Entrainment and export of Laptev Sea ice sediments, Siberian Arctic. *Journal of Geophysical Research*, *110*(7), 1–17. https://doi.org/10.1029/2004JC002740

Dethleff, D., & Kuhlmann, G. (2009). Entrainment of fine-grained surface deposits into new ice in the southwestern Kara Sea, Siberian Arctic. *Continental Shelf Research*, *29*(4), 691–701. https://doi.org/10.1016/j.csr.2008.11.009

Donegan, D., & Schrader, H. (1981). Modern Analogues of the Miocene Diatomaceous Monterey Shale of California: Evidence from Sedimentologic and Micropaleontologic Study. In R. E. Garrison & R. G. Douglas (Eds.), *The Monterey Formation and Related Siliceous Rocks of California: Soiety of Economic Paleontologists and Mineralogists* (pp. 149–157). Pacific Section SEPM.

Dowdeswell, J. A. (1986). The distribution and character of sediments in a tidewater glacier, Southern Baffin Island. *Arctic and Alpine Research*, *18*, 45–56. Retrieved from http://www.jstor.org/stable/30065541

Dowdeswell, J. A., & Dowdeswell, E. K. (1989). Debris in Icebergs and Rates of

Glaci-Marine Sedimentation: Observations from Spitsbergen and a Simple Model. *The Journal of Geology*, *97*(2), 221–231.

Drake, M. K., Aiello, I. W., & Ravelo, A. C. (2014). New Method for the Quantitative Analysis of Smear Slides in Pelagic and Hemi-Pelagic Sediments of the Bering Sea. *Fall Meeting, AGU*, *December 1*.

Drury, A. J., Lee, G. P., Gray, W. R., Lyle, M., Westerhold, T., Shevenell, A. E., & John, C. M. (2018). Deciphering the State of the Late Miocene to Early Pliocene Equatorial Pacific. *Paleoceanography and Paleoclimatology*, *33*(3), 246–263. https://doi.org/10.1002/2017PA003245

Dunhill, G. (1998). *Comparison of Sea-ice and Glacial-ice Rafted Debris: Grain Size, Surface Features, and Grain Shape*. U.S. Geological Survey. https://doi.org/10.3133/ofr98367

Dyez, K. A., Hönisch, B., & Schmidt, G. A. (2018). Early Pleistocene Obliquity-Scale pCO2 Variability at ~1.5 Million Years Ago. *Paleoceanography and Paleoclimatology*, *33*(11), 1270–1291. https://doi.org/10.1029/2018PA003349

Dyez, K. A., & Ravelo, A. C. (2014). Dynamical changes in the tropical Pacific warm pool and zonal SST gradient during the Pleistocene. *Geophysical Research Letters*, *871*, 7626–7633. https://doi.org/10.1002/2014GL061639

Edwards, CP, O., CA, S., SA, S., WJ, B., PA, C., … RP, F. (2010). The origins of C4 grasslands: integrating evolutionary and ecosystem science. *Science*, *328*, 587–591. 10.1126/science.1177216

Elias, S., & Brigham-Grette, J. (2007). Late Pleistocene Glacial Events in Beringia. *Encyclopedia of Quaternary Science*, (1), 191–201. https://doi.org/10.1016/B978-0-444-53643-3.00116-3

Emeis, K.-C., Schulz, H., Struck, U., Rossignol-Strick, M., Erlenkeuser, H., Howell, M. W., … Koizumi, I. (2003). Eastern Mediterranean surface water temperatures and δ ^{18} O composition during deposition of sapropels in the late Quaternary. *Paleoceanography*, *18*(1). https://doi.org/10.1029/2000PA000617

Emeis, K. C., Struck, U., Schulz, H. M., Rosenberg, R., Bernasconi, S., Erlenkeuser, H., … Martinez-Ruiz, F. (2000). Temperature and salinity variations of Mediterranean Sea surface waters over the last 16,000 years from records of planktonic stable oxygen isotopes and alkenone unsaturation ratios. *Palaeogeography, Palaeoclimatology, Palaeoecology*, *158*(3–4), 259–280. https://doi.org/10.1016/S0031-0182(00)00053-5

Fedorov, A. V., Dekens, P. S., McCarthy, M., Ravelo, A. C., DeMenocal, P. B., Barreiro, M., … Philander, S. G. (2006). The Pliocene Paradox (Mechanisms for a Permanent El Nino). *Science*, *312*, 1485–1489. https://doi.org/10.1126/science.1122666

Fedorov, Alexey V., Brierley, C. M., Lawrence, K. T., Liu, Z., Dekens, P. S., & Ravelo, A. C. (2013). Patterns and mechanisms of early Pliocene warmth. *Nature*, *496*(7443), 43–49. https://doi.org/10.1038/nature12003

Fedorov, Alexey V., Burls, N. J., Lawrence, K. T., & Peterson, L. C. (2015). Tightly linked zonal and meridional sea surface temperature gradients over the past five million years. *Nature Geoscience*, *8*(12), 975–980. https://doi.org/10.1038/ngeo2577

Ferretti, P., Crowhurst, S. J., Naafs, B. D. A., & Barbante, C. (2015). The Marine Isotope Stage 19 in the mid-latitude North Atlantic Ocean: Astronomical signature and intra-interglacial variability. *Quaternary Science Reviews*, *108*, 95–110. https://doi.org/10.1016/j.quascirev.2014.10.024

Fetterer, F., Knowles, K., Meier, W., Savoie, M., & Windnagel, A. K. (2016). *Sea Ice Index, Version 2 [Monthly Sea Ice Extent]*. Boulder, Colorado USA. https://doi.org/http://dx.doi.org/10.7265/N5736NV7

Fiedler, P. C., & Talley, L. D. (2006). Hydrography of the eastern tropical Pacific: A review. *Progress in Oceanography*, *69*(2–4), 143–180. https://doi.org/10.1016/j.pocean.2006.03.008

Ford, H. L., & Ravelo, A. C. (2019). Estimates of Pliocene Tropical Pacific Temperature Sensitivity to Radiative Greenhouse Gas Forcing. *Paleoceanography and Paleoclimatology*, *34*(1), 2–15. https://doi.org/10.1029/2018PA003461

Ford, H. L., Ravelo, A. C., Dekens, P. S., Lariviere, J. P., & Wara, M. W. (2015). The evolution of the equatorial thermocline and the early Pliocene El Padre mean state. *Geophysical Research Letters*, *42*(12), 4878–4887. https://doi.org/10.1002/2015GL064215

Ford, H. L., Ravelo, A. C., & Hovan, S. (2012). A deep Eastern Equatorial Pacific thermocline during the early Pliocene warm period. *Earth and Planetary Science Letters*, *355–356*, 152–161. https://doi.org/10.1016/j.epsl.2012.08.027

Ford, H. L., Ravelo, A. C., & Polissar, P. J. (2015). Reduced El Niño–Southern Oscillation during the Last Glacial Maximum. *Science*, *347*(6219), 255–258. https://doi.org/10.1126/science.1258437

Francke, A., Wennrich, V., Sauerbrey, M., Juschus, O., Melles, M., & Brigham-Grette, J. (2013). Multivariate statistic and time series analyses of grain-Size data in quaternary sediments of Lake El'gygytgyn, NE Russia. *Climate of the Past*, *9*(6), 2459–2470. https://doi.org/10.5194/cp-9-2459-2013

Frey, K. E., Moore, G. W. K., Cooper, L. W., & Grebmeier, J. M. (2015). Divergent patterns of recent sea ice cover across the Bering, Chukchi, and Beaufort seas of the Pacific Arctic Region. *Progress in Oceanography*, *136*, 32–49. https://doi.org/10.1016/j.pocean.2015.05.009

Garrison, R. E., & Fischer, A. G. (1969). Deep Water Limestones and Radiolarites of the Alpine Jurassic. In G. M. Friedman (Ed.), *Depositional Enviornments in Carbonate Rocks* (pp. 20–56). https://doi.org/10.2110/pec.69.03.0020

Garzione, C. N., McQuarrie, N., Perez, N. D., Ehlers, T. A., Beck, S. L., Kar, N., … Horton, B. K. (2017). Tectonic Evolution of the Central Andean Plateau and Implications for the Growth of Plateaus. *Annual Review of Earth and Planetary Sciences*, *45*, 529–559. https://doi.org/10.1146/annurev-earth-063016-020612

Ghil, M, Allen, M. R., Dettinger, M. D., Ide, K., Kondrashov, D., Mann, M. E., … Yiou, P. (2002). Advanced spectral methods for climate time series. *Reviews of Geophysics*, *40*(1), 3.1-3.41. https://doi.org/10.1029/2001RG000092

Ghil, Michael. (1994). Cryothermodynamics: the chaotic dynamics of paleoclimate. *Physica D: Nonlinear Phenomena*, *77*(1–3), 130–159. https://doi.org/10.1016/0167-2789(94)90131-7

Gildor, H., & Tziperman, E. (2000). Sea ice as the glacial cycles' climate switch Role of seasonal and orbital forcing. *Paleoceanography*, *15*(6), 605–615. https://doi.org/10.1029/1999PA000461

Goldner, A., Huber, M., Diffenbaugh, N., & Caballero, R. (2011). Implications of the permanent El Niño teleconnection "blueprint" for past global and North American hydroclimatology. *Climate of the Past*, *7*(3), 723–743. https://doi.org/10.5194/cp-7-723-2011

Gorbarenko, S. A., Wang, P., Wang, R., & Cheng, X. (2010). Orbital and suborbital environmental changes in the southern Bering Sea during the last 50kyr. *Palaeogeography, Palaeoclimatology, Palaeoecology*, *286*(1–2), 97–106. https://doi.org/10.1016/j.palaeo.2009.12.014

Graham, D. W., Bender, M. L., Williams, D. F., & Keigwin, L. D. (1982). Strontium-calcium ratios in Cenozoic planktonic foraminifera. *Geochimica et*

Cosmochimica Acta, *46*(7), 1281–1292. https://doi.org/10.1016/0016-7037(82)90012-6

Gray, W. R., & Evans, D. (2019). Nonthermal Influences on Mg/Ca in Planktonic Foraminifera: A Review of Culture Studies and Application to the Last Glacial Maximum. *Paleoceanography and Paleoclimatology*, *34*(3), 306–315. https://doi.org/10.1029/2018PA003517

Groth, A., & Ghil, M. (2015). Monte Carlo singular spectrum analysis (SSA) revisited: Detecting oscillator clusters in multivariate datasets. *Journal of Climate*, *28*(19), 7873–7893. https://doi.org/10.1175/JCLI-D-15-0100.1

Gu, D., & Philander, S. G. H. (1997). Interdecadal climate fluctuations that depend on exchanges between the tropics and extratropics. *Science*, *275*(5301), 805–807. https://doi.org/10.1126/science.275.5301.805

Gualtieri, L., Glushkova, O., & Brigham-Grette, J. (2000). Evidence for restricted ice extent during the last glacial maximum in the Koryak Mountains of Chukotka, far Eatern Russia. *Bulletin of the Geological Society of America*, *112*(7), 1106–1118. https://doi.org/10.1130/0016-7606(2000)112<1106:EFRIED>2.0.CO;2

Hagelberg, T. K., Bond, G., & DeMenocal, P. (1994). Milankovitch band forcing of sub-Milankovitch climate variability during the Pleistocene. *Paleoceanography*, *9*(4), 545–558. https://doi.org/10.1029/94PA00443

Hall, R. (2017). Southeast Asia: New Views of the Geology of the Malay Archipelago. *Annual Review of Earth and Planetary Sciences*, *45*, 331–358. https://doi.org/10.1146/annurev-earth-063016-020633

Hamilton, E. L. (1971). Elastic properties of marine sediments. *Journal Geophysical Research*, *76*(2), 579–604. https://doi.org/10.1029/JB076i002p00579

Hamilton, E. L. (1974). Prediction of deep-sea sediment properties: state-of-the-art. In A. L. Inderbitzen (Ed.), *Deep-Sea Sediments* (Vol. 2). New York: Springer, Boston, MA. https://doi.org/10.1007/978-1-4684-2754-7_1

Hamilton, E. L. (1976). Variations of density and porosity with depth in deep-sea sediments. *Journal of Sedimentary Petrology*, *46*(2), 280–300. https://doi.org/10.1306/212F6F3C-2B24-11D7-8648000102C1865D

Hamilton, E. L., & Bachman, R. (1982). Sound velocity and related properties of marine sediments. *The Journal of the Acoustical Society of America*, *72*(6), 1891. https://doi.org/10.1121/1.388539

Harper, B. S., Atmospheric, P., & Sciences, O. (2000). Thermocline ventilation and pathways of tropical – subtropical water mass exchange. *Tellus*, *0870*(April), 330–345. https://doi.org/10.3402/tellusa.v52i3.12269

Haug, G. H., Tiedemann, R., Zahn, R., & Ravelo, A. C. (2001). Role of Panama uplift on oceanic freshwater balance. *Geology*, *29*(3), 207–210. https://doi.org/10.1130/0091-7613(2001)029<0207:ROPUOO>2.0.CO;2

Hay, J. D., Imbrie, J., & Shackleton, N. J. (1976). Variations in the Earth's Orbit: Pacemaker of the Ice Ages. *Science*, *194*, 1121–1132. https://doi.org/10.1126/science.194.4270.1121

He, S., Gao, Y., Li, F., Wang, H., & He, Y. (2017). Impact of Arctic Oscillation on the East Asian climate: A review. *Earth-Science Reviews*, *164*, 48–62. https://doi.org/10.1016/j.earscirev.2016.10.014

Heath, G. R., & Moberly, R. (1971). Cherts from the Western Pacific, Leg 7, Deep Sea Drilling Project. In E. L. Winterer & et al. (Eds.), *Initial Reports of the Deep Sea Drilling Program, Volume 7* (pp. 991–1007). Washington (U.S. Government Printing Office). https://doi.org/10.2973/dsdp.proc.7.119.1971

Heiser, P. A., & Roush, J. J. (2001). Pleistocene glaciations in Chukotka, Russia; moraine mapping using satellite synthetic aperture radar (SAR) imagery. *Quaternary Science Reviews*, *20*(1–3), 393–404. https://doi.org/10.1016/S0277-3791(00)00109-8

Herbert, T. D., Lawrence, K. T., Tzanova, A., Peterson, L. C., Caballero-Gill, R., & Kelly, C. S. (2016). Late Miocene global cooling and the rise of modern ecosystems. *Nature Geoscience*, *9*(11), 843–847. https://doi.org/10.1038/ngeo2813

Herbert, T. D., & Mayer, L. A. (1991). Long climate time series from sediment physical property measurements. *Journal of Sedimentary Petrology*, *61*(7), 1089–1108. https://doi.org/10.1306/D4267843-2B26-11D7-8648000102C1865D

Herbert, T. D., Peterson, L. C., Lawrence, K. T., & Liu, Z. (2010). Tropical ocean temperatures over the past 3.5 million years. *Science*, *328*(5985), 1530–1534. https://doi.org/10.1126/science.1185435

Hertzberg, J. E., Schmidt, M. W., Bianchi, T. S., Smith, R. K., Shields, M. R., & Marcantonio, F. (2016). Comparison of eastern tropical Pacific TEX86 and Globigerinoides ruber Mg/Ca derived sea surface temperatures: Insights from the Holocene and Last Glacial Maximum. *Earth and Planetary Science Letters*, *434*, 320–332. https://doi.org/10.1016/j.epsl.2015.11.050

Hesse, R., & Schacht, U. (2011). Early diagenesis of deep-sea sediments. In H. Huneke & T. Mulder (Eds.), *Developments in Sedimentology* (Vol. 63, pp. 557–713). Amsterdam: Elsevier. https://doi.org/10.1016/B978-0-444-53000-4.00009-3

Ho, S. L., & Laepple, T. (2016). Flat meridional temperature gradient in the early Eocene in the subsurface rather than surface ocean. *Nature Geoscience*, *9*(8), 606–610. https://doi.org/10.1038/ngeo2763

Holbourn, A. E., Kuhnt, W., Clemens, S. C., Kochhann, K. G. D., Jöhnck, J., Lübbers, J., & Andersen, N. (2018). Late Miocene climate cooling and intensification of southeast Asian winter monsoon. *Nature Communications*, *9*, 1–13. https://doi.org/10.1038/s41467-018-03950-1

Hönisch, B., Allen, K. A., Lea, D. W., Spero, H. J., Eggins, S. M., Arbuszewski, J., … Elderfield, H. (2013). The influence of salinity on Mg/Ca in planktic foraminifers - Evidence from cultures, core-top sediments and complementary δ18O. *Geochimica et Cosmochimica Acta*, *121*, 196–213. https://doi.org/10.1016/j.gca.2013.07.028

Hopkins, D. M. (1982). Aspects of the paleogeography of Beringia during the late Pleistocene. In *Paleoecology of Beringia* (pp. 3–28). Elsevier. https://doi.org/10.1016/b978-0-12-355860-2.50008-9

Hopkins, D. M., & Einarsson, T. (1966). Pleistocene Glaciation on St . George , Pribilof Islands. *Science*, *152*(3720), 343–345. https://doi.org/10.1126/science.152.3720.343

Hori, R., Cho, C.-F., & Umeda, H. (1993). Origin of cyclicity in Triassic-Jurassic radiolarian bedded cherts of the Mino accretionary complex from Japan. *The Island Arc*, *3*, 170–180. https://doi.org/10.1111/j.1440-1738.1993.tb00084.x

Horikawa, K., Martin, E. E., Basak, C., Onodera, J., Seki, O., Sakamoto, T., … Kawamura, K. (2015). Pliocene cooling enhanced by flow of low-salinity Bering Sea water to the Arctic Ocean. *Nature Communications*, *6*, 7587. https://doi.org/10.1038/ncomms8587

Huguet, C., Schimmelmann, A., Thunell, R., Lourens, L. J., Damsté, J. S. S., & Schouten, S. (2007). A study of the TEX86 paleothermometer in the water column and sediments of the Santa Barbara Basin, California. *Paleoceanography*, *22*(3), 1–9. https://doi.org/10.1029/2006PA001310

Huybers, P. (2006). Early Pleistocene glacial cycles and the integrated summer

insolation forcing. *Science*, *313*(5786), 508–511.
https://doi.org/10.1126/science.1125249

Huybers, P. (2011). Combined obliquity and precession pacing of late Pleistocene
deglaciations. *Nature*, *480*(7376), 229–232. https://doi.org/10.1038/nature10626

Huybers, P., & Wunsch, C. (2005). Obliquity pacing of the late Pleistocene glacial
terminations. *Nature*, *434*(7032), 491–494. https://doi.org/10.1038/nature03401

Iijima, A., & Utada, M. (1983). Recent developments in the sedimentology of
siliceous deposits in Japan. *Developments in Sedimentology*, *36*, 45–64.
https://doi.org/10.1016/S0070-4571(08)70083-9

Ikenoue, T., Okazaki, Y., Takahashi, K., & Sakamoto, T. (2015). Bering sea
radiolarian biostratigraphy and paleoceanography at IODP site U1341 during the
last four million years. *Deep Sea Research Part II: Topical Studies in
Oceanography*, 1–18. https://doi.org/10.1016/j.dsr2.2015.03.004

Imbrie, J., Berger, A., Boyle, E. A., Clemens, S. C., Duffy, A., Howard, W. R., …
Lemaitre, G. (1993). On the structure and origin of major glaciation cycles 2.
The 100,000 year cycle. *Paleoceanography*, *8*(6), 699–735.
https://doi.org/10.1029/93PA02751

Isaacs, C. M., Pisciotto, K. A., & Garrison, R. E. (1983). Facies and Diagenesis of the
Miocene Monterey Formation, California: A Summary. *Developments in
Sedimentology*, *36*, 247–282. https://doi.org/10.1016/S0070-4571(08)70094-3

Iwasaki, S., Takahashi, K., Kanematsu, Y., Asahi, H., Onodera, J., & Ravelo, A. C.
(2016). Paleoproductivity and paleoceanography of the last 4.3 Myrs at IODP
Expedition 323 Site U1341 in the Bering Sea based on biogenic opal content.
Deep-Sea Research Part II: Topical Studies in Oceanography, *125–126*, 145–
154. https://doi.org/10.1016/j.dsr2.2015.04.005

Jaeger, J. M., & Koppes, M. N. (2016). The role of the cryosphere in source-to-sink
systems. *Earth-Science Reviews*, *153*, 43–76.
https://doi.org/10.1016/j.earscirev.2015.09.011

Janik, A., Lyle, M. W., & Liberty, L. M. (2004). Seismic expression of Pleistocene
paleoceanographic changes in the California Borderland from digitally acquired
3.5 kHz subbottom profiles and Ocean Drilling Program Leg 167 drilling.
Journal of Geophysical Research, *109*, B07101.
https://doi.org/10.1029/2003JB002439

Jansen, E., Fronval, T., Rack, F., & Channell, J. E. T. (2000). Pliocene-Pleistocene

ice rafting history and cyclicity in the Nordic Seas during the last 3.5 Myr. *Paleoceanography*, *15*(6), 709–721. https://doi.org/10.1029/1999PA000435

Johnson, T. C. (1976). Controls on the Preservation of Biogenic Opal in Sediments of the Eastern Tropical Pacific. *Science*, *192*(4242), 887–890. 10.1126/science.192.4242.887

Karas, C., Nürnberg, D., Tiedemann, R., & Garbe-Schönberg, D. (2011). Pliocene Indonesian Throughflow and Leeuwin Current dynamics: Implications for Indian Ocean polar heat flux. *Paleoceanography*, *26*(2), 1–9. https://doi.org/10.1029/2010PA001949

Kastner, M., & Gieske, J. M. (1983). Opal-A to opal-CT transformations: A kinetic study. *Siliceous Deposits in the Pacific Region*, 211–226. https://doi.org/10.1017/CBO9781107415324.004

Kastner, M., Keene, J. B., & Gieske, J. M. (1977). Diagenesis of siliceous oozes-Chemical controls on the rate of opal-A to opal-CT transformation- an experimental study. *Geochimica et Cosmochimica Acta*, *41*(8), 1041–1059. https://doi.org/10.1016/0016-7037(77)90099-0

Katsuki, K., & Takahashi, K. (2005). Diatoms as paleoenvironmental proxies for seasonal productivity, sea-ice and surface circulation in the Bering Sea during the late Quaternary. *Deep-Sea Research Part II: Topical Studies in Oceanography*, *52*(16–18), 2110–2130. https://doi.org/10.1016/j.dsr2.2005.07.001

Kaufman, D. S., Briner, J. P., & Manley, W. F. (2004). Pleistocene maximum and Late Wisconsinan glacier extents across Alaska, USA. *Developments in Quaternary Sciences*, *2*, 9–27. https://doi.org/https://doi.org/10.1016/S1571-0866(04)80182-9

Kaufman, D. S., & Manley, W. F. (2004). Pleistocene Maximum and Late Wisconsinan glacier extents across Alaska, U. S. A. *Developments in Quaternary Sciences*, *2*, 9–27. https://doi.org/10.1016/S1571-0866(04)80182-9

Keigwin, L. D. (1982). Isotopic paleoceanography of the Caribbean and East pacific: role of panama uplift in late neogene time. *Science*, *217*(4557), 350–353. https://doi.org/10.1126/science.217.4557.350.

Kempema, E. W., Reimnitz, E., & Barnes, P. W. (1989). Sea Ice Sediment Entrainment and Rafting in the Arctic. *Journal of Sedimentary Petrology*, *59*(2), 308–317. https://doi.org/10.1306/212F8F80-2B24-11D7-8648000102C1865D

Kim, J. H., van der Meer, J., Schouten, S., Helmke, P., Willmott, V., Sangiorgi, F., … Damsté, J. S. S. (2010). New indices and calibrations derived from the distribution of crenarchaeal isoprenoid tetraether lipids: Implications for past sea surface temperature reconstructions. *Geochimica et Cosmochimica Acta*, *74*(16), 4639–4654. https://doi.org/10.1016/j.gca.2010.05.027

Knight, P. G. (1997). The basal ice layer of glaciers and ice sheets. *Quaternary Science Reviews*, *16*, 975–993. https://doi.org/0277-3791/97

Knorr, G., Butzin, M., Micheels, A., & Lohmann, G. (2011). A warm Miocene climate at low atmospheric CO2 levels. *Geophysical Research Letters*, *38*(20), 1–5. https://doi.org/10.1029/2011GL048873

Knutson, T., & Manabe, S. (1995). Time-Mean Response over the Tropical Pacific to Increeased CO2 in a Coupled Ocean-Atmoshere Model. *Journal of Climate*, *8*(9), 2181–2199. https://doi.org/10.1175/1520-0442(1995)008<2181:TMROTT>2.0.CO;2

Koizumi, I., & Yamamoto, H. (2018). Diatom ooze and diatomite–diatomaceous sediments in and around the North Pacific Ocean. *JAMSTEC Report of Research and Development*, *27*(0), 26–46. https://doi.org/10.5918/jamstecr.27.26

Kotilainen, A. T., & Shackleton, N. J. (1995). Rapid climate variability in the North Pacific Ocean during the past 95,000 years. *Nature*, *377*(6547), 323–326. https://doi.org/10.1038/377323a0

Kozdon, R., Kelly, D. C., Kitajima, K., Strickland, A., Fournelle, J. H., & Valley, J. W. (2013). In situ δ18O and Mg/Ca analyses of diagenetic and planktic foraminiferal calcite preserved in a deep-sea record of the Paleocene-Eocene thermal maximum. *Paleoceanography*, *28*(3), 517–528. https://doi.org/10.1002/palo.20048

Krissek, L. A. (1995). Late Cenozoic ice-rafting records from Leg 145 sites in the North Pacific: Late Miocene onset, late Pliocene intensification, and Pliocene-Pleistocene events. In D. K. Rea, I. A. Basov, D. W. Scholl, & J. F. Allan (Eds.), *Proc. ODP, Sci. Results, 145* (pp. 179–194). College Station, TX: Ocean Drilling Program. https://doi.org/10.2973/odp.proc.sr.145.118.1995

Kutzbach, J. E., & Guetter, P. J. (1986). The influence of changing orbital parameters and surface boundary conditions on climate simulatinos for the past 18000 years. *Journal of the Atmospheric Sciences*, *43*(16), 1726–1759. https://doi.org/10.1175/1520-0469(1986)043<1726:TIOCOP>2.0.CO;2

Lagoe, M. B., Eyles, C. H., Eyles, N., & Hale, C. (1993). Timing of late Cenozoic

tidewater glaciation in the far North Pacific Timing of late Cenozoic tidewater glaciation in the far North Pacific. *Geological Society Of America Bulletin*, (12), 1542–1560. https://doi.org/10.1130/0016-7606(1993)105<1542

LaRiviere, J. P., Ravelo, A. C., Crimmins, A., Dekens, P. S., Ford, H. L., Lyle, M., & Wara, M. W. (2012). Late Miocene decoupling of oceanic warmth and atmospheric carbon dioxide forcing. *Nature*, *486*(7401), 97–100. https://doi.org/10.1038/nature11200

Larsen, H. C., Saunders, a D., Clift, P. D., Beget, J., Wei, W., & Spezzaferri, S. (1994). Seven million years of glaciation in greenland. *Science*, *264*(5161), 952–955. https://doi.org/10.1126/science.264.5161.952

Laskar, J., Robutel, P., Joutel, F., Gastineau, M., Correia, a. C. M., & Levrard, B. (2004). A long-term numerical solution for the insolation quantities of the Earth. *Astronomy and Astrophysics*, *428*(1), 261–285. https://doi.org/10.1051/0004-6361:20041335

Lawrence, K. T., Pearson, A., Castañeda, I. S., Ladlow, C., Peterson, L. C., & Lawrence, C. E. (2020). Comparison of Late Neogene Uk′37 and TEX86 Paleotemperature Records From the Eastern Equatorial Pacific at Orbital Resolution. *Paleoceanography and Paleoclimatology*, *35*(7), 1–7. https://doi.org/10.1029/2020PA003858

Lawrence, K. T., Sosdian, S., White, H. E., & Rosenthal, Y. (2010). North Atlantic climate evolution through the Plio-Pleistocene climate transitions. *Earth and Planetary Science Letters*, *300*(3–4), 329–342. https://doi.org/10.1016/j.epsl.2010.10.013

Lawrence, Kira T., Liu, Z., & Herbert, T. D. (2006). Evolution of the Eastern Tropical Pacific Through Plio-Pleistocene Glaciation. *Science*, *312*, 79–84. https://doi.org/10.1126/science.1120395

Le Treut, H., & Ghil, M. (1983). Orbital forcing, climatic interactions, and glaciation cycles. *Journal of Geophysical Research: Oceans*, *88*(C9), 5167–5190. https://doi.org/10.1029/JC088iC09p05167

Lear, C. H., Elderfield, H., & Wilson, P. A. (2003). A Cenozoic seawater Sr/Ca record from benthic foraminiferal calcite and its application in determining global weathering fluxes. *Earth and Planetary Science Letters*, *208*(1–2), 69–84. https://doi.org/10.1016/S0012-821X(02)01156-1

Lee, S. Y., & Poulsen, C. J. (2009). Obliquity and precessional forcing of continental snow fall and melt: implications for orbital forcing of Pleistocene ice ages.

Quaternary Science Reviews, *28*(25–26), 2663–2674. https://doi.org/10.1016/j.quascirev.2009.06.002

Levitus, S., & Boyer, T. P. (1994). *World Ocean Atlast 1994*. United States.

Li, F., & Wang, H. (2013). Relationship between Bering Sea ice cover and East Asian winter monsoon year-to-year variations. *Advances in Atmospheric Sciences*, *30*(1), 48–56. https://doi.org/10.1007/s00376-012-2071-2

Lisiecki, L. E., & Raymo, M. E. (2004). A Pliocene-Pleistocene stack of 57 globally distributed benthic δ 18 O records. *Paleoceanography*, (1). https://doi.org/10.1029/2004PA001071

Lisiecki, L. E., & Raymo, M. E. (2005). A Pliocene-Pleistocene stack of 57 globally distributed benthic 18O records. *Paleoceanography*, *20*(1), 1–17. https://doi.org/10.1029/2004PA001071

Lisitsyn, A. ., Belyayev, Y., Bogdanov, Y., & Bogoyavlenskiy, A. (1967). Distribution relationships and forms of silicon suspended in the waters of the World Ocean. *International Geology Review*, *9*(4), 604–623. https://doi.org/10.1080/00206816709474491

Lisitzin, A. (2002). Stages of lithogenesis in ice zones: Three types of sea ice sedimentation and two vertical levels of the process. In *Sea-ice and iceberg sedimentation in the ocean* (pp. 79–115). Berlin Heidelberg: Springer. https://doi.org/https://doi.org/10.1007/978-3-642-55905-1_6

Liu, J., Tian, J., Liu, Z., Herbert, T. D., Fedorov, A. V., & Lyle, M. (2019). Eastern equatorial Pacific cold tongue evolution since the late Miocene linked to extratropical climate. *Science Advances*, *5*(4), 1–8. https://doi.org/10.1126/sciadv.aau6060

Liu, Z., & Herbert, T. D. (2004). High-latitude influence on the eastern equatorial Pacific climate in the early Pleistocene epoch. *Nature*, *427*, 720–723. https://doi.org/10.1038/nature02338

Locarnini, R. A., Mishonov, A. V., Antonov, J. I., Boyer, T. P., Garcia, H. E., Baranova, O. K., … Seidov, D. (2013). World Ocean Atlas 2013. Vol. 1: Temperature. *S. Levitus, Ed.; A. Mishonov, Technical Ed.; NOAA Atlas NESDIS*. https://doi.org/10.7289/V55X26VD

Lovell, H., Fleming, E., Benn, D., Hubbard, B., Lukas, S., Rea, B. R., … Flink, A. E. (2015). Debris entrainment and landorm genesis during tidewater glacier surges. *Journal of Geophysical Research: Earth Surface*, *120*, 1574–1595. https://doi.org/10.1002/2015JF003509

Lyle, M. (2003). Neogene carbonate burial in the Pacific Ocean. *Paleoceanography*, *18*(3), 1059-undefined. https://doi.org/10.1029/2002PA000777

Lyle, M., & Baldauf, J. (2015). Biogenic sediment regimes in the Neogene equatorial Pacific, IODP Site U1338: Burial, production, and diatom community. *Palaeogeography, Palaeoclimatology, Palaeoecology*, *433*, 106–128. https://doi.org/10.1016/j.palaeo.2015.04.001

Manley, W. F., Kaufman, D. S., & Briner, J. P. (2001). Pleistocene glacial history of the southern Ahklun Mountains, southwestern Alaska: Soil-development, morphometric, and radiocarbon constraints. *Quaternary Science Reviews*, *20*(1–3), 353–370. https://doi.org/10.1016/S0277-3791(00)00111-6

Marsaglia, K., Milliken, K., & Doran, L. (2013). *IODP Digital Reference for Smear Slides Analysis of Marine Mud*. *Part 1 : Methodology and Atlas of Siliciclastic and Volcanogenic Components*. IODP Technical Note 1. https://doi.org/10.2204/iodp.tn.1.2013

Marsaglia, K., Milliken, K., Leckie, R. M., Tentori, D., & Doran, L. (2015). *IODP Smear Slide Digital Reference for Sediment Analysis of Marine Mud*. *Part 2: Methodology and Atlas of Biogenic Components*. IODP Technical Note 2. https://doi.org/10.2204/iodp.tn.2.2015

Martin, P. A., & Lea, D. W. (2002). A simple evaluation of cleaning procedures on fossil benthic foraminiferal Mg/Ca. *Geochemistry, Geophysics, Geosystems*, *3*(10), 1–8. https://doi.org/10.1029/2001GC000280

Martinez-Garcia, A., Rosell-Melé, A., McClymont, E. L., Gersonde, R., & Haug, G. H. (2010). Subpolar Link to the Emergence of the Modern Equatorial Pacific Cold Tongue. *Science*, *5985*, 1550–1553. https://doi.org/10.1126/science.1184480

Martínez-Garcia, A., Rosell-Melé, A., McClymont, E. L., Gersonde, R., & Haug, G. H. (2010). Subpolar link to the emergence of the modern equatorial pacific cold tongue. *Science*, *328*(5985), 1550–1553. https://doi.org/10.1126/science.1184480

Maslin, M. A., Haug, G. H., Sarnthein, M., Tiedemann, R., Erlenkeuser, H., & Stax, R. (1995). Northwest Pacific Site 882: The Initiation of Northern Hemisphere Glaciation. In D.K. Rea, L. A. Basov, D. W. Scholl, & J. F. Allan (Eds.), *Proc. ODP, Sci. Results, 145* (pp. 315–329). College Station, TX: Ocean Drilling Program. https://doi.org/10.2973/odp.proc.sr.145.119.1995

McGuire, A. D., Chapin, F. S., Walsh, J. E., & Wirth, C. (2006). Integrated regional changes in arctic climate feedbacks: Implications for the global climate system. *Annual Review of Environment and Resources*, *31*, 61–91. https://doi.org/10.1146/annurev.energy.31.020105.100253

McIntyre, A., & Molfino, B. (1996). Forcing of Atlantic Equatorial and Subpolar Millennial Cycles by Precession. *Science*, *274*(5294), 1867–1870. https://doi.org/10.1126/science.274.5294.1867

McIntyre, K., Delaney, M. L., & Ravelo, A. C. (2001). Millennial-scale climate change and oceanic processes in the late Pliocene and early Pleistocene. *Paleoceanography*, *16*(5), 535–543. https://doi.org/10.1029/2000PA000526

McKelvey, B., Chen, W., & Arculus, R. (1995). Provenance of Pliocene-Pleistocene ice-rafted debris, Leg 145, Northern Pacific Ocean. In D. K. Rea, I. A. Basov, D. W. Scholl, & J. F. Allan (Eds.), *Proc. ODP, Sci. Results, 145* (pp. 195–204). College Station, TX: Ocean Drilling Program. https://doi.org/10.2973/odp.proc.sr.145.120.1995

McRae, S. G. (1972). Glauconite. *Earth-Science Reviews*, *8*(4), 397–440. https://doi.org/10.1016/0012-8252(72)90063-3

Medina-Elizalde, M., & Lea, D. W. (2010). Late Pliocene equatorial Pacific. *Paleoceanography*, *25*(2), 1–10. https://doi.org/10.1029/2009PA001780

Medina-Elizalde, M., Lea, D. W., & Fantle, M. S. (2008). Implications of seawater Mg/Ca variability for Plio-Pleistocene tropical climate reconstruction. *Earth and Planetary Science Letters*, *269*(3–4), 584–594. https://doi.org/10.1016/j.epsl.2008.03.014

Mejía, L. M., Méndez-Vicente, A., Abrevaya, L., Lawrence, K. T., Ladlow, C., Bolton, C., … Stoll, H. (2017). A diatom record of CO2 decline since the late Miocene. *Earth and Planetary Science Letters*, *479*, 18–33. https://doi.org/10.1016/j.epsl.2017.08.034

Mestas-Nuñez, A. M., & Molnar, P. (2014). A mechanism for freshening the Caribbean Sea in pre-Ice Age time. *Paleoceanography*, *29*(6), 508–517. https://doi.org/10.1002/2013PA002515

Meyers, S. R. (2012). Seeing red in cyclic stratigraphy: Spectral noise estimation for astrochronology. *Paleoceanography*, *27*(3), 1–12. https://doi.org/10.1029/2012PA002307

Meyers, S. R. (2015). Testing and Time Scale Optimization. *Paleoceanography*, *30*,

1625–1640. https://doi.org/10.1002/2015PA002850

Milankovitch, M. K. (1941). Kanon der Erdbestrahlung und seine Anwendung auf das Eiszeitenproblem. *Royal Serbian Academy Special Publication*, *133*, 1–633. Retrieved from https://ci.nii.ac.jp/naid/10009278924

Miller, K. G., Browning, J. V., John Schmelz, W., Kopp, R. E., Mountain, G. S., & Wright, J. D. (2020). Cenozoic sea-level and cryospheric evolution from deep-sea geochemical and continental margin records. *Science Advances*, *6*(20). https://doi.org/10.1126/sciadv.aaz1346

Miller, K. G., Mountain, G. S., Wright, J. D., & Browning, J. V. (2011). Sea level and ice volume variations from continental margin and deep-sea isotopic records. *Oceanography*, *24*(2), 40–53. https://doi.org/10.5670/oceanog.2011.26

Molnar, P. (2008). Closing of the Central American Seaway and the ice age: A critical review. *Paleoceanography*, *23*(2), 1–15. https://doi.org/10.1029/2007PA001574

Molnar, P., & Cane, M. (2002). El Niño's tropical climate and teleconnections as a blueprint for pre-Ice Age climates. *Paleoceanography*, *17*(2), 1021-undefined. https://doi.org/10.1029/2001PA000663

Molnar, P., & Cane, M. A. (2007). Early Pliocene (pre-Ice age) El Niño-like global climate: Which El Niño? *Geosphere*, *3*(5), 337–365. https://doi.org/10.1130/GES00103.1

Molnia, B. F. (2007). Late nineteenth to early twenty-first century behavior of Alaskan glaciers as indicators of changing regional climate. *Global and Planetary Change*, *56*(1–2), 23–56. https://doi.org/10.1016/j.gloplacha.2006.07.011

Montes, C., Cardona, A., Jaramillo, C., Pardo, A., Silva, J. C., Valencia, V., … Niño, H. (2015). Middle Miocene closure of the Central American Seaway. *Science*, *348*(6231), 226–229. https://doi.org/10.1126/science.aaa2815

Montes, Camilo, Bayona, G., Cardona, A., Buchs, D. M., Silva, C. A., Morón, S., … Valencia, V. (2012). Arc-continent collision and orocline formation: Closing of the Central American seaway. *Journal of Geophysical Research: Solid Earth*, *117*(4), 1–25. https://doi.org/10.1029/2011JB008959

Montes, Camilo, Cardona, A., McFadden, R., Morón, S. E., Silva, C. A., Restrepo-Moreno, S., … Flores, J. A. (2012). Evidence for middle Eocene and younger land emergence in central Panama: Implications for Isthmus closure. *Bulletin of*

the *Geological Society of America*, *124*(5–6), 780–799.
https://doi.org/10.1130/B30528.1

Mortlock, R., & Froelich, P. (1989). A simple method of the rapid determination of biogenic opal in pelagic marine sediments. *Deep Sea Research Part I: Oceanographic Research Papers*, *36*(9), 1415–1426.

Muller, P. J., Kirst, G., Ruhland, G., von Storch, I., & Rosell-Mele, A. (1998). Calibration of the alkenone paleotemperature index U-37(K ') based on core-tops from the eastern South Atlantic and the global ocean (60 degrees N-60 degrees S). *Geochimica Et Cosmochimica Acta*, *62*(10), 1757–1772. https://doi.org/10.1016/S0016-7037(98)00097-0

Murray, R. W., Jones, D. L., & Buchholtz ten Brink, M. R. (1992). Diagenetic formation of bedded chert: Evidence from chemistry of the chert-shale couplet. *Geology*, *20*(3), 271–274. https://doi.org/10.1130/0091-7613(1992)020<0271:DFOBCE>2.3.CO;2

Naafs, B. D. A., Hefter, J., Acton, G., Haug, G. H., Martínez-Garcia, A., Pancost, R., & Stein, R. (2012). Strengthening of North American dust sources during the late Pliocene (2.7Ma). *Earth and Planetary Science Letters*, *317–318*, 8–19. https://doi.org/10.1016/j.epsl.2011.11.026

Nathan, S. a., & Leckie, R. M. (2009). Early history of the Western Pacific Warm Pool during the middle to late Miocene (~13.2–5.8 Ma): Role of sea-level change and implications for equatorial circulation. *Palaeogeography, Palaeoclimatology, Palaeoecology*, *274*(3–4), 140–159. https://doi.org/10.1016/j.palaeo.2009.01.007

Nechaev, V. P., Sorochinskaya, A. V., Tsoy, I. B., & Gorbarenko, S. A. (1994). Clastic components in Quaternary sediments of the northwest Pacific and their paleo-oceanic significance. *Marine Geology*, *118*(1–2), 119–137. https://doi.org/10.1016/0025-3227(94)90116-3

Newkirk, D. R., & Martin, E. E. (2009). Circulation through the Central American Seaway during the Miocene carbonate crash. *Geology*, *37*(1), 87–90. https://doi.org/10.1130/G25193A.1

Niebauer, H. J. (1988). Interannual Variability in the Subarctic Bering Sea. *Journal Geophysical Research*, *93*, 5051–5068. https://doi.org/10.1029/JC093iC05p05051

Nobes, D. C., Mienert, J., & Dirksen, G. J. (1991). Lithologic control of physical-property interrelationships. In P. Ciesielski & Y. Kristoffersen (Eds.), *Proc*.

ODP, Sci. Results, 114 (pp. 657–669). College Station, TX: Ocean Drilling Program. https://doi.org/10.2973/odp.proc.sr.114.162.1991

O'Brien, C. L., Foster, G. L., Martínez-Botí, M. a., Abell, R., Rae, J. W. B., & Pancost, R. D. (2014). High sea surface temperatures in tropical warm pools during the Pliocene. *Nature Geoscience*, *7*(8), 606–611. https://doi.org/10.1038/ngeo2194

O'Dea, A., Lessios, H. A., Coates, A. G., Eytan, R. I., Restrepo-Moreno, S. A., Cione, A. L., … Jackson, J. B. C. (2016). Formation of the Isthmus of Panama. *Science Advances*, *2*(8), 1–12. https://doi.org/10.1126/sciadv.1600883

Onodera, J., Takahashi, K., & Nagatomo, R. (2013). Diatoms, silicoflagellates, and ebridians at Site U1341 on the western slope of Bowers Ridge, IODP Expedition 323. *Deep Sea Research Part II: Topical Studies in Oceanography*, 1–10. https://doi.org/10.1016/j.dsr2.2013.03.025

Osborne, A., Newkirk, D. R., Groeneveld, J., Martin, E. E., Tiedemann, R., & Frank, M. (2014). The seawater neodymium and lead isotope record of the final stages of Central American Seaway closure. *Paleoceanography*, *29*, 715–729. https://doi.org/10.1002/2014PA002676

Overland, J. E., & Pease, C. H. (1982). Cyclone Climatology of the Bering Sea and Its Relation to Sea Ice Extent. *Monthly Weather Review*, *110*(1), 5–13. https://doi.org/10.1175/1520-0493(1982)110<0005:CCOTBS>2.0.CO;2

Pagani, M., Liu, Z., Lariviere, J., & Ravelo, A. C. (2010). High Earth-system climate sensitivity determined from Pliocene carbon dioxide concentrations. *Nature Geoscience*, *3*(1), 27–30. https://doi.org/10.1038/ngeo724

Pagani, M., Zachos, J. C., Freeman, K. H., Tipple, B., & Bohaty, S. (2005). Marked decline in atmospheric carbon dioxide concentrations during the Paleogene. *Science*, *309*(5734), 600–603. https://doi.org/10.1126/science.1110063

Palmer, T. N., & Mansfield, D. A. (1984). Response of two atmospheric general circulation models to sea- surface temperature anomalies in the tropical East and West Pacific. *Nature*, *310*(5977), 483–485. https://doi.org/10.1038/310483a0

Pearson, A., & Ingalls, A. E. (2013). Assessing the use of archaeal lipids as marine environmental proxies. *Annual Review of Earth and Planetary Sciences*, *41*, 359–384. https://doi.org/10.1146/annurev-earth-050212-123947

Pease, C. H. (1980). Eastern Bering Sea Ice Processes. *Monthly Weather Review*, *108*(12), 2015–2023. https://doi.org/https://doi.org/10.1175/1520-

0493(1980)108<2015:EBSIP>2.0.CO;2

Pena, L. D., Cacho, I., Calvo, E., Pelejero, C., Eggins, S., & Sadekov, A. (2008). Characterization of contaminant phases in foraminifera carbonates by electron microprobe mapping. *Geochemistry, Geophysics, Geosystems*, *9*(7). https://doi.org/10.1029/2008GC002018

Pena, L. D., Calvo, E., Cacho, I., Eggins, S., & Pelejero, C. (2005). Identification and removal of Mn-Mg-rich contaminant phases on foraminiferal tests: Implications for Mg/Ca past temperature reconstructions. *Geochemistry, Geophysics, Geosystems*, *6*(9). https://doi.org/10.1029/2005GC000930

Pettijohn, F. (1975). *Sedimentary Rocks*. Harper & Row.

Philander, S. G., & Fedorov, A. V. (2003). Role of tropics in changing the response to Milankovich forcing some three million years ago. *Paleoceanography*, *18*(2). https://doi.org/10.1029/2002PA000837

Pisciotto, K. A., & Garrison, R. E. (1981). Lithofacies and Depositional environments of the Monterey Formation, California. In R. E. Garrison & R. G. Douglas (Eds.), *The Monterey Formation and Related Siliceous Rocks of California, special publicatoin of the Pacific Section Soiety of Economic Paleontologists and Mineralogists* (pp. 97–112). Pacific Section SEPM.

Pound, M. J., Haywood, A. M., Salzmann, U., & Riding, J. B. (2012). Global vegetation dynamics and latitudinal temperature gradients during the Mid to Late Miocene (15.97-5.33Ma). *Earth-Science Reviews*, *112*, 1–22. https://doi.org/10.1016/j.earscirev.2012.02.005

Pound, M. J., Haywood, A. M., Salzmann, U., Riding, J. B., Lunt, D. J., & Hunter, S. J. (2011). A Tortonian (Late Miocene, 11.61-7.25Ma) global vegetation reconstruction. *Palaeogeography, Palaeoclimatology, Palaeoecology*, *300*, 29–45. https://doi.org/10.1016/j.palaeo.2010.11.029

Rack, F. R., & Palmer-Julson, A. (1992). Sediment microfabric and physical properties record of late Neogene Polar Front migration, Site 751. In S. W. Wise, R. Schlich, & et al. (Eds.), *Proc. ODP, Sci. Results, 120* (pp. 179–205). College Station, TX: Ocean Drilling Program. https://doi.org/10.2973/odp.proc.sr.120.145.1992

Ragueneau, O., Treguer, P., Leynaert, A., Anderson, R. F., Brzezinski, M. A., DeMaster, D. J., … Queguiner, B. (2000). A review of the Si cycle in the modern ocean : recent progress and missing gaps in the application of biogenic opal as a paleoproductivity proxy. *Global and Planetary Change*, *26*, 317–365.

https://doi.org/10.1016/S0921-8181(00)00052-7

Ravelo, A. C., Andreasen, D. H., Lyle, M., Olivarez Lyle, A., & Wara, M. W. (2004). Regional climate shifts caused by gradual global cooling in the Pliocene epoch. *Nature*, *429*, 263–267. https://doi.org/10.1038/nature02567

Ravelo, A. C., Lawrence, K. T., Fedorov, A., & Ford, H. L. (2014). Comment on "A 12-million-year temperature history of the tropical Pacific Ocean." *Science*, *344*(6179), 84–87. https://doi.org/10.1126/science.1246172

Raymo, M. E., Lisiecki, L. E., & Nisancioglu, K. H. (2006). Plio-Pleistocene Ice Volume, Antarctic Climate, and the Global 18O Record. *Science*, *313*, 492–495. https://doi.org/10.1126/science.1123296

Raymo, Maureen E., & Huybers, P. (2008). Unlocking the mysteries of the ice ages. *Nature*, *451*, 284–285. https://doi.org/10.1038/nature06589

Raymo, Maureen E., Lisiecki, L. E., & Nisancioglu, K. H. (2006). Plio-Pleistocene ice volume, Antarctic climate, and the global delta18O record. *Science*, *313*(5786), 492–495. https://doi.org/10.1126/science.1123296

Raymo, Maureen E., & Nisancioglu, K. (2003). The 41 kyr world: Milankovitch's other unsolved mystery. *Paleoceanography*, *18*(1), 1–6. https://doi.org/10.1029/2002PA000791

Regenberg, M., Nürnberg, D., Schönfeld, J., & Reichart, G. J. (2007). Early diagenetic overprint in Caribbean sediment cores and its effect on the geochemical composition of planktonic foraminifera. *Biogeosciences*, *4*(6), 957–973. https://doi.org/10.5194/bg-4-957-2007

Retallack, G. J. (2004). Late Miocene climate and life on land in Oregon within a context of Neogene global change. *Palaeogeography, Palaeoclimatology, Palaeoecology*, *214*(1–2), 97–123. https://doi.org/10.1016/j.palaeo.2004.07.024

Retallack, G. J., Tanaka, S., & Tate, T. (2002). Late Miocene advent of tall grassland paleosols in Oregon. *Palaeogeography, Palaeoclimatology, Palaeoecology*, *183*(3–4), 329–354. https://doi.org/10.1016/S0031-0182(02)00250-X

Rial, J. A., & Anaclerio, C. A. (2000). Understanding nonlinear responses of the climate system to orbital forcing. *Quaternary Science Reviews*, *19*, 1709–1722. https://doi.org/10.1016/S0277-3791(00)00087-1

Ridgwell, A. J., Watson, A. J., & Raymo, M. E. (1999). Is the spectral signature of the 100 kyr glacial cycle consistent with a Milankovitch origin?

Paleoceanography, *14*(4), 437–440. https://doi.org/10.1029/1999PA900018

Rodionov, S. N., Bond, N. a., & Overland, J. E. (2007). The Aleutian Low, storm tracks, and winter climate variability in the Bering Sea. *Deep-Sea Research Part II: Topical Studies in Oceanography*, *54*(23–26), 2560–2577. https://doi.org/10.1016/j.dsr2.2007.08.002

Rodionov, Sergei N., Overland, J. E., & Bond, N. A. (2005). The Aleutian low and winter climatic conditions in the Bering Sea. Part I: Classification. *Journal of Climate*, *18*(1), 160–177. https://doi.org/10.1175/JCLI3253.1

Romero, O. E., & Hebbeln, D. (2003). Biogenic silica and diatom thanatocoenosis in surface sediments below the Peru–Chile Current: controlling mechanisms and relationship with productivity of surface waters. *Marine Micropaleontology*, *48*(1–2), 71–90. https://doi.org/10.1016/S0377-8398(02)00161-5

Romero, O. E., Hebbeln, D., & Wefer, G. (2001). Temporal and spatial variability in export production in the SE Pacific Ocean: evidence from siliceous plankton fluxes and surface sediment assemblages. *Deep Sea Research Part I: Oceanographic Research Papers*, *48*(12), 2673–2697. https://doi.org/10.1016/S0967-0637(01)00037-1

Rommerskirchen, F., Condon, T., Mollenhauer, G., Dupont, L., & Schefuss, E. (2011). Miocene to Pliocene development of surface and subsurface temperatures in the Benguela Current system. *Paleoceanography*, *26*(3), 1–15. https://doi.org/10.1029/2010PA002074

Rosenthal, Y., Holbourn, A., Kullhanek, D. K., & Expedition 363 Scientists. (2017). *Expedition 363 Preliminary Report: Western Pacific Warm Pool*. International Ocean Discovery Program. https://doi.org/10.14379/iodp.pr.363.2017

Rothwell, R. (1989). *Minerals & Mineraloids in Marine Sediments*. (R. G. Rothwell, Ed.) (1st ed.). Crown House, England: Springer Netherlands. https://doi.org/10.1007/978-94-009-1133-8

Rothwell, R. G., & Rack, F. R. (2006). New techniques in sediment core analysis: an introduction. *Geological Society, London, Special Publications*, *267*(1), 1–29. https://doi.org/10.1144/GSL.SP.2006.267.01.01

Rousselle, G., Beltran, C., Sicre, M. A., Raffi, I., & De Rafélis, M. (2013). Changes in sea-surface conditions in the Equatorial Pacific during the middle Miocene-Pliocene as inferred from coccolith geochemistry. *Earth and Planetary Science Letters*, *361*, 412–421. https://doi.org/10.1016/j.epsl.2012.11.003

Sancetta, C., Heusser, L., Labeyrie, L., Naidu, A. S., & Robinson, S. W. (1985). Wisconsin—Holocene paleoenvironment of the Bering Sea: Evidence from diatoms, pollen, oxygen isotopes and clay minerals. *Marine Geology*, *62*(1–2), 55–68. https://doi.org/10.1016/0025-3227(84)90054-9

Sancetta, C., & Robinson, S. W. (1983). Diatom evidence on Wisconsin and Holocene events in the Bering Sea. *Quaternary Research*, *20*(2), 232–245. https://doi.org/10.1016/0033-5894(83)90079-0

Scherer, R. P., Sjunneskog, C. M., Iverson, N. R., & Hooyer, T. S. (2004). Assessing subglacial processes from diatom fragmentation patterns. *Geology*, *32*(7), 557–560. https://doi.org/10.1130/G20423.1

Schlung, S. A., Christina Ravelo, A., Aiello, I. W., Andreasen, D. H., Cook, M. S., Drake, M. K., … Takahashi, K. (2013). Millennial-scale climate change and intermediate water circulation in the Bering Sea from 90 ka: A high-resolution record from IODP Site U1340. *Paleoceanography*, *28*(1), 54–67. https://doi.org/10.1029/2012PA002365

Schmidt, D. N., Caromel, A. G. M., Seki, O., Rae, J. W. B., & Renaud, S. (2016). Morphological response of planktic foraminifers to habitat modifications associated with the emergence of the Isthmus of Panama. *Marine Micropaleontology*, *128*, 28–38. https://doi.org/10.1016/j.marmicro.2016.08.003

Schouten, S., Hopmans, E. C., Schefub, E., & Sinninghe Damste, J. S. (2002). Distributional variations in marine crenarchaeotal membrane lipids: A new tool for reconstructing ancient sea water temperatures? *Earth and Planetary Science Letters*, *204*(1–2), 265–274. https://doi.org/10.1016/S0012-821X(02)00979-2

Schouten, S., Hopmans, E. C., & Sinninghe Damsté, J. S. (2013). The organic geochemistry of glycerol dialkyl glycerol tetraether lipids: A review. *Organic Geochemistry*, *54*, 19–61. https://doi.org/10.1016/j.orggeochem.2012.09.006

Schrader, H. J., & Gersonde, R. (1976). Diatoms and Silicoflagellates. In W. J. Zachariasse, Riedel. W.R. A, R. R. Schmidt, A. Sanfilippo, M. J. Brolsma, H. J. Schrader, … J. A. Broekman (Eds.), *Micropaleontological Counting Methods and Techniques an Exercise on an Eight Metres Section of the Lower Pliocene of Capo Rosello, Sicily* (pp. 129–176). Utrecht: Utrecht Micropaleontology.

Schuette, G., & Schrader, H. (1981). Diatoms in surface sediments: A reflection of coastal upwelling. In F. A. Richards (Ed.), *Coastal and Esuarine Sciences* (Vol. 1, pp. 372–380). https://doi.org/10.1029/CO001p0372

Seager, R., Cane, M., Henderson, N., Lee, D. E., Abernathey, R., & Zhang, H.

(2019). Strengthening tropical Pacific zonal sea surface temperature gradient consistent with rising greenhouse gases. *Nature Climate Change*, *9*(7), 517–522. https://doi.org/10.1038/s41558-019-0505-x

Seki, O., Foster, G. L., Schmidt, D. N., Mackensen, A., Kawamura, K., & Pancost, R. D. (2010). Alkenone and boron-based Pliocene pCO2 records. *Earth and Planetary Science Letters*, *292*(1–2), 201–211. https://doi.org/10.1016/j.epsl.2010.01.037

Seki, O., Schmidt, D. N., Schouten, S., Hopmans, E. C., Sinninghe Damsté, J. S., & Pancost, R. D. (2012). Paleoceanographic changes in the Eastern Equatorial Pacific over the last 10 Myr. *Paleoceanography*, *27*(3), 1–14. https://doi.org/10.1029/2011PA002158

Sepulchre, P., Arsouze, T., Donnadieu, Y., Dutay, J. C., Jaramillo, C., Le Bras, J., … Waite, A. J. (2014). Consequences of shoaling of the Central American Seaway determined from modeling Nd isotopes. *Paleoceanography*, *29*(3), 176–189. https://doi.org/10.1002/2013PA002501

Short, D. A., Mengel, J. G., Crowley, T. J., Hyde, W. T., & North, G. R. (1991). Filtering of milankovitch cycles by earth's geography. *Quaternary Research*, *35*(2), 157–173. https://doi.org/10.1016/0033-5894(91)90064-C

Shunk, A. J., Driese, S. G., & Clark, G. M. (2006). Latest Miocene to earliest Pliocene sedimentation and climate record derived from paleosinkhole fill deposits, Gray Fossil Site, northeastern Tennessee, U.S.A. *Palaeogeography, Palaeoclimatology, Palaeoecology*, *231*(3–4), 265–278. https://doi.org/10.1016/j.palaeo.2005.08.001

Snyder, C. W. (2016). Evolution of global temperature over the past two million years. *Nature*, *538*(7624), 226–228. https://doi.org/10.1038/nature19798

Sosdian, S. M., Babila, T. L., Greenop, R., Foster, G. L., & Lear, C. H. (2020). Ocean Carbon Storage across the middle Miocene: a new interpretation for the Monterey Event. *Nature Communications*, *11*(1), 1–11. https://doi.org/10.1038/s41467-019-13792-0

Sosdian, S. M., Greenop, R., Hain, M. P., Foster, G. L., Pearson, P. N., & Lear, C. H. (2018). Constraining the evolution of Neogene ocean carbonate chemistry using the boron isotope pH proxy. *Earth and Planetary Science Letters*, *498*, 362–376. https://doi.org/10.1016/j.epsl.2018.06.017

Sosdian, S., & Rosenthal, Y. (2009). Deep-Sea Temperature and Ice Volume Changes Across the Pliocene-Pleistocene Climate Transitions. *Science*, *325*, 306–311.

https://doi.org/10.1126/science.1169938

Soutar, A., Johnson, S. R., & Baumgartner, T. R. (1981). In Search of Modern Depositional Analogs to the Monterey Formation. In R. E. Garrison & R. G. Douglas (Eds.), *The Monterey Formation and Related Siliceous Rocks of California, special publicatoin of the Pacific Section Soiety of Economic Paleontologists and mineralogists* (pp. 123–147). Pacific Section SEPM.

Spezzaferri, S., Kucera, M., Pearson, P. N., Wade, B. S., Rappo, S., Poole, C. R., … Stalder, C. (2015). Fossil and genetic evidence for the polyphyletic nature of the Planktonic foraminifera "Globigerinoides", and description of the new genus Trilobatus. *PLoS ONE*, *10*(5), 1–20. https://doi.org/10.1371/journal.pone.0128108

St John, K., & Krissek, L. A. (1999). Regional patterns of Pleistocene ice-rafted debris flux in the North Pacific. *Paleoceanography*, *14*(5), 653–662. https://doi.org/https://doi.org/10.1029/1999PA900030

Stabeno, P., Bond, N. A., Kachel, N. B., Salo, S. A., & Schumacher, J. D. (2001). On the temporal variability of the physical environment over the south-eastern Bering Sea. *Fisheries Oceanography*, *10*, 81–98. https://doi.org/10.1046/j.1365-2419.2001.00157.x

Stabeno, P. J., Kachel, N. B., Moore, S. E., Napp, J. M., Sigler, M., Yamaguchi, A., & Zerbini, A. N. (2012). Comparison of warm and cold years on the southeastern Bering Sea shelf and some implications for the ecosystem. *Deep-Sea Research Part II: Topical Studies in Oceanography*, *65–70*, 31–45. https://doi.org/10.1016/j.dsr2.2012.02.020

Steinthorsdottir, M., Coxall, H. K., de Boer, A. M., Huber, M., Barbolini, N., Bradshaw, C. D., … Strömberg, C. A. E. (2020). The Miocene: the Future of the Past. *Paleoceanography and Paleoclimatology*. https://doi.org/10.1029/2020pa004037

Steph, S., Tiedemann, R., Groeneveld, J., Sturm, A., & Nürnberg, D. (2006). Pliocene changes in tropical east Pacific upper ocean stratification: Response to tropical gateways? In R. Tiedemann, A. C. Mix, C. Richter, & W. F. Ruddiman (Eds.), *Proc. ODP, Sci. Results, 202* (pp. 1–51). College Station, TX: Ocean Drilling Program. https://doi.org/10.2973/odp.proc.sr.202.211.2006

Steph, S., Tiedemann, R., Prange, M., Groeneveld, J., Schulz, M., Timmermann, A., … Haug, G. H. (2010). Early Pliocene increase in thermohaline overturning: A precondition for the development of the modern equatorial Pacific cold tongue. *Paleoceanography*, *25*(2), 1–17. https://doi.org/10.1029/2008PA001645

Stringer, W. J., & Groves, J. E. (1991). Location and Areal Extent of Polynyas in the Bering and Chukchi Seas. *Arctic*, *44*, 164–171. Retrieved from http://www.jstor.org/stable/40510994

Strömberg, C. A. E. (2011). Evolution of grasses and grassland ecosystems. *Annual Review of Earth and Planetary Sciences*, *39*, 517–544. https://doi.org/10.1146/annurev-earth-040809-152402

Stroynowski, Z., Abrantes, F., & Bruno, E. (2017). The response of the Bering Sea Gateway during the Mid-Pleistocene Transition. *Palaeogeography, Palaeoclimatology, Palaeoecology*, *485*, 974–985. https://doi.org/10.1016/j.palaeo.2017.08.023

Stroynowski, Z., Ravelo, A. C., & Andreasen, D. (2015). A Pliocene to recent history of the Bering Sea at Site U1340A, IODP Expedition 323. *Paleoceanography*, *30*(12), 1641–1656. https://doi.org/10.1002/2015PA002866

Strum, M., Schimel, J., Michaelson, G., Welker, J. M., Oberbauer, S. F., Liston, G. E., … Romanovsky, V. E. (2005). Winter biological processes could help convert Arctic tundra to shrubland. *BioScience*, *55*, 323–334. https://doi.org/10.1641/0006-3568(2005)055

Sun, J., & Huang, X. (2006). Half-precessional cycles recorded in Chinese loess: response to low-latitude insolation forcing during the Last Interglaciation. *Quaternary Science Reviews*, *25*(9–10), 1065–1072. https://doi.org/10.1016/j.quascirev.2005.08.004

Sun, Y., Clemens, S. C., An, Z., & Yu, Z. (2006). Astronomical timescale and palaeoclimatic implication of stacked 3.6-Myr monsoon records from the Chinese Loess Plateau. *Quaternary Science Reviews*, *25*, 33–48. https://doi.org/10.1016/j.quascirev.2005.07.005

Tabor, C. R., Poulsen, C. J., & Pollard, D. (2015). How obliquity cycles powered early Pleistocene global ice-volume variability. *Geophysical Research Letters*, *42*, 1871–1879. https://doi.org/10.1002/2015GL063322

Tada, R. (1991). Compaction and cementation in siliceous rocks and their possible effect on bedding enhancement. In G. Einsele, W. Ricken, & A. Seilacher (Eds.), *Cycles and Events in Stratigraphy* (pp. 480–491). Springer-Verlag.

Takahashi, K., Fujitani, N., & Yanada, M. (2002). Long term monitoring of particle fluxes in the Bering Sea and the central subarctic Pacific Ocean, 1990-2000. *Progress in Oceanography*, *55*(1–2), 95–112. https://doi.org/10.1016/S0079-

6611(02)00072-1

Takahashi, K., Ravelo, A. C., Alvarez Zarikian, C., & Expedition 323 Scientists. (2011). *Proc. IODP, 323*. Tokyo. https://doi.org/10.2204/ iodp.proc.323.2011

Takahashi, Kozo, Fujitani, N., Yanada, M., & Maita, Y. (2000). Long-term biogenic particle fluxes in the Bering Sea and the central subarctic Pacific Ocean, 1990-1995. *Deep Sea Research Part I: Oceanographic Research Papers*, *47*, 1723–1759. https://doi.org/10.1016/S0967-0637(00)00002-9

Tanner, T., Hernández-Almeida, I., Drury, A. J., Guitián, J., & Stoll, H. (2020). Decreasing Atmospheric CO2 During the Late Miocene Cooling. *Paleoceanography and Paleoclimatology*, *35*(12), 1–25. https://doi.org/10.1029/2020PA003925

Taschetto, A. S., Ummenhofer, C. C., Stuecker, M. F., Dommenget, D., Ashok, K., Rodrigues, R. R., & Yeh, S. (2020). ENSO Atmospheric Teleconnections. In M. J. McPhaden, A. Santoso, & W. Cai (Eds.), *El Nino Southern Oscillation in a Changing Climate* (pp. 309–335). Wiley. https://doi.org/10.1002/9781119548164.ch14

Teraishi, A., Suto, I., Onodera, J., & Takahashi, K. (2013). Diatom, silicoflagellate and ebridian biostratigraphy and paleoceanography in IODP 323 Hole U1343E at the Bering slope site. *Deep Sea Research Part II: Topical Studies in Oceanography*, 1–11. https://doi.org/10.1016/j.dsr2.2013.03.026

Tierney, J. E., Haywood, A. M., Feng, R., Bhattacharya, T., & Otto-Bliesner, B. L. (2019). Pliocene Warmth Consistent With Greenhouse Gas Forcing. *Geophysical Research Letters*, *46*(15), 9136–9144. https://doi.org/10.1029/2019GL083802

Tierney, J. E., Malevich, S. B., Gray, W., Vetter, L., & Thirumalai, K. (2019). Bayesian calibration of the Mg/Ca paleothermometer in planktic foraminifera. *Paleoceanography and Paleoclimatology*. https://doi.org/10.1029/2019pa003744

Tierney, J. E., Poulsen, C. J., Montañez, I. P., Bhattacharya, T., Feng, R., Ford, H. L., … Zhang, Y. G. (2020). Past climates inform our future. *Science*, *370*(6517). https://doi.org/10.1126/science.aay3701

Tokinaga, H., Xie, S. P., Timmermann, A., McGregor, S., Ogata, T., Kubota, H., & Okumura, Y. M. (2012). Regional patterns of tropical indo-pacific climate change: Evidence of the walker circulation weakening. *Journal of Climate*, *25*(5), 1689–1710. https://doi.org/10.1175/JCLI-D-11-00263.1

Turich, C., Freeman, K. H., Bruns, M. A., Conte, M., Jones, A. D., & Wakeham, S. G. (2007). Lipids of marine Archaea: Patterns and provenance in the water-column and sediments. *Geochimica et Cosmochimica Acta*, *71*(13), 3272–3291. https://doi.org/10.1016/j.gca.2007.04.013

Tzanova, A., Herbert, T. D., & Peterson, L. (2015). Cooling Mediterranean Sea surface temperatures during the Late Miocene provide a climate context for evolutionary transitions in Africa and Eurasia. *Earth and Planetary Science Letters*, *419*, 71–80. https://doi.org/10.1016/j.epsl.2015.03.016

Tziperman, E., & Farrell, B. (2009). Pliocene equatorial temperature: Lessons from atmospheric superrotation. *Paleoceanography*, *24*(1), 1–6. https://doi.org/10.1029/2008PA001652

Ukita, J., Honda, M., Nakamura, H., Tachibana, Y., Cavalieri, D. J., Parkinson, C. L., … Yamamoto, K. (2007). Northern Hemisphere sea ice variability: Lag structure and its implications. *Tellus, Series A: Dynamic Meteorology and Oceanography*, *59*(2), 261–272. https://doi.org/10.1111/j.1600-0870.2006.00223.x

Vaughn, D. R., & Caissie, B. E. (2017). Effects of sea-level, sea-ice extent, and nutrient availability on primary production at the Umnak Plateau, Bering Sea (IODP Site U1339) during Marine Isotope Stage (MIS) 5. *Palaeogeography, Palaeoclimatology, Palaeoecology*, *485*, 283–292. https://doi.org/10.1016/j.palaeo.2017.06.020

Vautard, R., Yiou, P., & Ghil, M. (1992). Singular-spectrum analysis: A toolkit for short, noisy chaotic signals. *Physica D: Nonlinear Phenomena*, *58*(1–4), 95–126. https://doi.org/10.1016/0167-2789(92)90103-T

Venti, N. L., Billups, K., & Herbert, T. D. (2013). Increased sensitivity of the Plio-Pleistocene northwest Pacific to obliquity forcing. *Earth and Planetary Science Letters*, *384*, 121–131. https://doi.org/10.1016/j.epsl.2013.10.007

Waller, R. I., Hart, J. K., & Knight, P. G. (2000). The influence of tectonic deformation on facies variability in stratifed debris-rich basal ice. *Quaternary Science Reviews*, *19*, 775–786. https://doi.org/10.1016/S0277-3791(99)00035-9

Wang, C., Dai, J., Zhao, X., Li, Y., Graham, S. A., He, D., … Meng, J. (2014). Outward-growth of the Tibetan Plateau during the Cenozoic: A review. *Tectonophysics*, *621*, 1–43. https://doi.org/10.1016/j.tecto.2014.01.036

Wara, M W, Ravelo, A. C., & Revenaugh, J. S. (2000). The pacemaker always rings twice. *Paleoceanography*, *15*(6), 616–624. https://doi.org/https://doi.org/10.1029/2000PA000500

Wara, Michael W, Ravelo, A. C., & Delaney, M. L. (2005). Permanent El Niño-like Conditions during the Pliocene Warm Period. *Science*, *309*(5735), 758–761. https://doi.org/10.1126/science.1112596

Warner, N. R., & Domack, E. (2002). Millennial- to decadal-scale paleoenvironmental change during the Holocene in the Palmer Deep, Antarctica, as recorded by particle size analysis. *Paleoceanography*, *17*(3). https://doi.org/10.1029/2000PA000602

Wendler, G., Chen, L., & Moore, B. (2014). Recent sea ice increase and temperature decrease in the Bering Sea area, Alaska. *Theoretical and Applied Climatology*, *117*(3–4), 393–398. https://doi.org/10.1007/s00704-013-1014-x

White, J. M., Ager, T. A., Adam, D. P., Leopold, E. B., Liu, G., Jetté, H., & Schweger, C. E. (1997). An 18 million year record of vegetation and climate change in northwestern Canada and Alaska: Tectonic and global climatic correlates. *Palaeogeography, Palaeoclimatology, Palaeoecology*, *130*(1–4), 293–306. https://doi.org/10.1016/S0031-0182(96)00146-0

Wilkens, R. H., & Handyside, T. (1985). Physical properties of equatorial Pacific sediments. In L. Mayer, F. Theyer, & et al. (Eds.), *Initial Reports Deep Sea Drilling Project, Volume 85* (pp. 839–847). Washington: U.S. Govt. Printing Office. https://doi.org/10.2973/dsdp.proc.85.128.1985

Wolfe, J. A. (1994a). An analysis of Neogene climates in Beringia. *Palaeogeography, Palaeoclimatology, Palaeoecology*, *108*(3–4), 207–216. https://doi.org/10.1016/0031-0182(94)90234-8

Wolfe, J. A. (1994b). Tertiary climatic changes at middle latitudes of western North America. *Palaeogeography, Palaeoclimatology, Palaeoecology*, *108*(3–4), 195–205. https://doi.org/10.1016/0031-0182(94)90233-X

Woodgate, R. A., & Aagaard, K. (2005). Revising the Bering Strait freshwater flux into the Arctic Ocean. *Geophysical Research Letters*, *32*(2), 1–4. https://doi.org/10.1029/2004GL021747

Wuchter, C., Schouten, S., Wakeham, S. G., & Sinninghe Damsté, J. S. (2005). Temporal and spatial variation in tetraether membrane lipids of marine Crenarchaeota in particulate organic matter: Implications for TEX86 paleothermometry. *Paleoceanography*, *20*(3), 1–11. https://doi.org/10.1029/2004PA001110

Wycech, J. B., Gill, E., Rajagopalan, B., Marchitto, T. M., & Molnar, P. H. (2020).

Multiproxy Reduced-Dimension Reconstruction of Pliocene Equatorial Pacific Sea Surface Temperatures. *Paleoceanography and Paleoclimatology*, *35*(1), 1–20. https://doi.org/10.1029/2019PA003685

Xie, S. P., Deser, C., Vecchi, G. A., Ma, J., Teng, H., & Wittenberg, A. T. (2010). Global warming pattern formation: Sea surface temperature and rainfall. *Journal of Climate*, *23*(4), 966–986. https://doi.org/10.1175/2009JCLI3329.1

Yiou, P., Ghil, M., Jouzel, J., Paillard, D., & Vautard, R. (1994). Nonlinear variability of the climatic system from singular and power spectra of Late Quaternary records. *Climate Dynamics*, *9*(8), 371–389. https://doi.org/10.1007/BF00207933

Zhang, Y. G., & Liu, X. (2018). Export Depth of the TEX86 Signal. *Paleoceanography and Paleoclimatology*, *33*(7), 666–671. https://doi.org/10.1029/2018PA003337

Zhang, Y. G., Pagani, M., & Liu, Z. (2014). A 12-Million-Year Temperature History of the Tropical Pacific Ocean. *Science*, *344*(6179), 84–87. https://doi.org/10.1126/science.1246172

Zhang, Y. G., Pagani, M., Liu, Z., Bohaty, S. M., Deconto, R., & A, P. T. R. S. (2013). A 40-million-year history of atmospheric CO2. *Phil. Trans. R. Soc. B*, *371*(2001). https://doi.org/10.1098/rsta.2013.0096